INTERACTION OF CARBON MONOXIDE WITH PARTIALLY REDUCED CERIA-ZIRCONIA SUPPORTED CATALYSTS

by

Meghan Elizabeth Swanson

Bachelor of Science in Chemical Engineering, Case Western Reserve University, 2002

Master of Science in Chemical Engineering, Case Western Reserve University, 2003

Submitted to the Graduate Faculty of

Swanson School of Engineering in partial fulfillment

of the requirements for the degree of

Doctor of Philosophy

University of Pittsburgh

2008

UNIVERSITY OF PITTSBURGH

SWANSON SCHOOL OF ENGINEERING

This dissertation was presented

by

Meghan E. Swanson

It was defended on

March 25, 2008

and approved by

Robert Parker, Associate Professor, Chemical and Petroleum Engineering Department

Sachin Velankar, Assistant Professor, Chemical and Petroleum Engineering Department

James Miller, Research Scientist, Chemical Engineering Department, Carnegie Mellon University

Dissertation Director: Julie d'Itri, Associate Professor, Chemical and Petroleum Engineering Department

INTERACTION OF CARBON MONOXIDE WITH

PARTIALLY REDUCED CERIA-ZIRCONIA SUPPORTED CATALYSTS

Meghan E. Swanson, Ph.D.

University of Pittsburgh, 2008

As either a catalyst and/or catalyst support, metal oxides may contribute surface area, chemically active sites, or both. With cerium dioxide (CeO_2), the redox conversion between Ce^{3+} and Ce^{4+} is facile under conditions of industrial interest. This redox function imparts CeO_2 with the capacity to store and release oxygen as reaction conditions, especially oxidant partial pressure, vary.

This work investigated the interaction of CO with stoichiometric and sub-stoichiometric materials. *In situ* Raman spectroscopy studies provided direct evidence of surface carbon deposits on CeO_2, $Ce_{0.75}Zr_{0.25}O_2$, and Pd catalysts following CO exposure at 10% CO/He and 623 K. A band attributed to Ce^{3+} demonstrated the presence of reduced Ce sites, viz. the presence of oxygen vacancies, and appeared concomitantly with carbon formation.

It was inferred from the increase in intensity of the carbon bands with increasing time of exposure to CO that CeO_{2-x} catalyzes CO disproportionation. After prolonged exposure to CO at 623 K, the reaction becomes autocatalytic, as evidenced by the increase in the rate of carbon formation. Based on this result, a mechanistic description of the surface chemistry was put forth. It was speculated that at the aggregated vacancy, the degree of electron density localization controls the rates at which CO acts as an electron donor or acceptor to form an energetically activated complex.

After disproportionation of CO on the CeO_2 surface at 623 K, subsequent exposure to O_2 at room temperature decreased the intensities of the carbon bands and Raman modes characteristic of formate surface species appeared. A mechanism to account for the C/CeO_{2-x} to formate formation was suggested. Namely, CO interacts with the oxygen vacancy through the oxygen end of the molecule to form the intermediate to the surface formate product. This mechanism utilizes the principle of microscopic reversibility and thus may be considered more viable than interaction of a ceria oxygen vacancy with the carbon end of CO.

Similar CO exposure studies performed using a complementary technique, IR spectroscopy, indicate that site blocking by carbonates may play a role in the increased oxygen storage capacity of ceria-zirconia catalysts compared to ceria.

TABLE OF CONTENTS

LIST OF TABLES

LIST OF FIGURES

PREFACE

I have had a few starts and stops on my way to this terminal degree, and I would like to thank several people who have helped to make it happen. Though he may not have consistently felt my appreciation over the previous four years, I would like to thank my husband, Ralph, for encouraging me to go back to school (and living with the consequences)! My advisor, Prof. Julie d'Itri, gave up countless weekend mornings to discuss and question my research and others'. I would like to thank Dr. Vladimir Kovalchuk, Vladimir Pushkarev, Dmitri Kazachkin, Prof. Victor Borovkov, Dr. Tom Vanderspurt, Dr. Dominic Alfonso, and Dave Bivens for their discussions and contributions to this work. Last but not least, my boss Dr. Zane Frund has consistently supported me, and even took a few extra business trips on my behalf so I could keep on track- even though I heard the view from Brazil wasn't bad.

Support from the Petroleum Research Fund (grant No PRF 39801 AC5S) of the American Chemical Society, the Coordinating Research Council (Grant No E-7a-3), and Mine Safety Appliances Co. is gratefully acknowledged. The National Science Foundation also provided a graduate research fellowship that partially supported my Ph.D. coursework.

1.0 INTRODUCTION

Metal oxides are widely used as refractory materials, and are ubiquitous in glasses and ceramics. Catalyst supports composed of metal oxides may contribute surface area, chemically active sites, thermal stability, or a combination to the catalytic reaction. Generally, metal oxides consist of metal cations ionically bonded to oxygen anions in a defined crystal lattice.

The oxidation state of a metal refers to the number of valence electrons available to bond with oxygen (forming O^{2-}). For example, aluminum has a 3+ oxidation state, which means two atoms of aluminum are able to contribute three electrons each to three oxygen atoms, thus forming aluminum oxide (Al_2O_3). Many metals, especially transition metals, are able to assume multiple oxidation states depending on the chemical conditions. For instance, iron commonly forms Fe^{2+} oxide, (FeO or ferrous oxide) as well as Fe^{3+} oxide (Fe_2O_3 or ferric oxide). The ability of a material to assume different oxidation states is called redox capability. Several metal oxides used in catalysts exhibit redox properties, including oxides of copper, chromium, cobalt, and cerium.

The research presented in this dissertation focuses on ceria. Regarding cerium dioxide, the redox conversion between Ce^{3+} and Ce^{4+} is facile at conditions of industrial interest. When used as a catalyst support, this redox ability imparts CeO_2 with the capability to store and release oxygen to the catalytic reaction under various conditions of oxidant partial pressure. An understanding of ceria redox and oxygen mobility is crucial for applications such as water-gas

shift catalysts, solid oxide fuel cell electrodes, and automotive emissions catalysts. For automotive exhaust abatement, ceria supplies oxygen necessary for CO and hydrocarbon oxidation under fuel rich conditions.

The catalysts used to control auto exhaust are called three way catalysts (TWC) because they oxidize CO and hydrocarbons, as well as reduce NO_x to N_2.[1] Modern automobiles operate near the stoichiometric air/fuel ratio in order to simultaneously perform oxidation and reduction, and the TWC conversion efficiency drops off sharply as the ratio fluctuates. In order to minimize the air/fuel ratio fluctuations, ceria is added to the TWC support.

1.1 CERIA STRUCTURE AND REDUCTION CHEMISTRY

Cerium dioxide crystallizes in the cubic fluorite structure (space group *Fm3m*), so called because it is the same structure as calcium fluoride.[2] The lattice structure refers to the orientation of cerium cations and oxygen anions in space. The cerium cations crystallize in a face centered cube, and the oxygen anions fill the tetrahedral positions in the metal cage. The ceria structure is shown in Fig. 1.

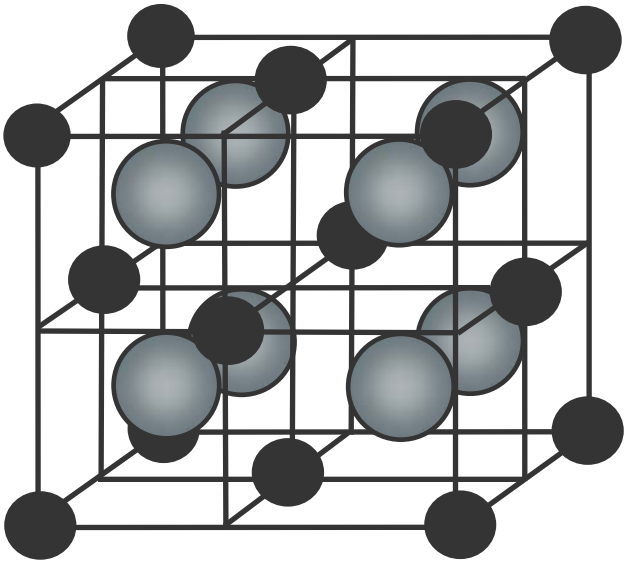

Figure 1. Unit cell of CeO_2. Dark atoms are Ce^{4+} and light atoms are O^{2-}.

Among metal oxides with redox capabilities, cerium dioxide is particularly suited for use as a catalyst support because the CeO_2 lattice structure remains intact even after a significant portion of the cerium cations have been reduced from the 4+ to 3+ oxidation state.[3] The most reduced sub-stoichiometric CeO_{2-x} oxide that may be formed from CeO_2 without a phase change is widely reported to be $CeO_{1.714}$.[2] Ceria may be reduced by increasing temperature or decreasing the oxygen partial pressure. For example, at an O_2 fugacity of 10^{-10} atm, the oxide is CeO_2 at 1020 K, $CeO_{1.9}$ at 1098 K, and $CeO_{1.8}$ at 1189 K.[4]

Additionally, a chemical reductant may be used to accomplish the reduction of ceria at less robust temperatures than the thermal O_2 route. During the abstractive reduction of ceria, gas phase CO interacts with the ceria resulting in carbon dioxide formation; this is similar to the mechanism proposed by Kung on NiO and TiO_2.[5] Each reaction of a CO molecule with the ceria to form CO_2 removes one oxygen atom from the ceria lattice. The empty lattice site from which the oxygen atom was taken is termed a vacancy. As the lattice oxygen is abstracted as an atom, two electrons remain at the vacancy. A mechanism for abstractive reduction of ceria by CO is shown in Scheme 1:

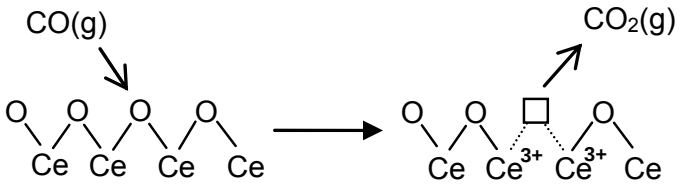

Scheme 1. Abstractive reduction of CeO_2 by CO.

As more oxygen atoms are abstracted, the concentration of vacancies increases. To this end, the probability of vacancies adjacent to one another increases, and indeed vacancy clusters

have been experimentally observed on cerium oxide surfaces. Dimers, trimers, lines, and larger aggregate vacancies have been observed on ceria using STM and AFM,[6,7] as well as inferred from Raman investigations using dioxygen as a probe molecule.[8] Dioxygen adsorbs on ceria-based oxides as peroxide (O_2^{2-}) or superoxide (O_2^-) species. Though the species have been observed at room temperature on ceria[9] and ceria-zirconia[10] using FTIR spectroscopy, Raman spectroscopy is an excellent tool for observing the interaction of dioxygen with oxide surfaces because dioxygen is a non-polar molecule. Temperature-programmed dioxygen adsorption experiments were performed in this laboratory using *in situ* Raman spectroscopy on partially reduced ceria.[8] It was observed that surface peroxides formed on the oxygen vacancy sites. Three types of peroxides were observed: peroxides on aggregate vacancies, peroxides on line vacancies, and peroxides on point vacancies. The thermal stability of peroxide species followed the trend of aggregate < line < point.[8]

1.2 REDOX PROPERTIES OF CERIA-BASED CATALYSTS

Control and understanding of the extent and rate of ceria reduction and oxidation is necessary for many reactions in which ceria exhibits redox behavior. For example, as a component of water-gas shift catalysts ceria may reduce H_2O and oxidize CO in the production of H_2 and CO_2.[11] Also, for solid oxide fuel cell electrodes ceria is a mixed ionic and electronic conductor, which may increase the available area for anodic oxidation of the CO or H_2 fuel.[12] However, the most industrially important application of ceria is in automotive emissions.

Gasoline powered automobile exhaust oscillates between oxidizing and reducing conditions, so the ceria component of the three way emissions catalyst stores and releases

oxygen as necessary. Development of oxygen storage materials precipitated the use of oxygen storage capacity (OSC) measurements to quantify the effectiveness of the catalyst redox. The OSC experiments essentially titrate the catalyst with O_2 and CO in order to determine the amount of labile oxygen available under defined conditions.[13] The amount of CO_2 produced or the amount of O_2 consumed by a single pulse of CO is termed the OSC, a useful measure of the redox rate under the reducing/oscillating conditions typical of automotive emissions. The total amount of oxygen a material will supply is typically measured by exposing the oxidized catalyst to pulses of CO until the consumption of CO ceases. The total amount of CO_2 produced during all pulses, or the amount of O_2 consumed during all pulses, is referred to as the OSC complete (OSCC).[13]

Two main factors influence the amount of labile oxygen available under reaction conditions. First is the ceria surface area; several studies have shown that the larger the surface area, the greater the low-temperature OSC.[13-17] These results indicate that surface oxygen participates in ceria low-temperature OSC rather than oxygen from the bulk. Thus, under sintering conditions when surface area is lost permanently, OSC is also lost permanently; for example, ceria treated at 1073 K experienced > 90% loss in OSC.[18] Second, incorporation of a foreign metal cation in the ceria lattice also affects the OSC of the material. Though numerous transition metal oxides have been investigated,[19-21] zirconia added to ceria has been shown to increase the OSC several times compared to ceria alone. [16,18,22-25]

With respect to commercial performance, ceria-zirconia is widely used and exhibits consistent improved OSC properties compared to ceria alone.[16,18,22-25] One reason for the prevalence of $Ce_xZr_{1-x}O_2$ mixed oxides is ease of incorporation. Depending on the catalyst preparation, zirconia can form a solid solution with ceria, in the cubic crystal structure, for CeO_2

content between 20 – 80%.[26] Addition of zirconia also enhances the thermal stability of ceria. The $Ce_xZr_{1-x}O_2$ oxides are more resistant to sintering and loss of surface area at high temperature compared to ceria.[27-29] In short, $Ce_xZr_{1-x}O_2$ is one of the most widely used and studied ceria-based mixed oxides. The $Ce_xZr_{1-x}O_2$ mixed oxide was a focus of this research.

It is well established that $Ce_xZr_{1-x}O_2$ oxides exhibit an OSC several times[14,30,31] higher than that of CeO_2. Indeed, experiments were performed using H_2/H_2O atmospheres to control O_2 fugacity while the equilibrium oxidation state of exposed ceria was monitored using electrochemical methods; results indicated that reduction of $Ce_xZr_{1-x}O_2$ mixed oxides is more thermodynamically favored than CeO_2 reduction under equivalent conditions of temperature and oxygen fugacity.[32] The most popular explanations for the increased OSC of the mixed oxide involve geometric effects; for example, lattice relaxation may be induced by the smaller size of the Zr^{4+} cation compared to the Ce^{3+} cation.[16,33-38] It is speculated that the smaller radius of zirconia reduces the lattice strain during Ce^{4+} reduction, thereby enhancing the stability of oxygen defects.[34] However, electronic effects of the role of zirconia addition in the oxygen storage capacity enhancement have also been considered. For example, the possible localization of electrons on Ce^{3+} near oxygen vacancies has been calculated.[6] A computational method, density functional theory, (DFT) predicted that the single vacancy formation adjacent to single Zr^{4+} cation would be facilitated by 0.9 eV.[6] In short, the reason for the enhanced OSC of the ceria-zirconia mixed oxide compared to ceria is still a matter of debate. To this end, this dissertation research entertains the idea that electronic effects caused by oxygen vacancies aid the reduction of $Ce_xZr_{1-x}O_2$ oxides.

1.3 SURFACE CHEMISTRY AND SURFACE SPECIES INVOLVING CARBON OXIDES

The molecular orbital-energy level diagram for the CO molecule is shown in Fig. 2. The ten valence electrons are distributed in the 3σ, 4σ, $1\pi_y$, $1\pi_z$, and 5σ molecular orbitals as shown.[39,40] The four nonbonding electrons, located in the 1σ (O 1s) and $2\sigma^*$ (C 1s) orbitals, are not shown. Bonding between CO and a metal or metal oxide surface is believed to occur through electron donation from CO to the surface through the 5σ highest occupied molecular orbital (HOMO), accompanied by back-donation from the surface to the CO $2\pi^*$ lowest unoccupied molecular orbital (LUMO). Because the $2\pi^*$ LUMO is antibonding, the CO bond is weakened upon adsorption.

Because ceria is a basic oxide, carbonate and carboxylate species form on ceria-based oxide surfaces when CO or CO_2 impurities are present, such as in air. Whereas carbonate species consist of a carbon and three oxygen atoms, a carboxylate species contains only two oxygen atoms. In the presence of hydrogen, usually in the form of surface hydroxyl species, hydrogen carbonates and surface formate species may form. Formate formation has been observed on ceria at temperatures ranging from room temperature to over 673 K, on oxides pretreated in O_2 or H_2.[41-43] The different classes of ceria surface species are shown in Scheme 2.

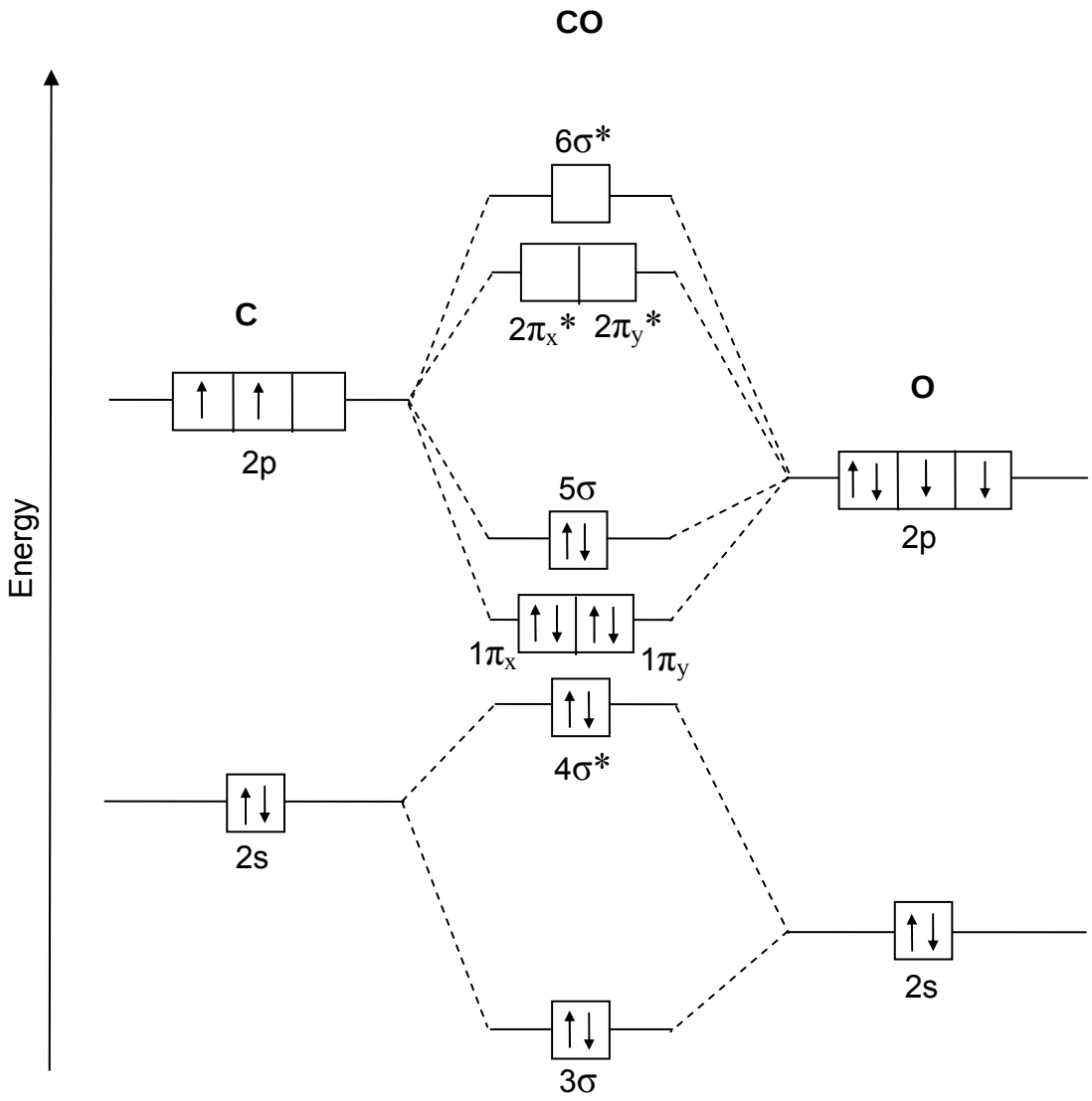

Figure 2. Molecular orbital energy level diagram for the CO molecule[40]

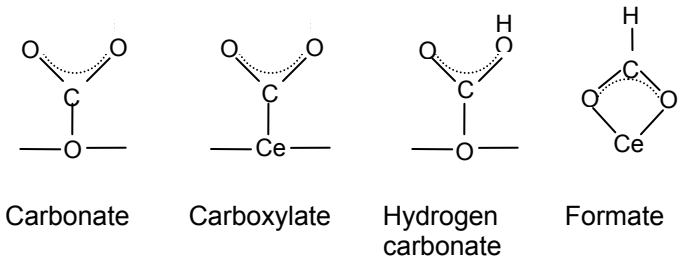

Scheme 2. Types of carbon/oxygen surface species

The carbonate may adsorb in a variety of orientations and coordinations with respect to the oxide surface. When only one oxygen of the carbonate is shared with the oxide surface, the species is classified as a monodentate coordinated species. Two oxygen coordinated carbonates may be bidentate, if both oxygen atoms bind to one surface site, or bridged if the oxygen atoms bind to different sites. When all three oxygen atoms are bound to the surface, the species is called polydentate, or bulk carbonate.[44] Scheme 3 illustrates the possible carbonate coordinations.

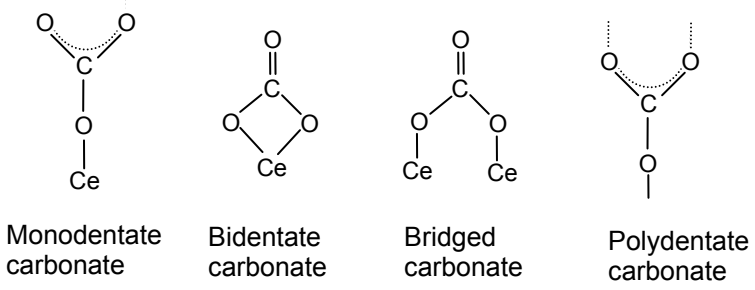

Scheme 3. Carbonate surface species

The thermal stability of a carbonate species depends, in part, on its type and nature. Typically, the carbonates desorb under evacuation at the following temperatures: hydrogen carbonate, bridged carbonate (298 K) < bidentate carbonate (423 K) < monodentate carbonate (473 K) < polydentate carbonate (573 and above).[41,45,46] High temperature outgassing (1000 K) and/or oxygen treatments (873 K) are required to remove the most stable species, polydentate carbonates, from ceria-based catalysts.[41,42,47]

1.4 RAMAN SPECTRA OF RELEVANT MATERIALS

The nomenclature for the Raman band assignments given in this work are based on group theory and crystalline symmetry. The CeO_2 cubic fluorite lattice has the space group *Fm3m,*[2] which corresponds to point group $\mathbf{O_h^5}$.[48] The $\mathbf{O_h}$ point group indicates that the molecule has three axes with 2-fold rotational symmetry, four axes with 3-fold rotational symmetry, and inversion symmetry.[48] The allowed symmetry for point groups have been tabulated in character tables that list the available symmetry operations, denoted by I, A, B, C, etc., for each type of symmetry. The character table for the point group $\mathbf{O_h}$ shows that the A_{1g}, E_g, and F_{2g} vibrations are Raman active, because the vibrations belong to the same species as one of the components of the polarizability.[48] Indeed, the Raman spectrum of CeO_2 shows a strong line at 465 cm^{-1} which is consistent with the first order F_{2g} symmetry mode.[49] Additional features have been observed which may be attributed to second order combinations of the Raman active vibrations, A_{1g}, E_g, and F_{2g}. These include weak bands at 207, 250, 428, 578, and 1174 cm^{-1}.[8]

Considering the Raman spectrum of graphite and other sp^2 hybridized carbon, the carbon is bonded in hexagonal sheets; the sheets are weakly held together with Van der Waals forces.

The unit cell for graphite has symmetry corresponding to point group D_{6h}, and the character table shows that E_{2g} is the only Raman active vibrational mode.[50] The E_{2g} mode corresponds to C-C stretching in the plane of the carbon atoms, and is called the G mode (from "graphite").[51] Additionally, a symmetry-forbidden mode has been observed for small sp^2 carbon crystals, which corresponds to the A_{1g} mode.[52] This mode has been termed the D mode (from "defect"), and arises because of edge effects in the crystal.[52] The G and D carbon modes are illustrated in Fig. 3.

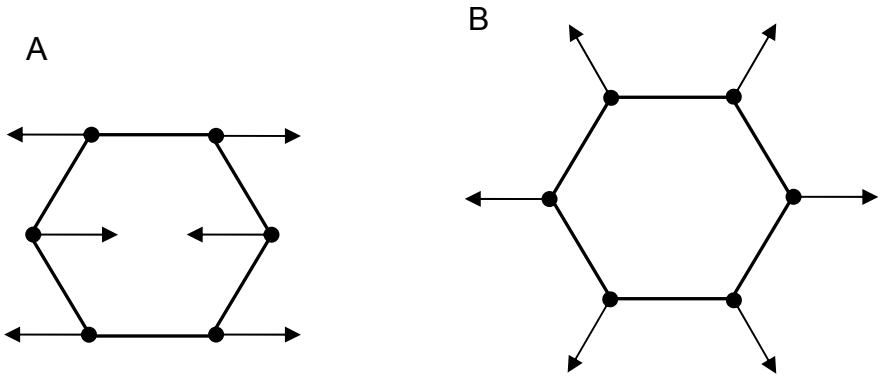

Figure 3. Observed vibrational modes for sp^2 carbon: (A) E_{2g} "G mode", (B) A_{1g} "D mode"

1.5 SCOPE OF THE CURRENT WORK

This research investigates the interaction of ceria-based catalysts with CO, a common reactant and molecular probe. The effects of catalyst composition and treatment conditions on the oxidation state and surface species are surmised. This work also introduces the concept of reduced ceria metallic nano-domains as active sites for CO disproportionation after long times on stream. Understanding the surface chemistry of ceria based oxides is essential for future developments in total and selective oxidation catalysts.

In order to elucidate the molecular behavior occurring during the reduction of ceria based catalysts, their interactions with CO were explored. In addition to CO oxidation, another possible reaction is CO disproportionation. Carbon monoxide disproportionation results in the formation of CO_2 and carbon, as shown:

$$2\ CO \rightarrow CO_2 + C_s$$

The reaction is favored thermodynamically at temperatures less than 1000 K, as shown in the equilibrium plot in Fig. 4. Though the gas phase reaction kinetics are extremely slow,[53] metals such as Ni,[54-58] Fe,[59,60] Co,[56,60,61] Pt,[62] Pd,[63-65] Ru,[66] and Rh[67] readily catalyze the reaction. It has also been reported that CO disproportionation is facile on metal oxides such as MgO[68] and Fe_3O_4,[69] albeit these metal oxides are considered as less active catalysts than the metals. With respect to the interaction of CO with ceria, results from an FTIR investigation of the surface species led to the inference that CeO_2 catalyzes CO disproportionation.[70] One goal of this dissertation research was to probe directly the catalysis of CO disproportionation on ceria. In particular, Raman spectroscopy is an appropriate tool to study CO disproportionation because graphite and other carbonaceous moieties are good Raman scatterers with well-established spectra.[50,71-78]

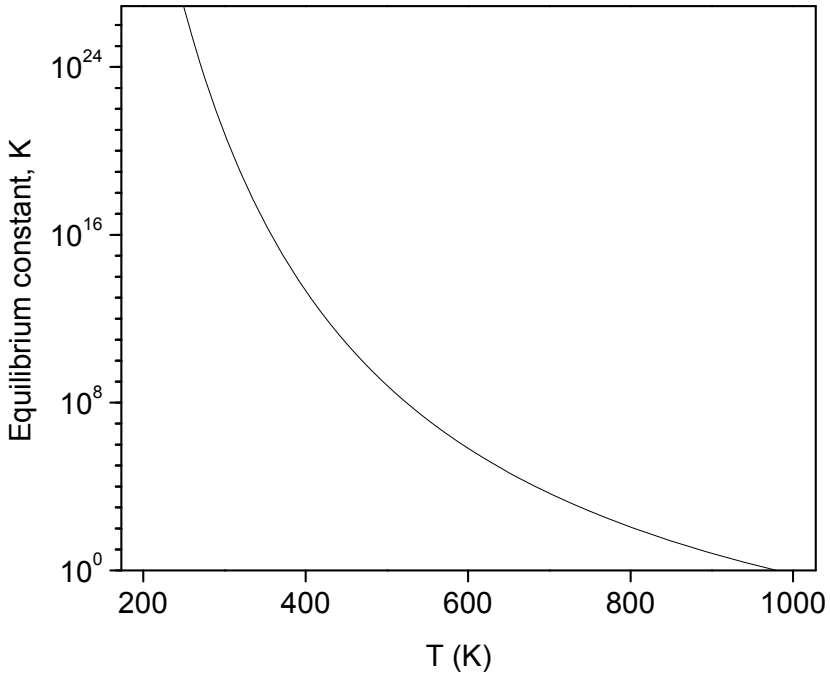

Figure 4. Thermodynamic equilibrium constant for CO disproportionation[79]

Chapter 2 describes the experimental materials and methods used for this work. Chapter 3[80] introduces probing studies of the carbon monoxide interaction with CeO_2, explored using Raman spectroscopy. Chapter 4[81] expands the study to include Pd/CeO_2, $Pd/Ce_{0.75}Zr_{0.25}O_2$, Pd/ZrO_2, and the supports alone. The spectroscopic evidence of reaction products on the ceria surface were interpreted as carbonaceous deposits similar to microcrystalline graphite. The reactivity of the products to room temperature oxidation was also explored.

The macroscopic behavior observed for reactions of reductants or oxidants on ceria is modified substantially by the addition of noble metal particles placed on the oxide. In order to understand the molecular-level phenomena controlling the overall rates of reactions, it is necessary to understand which elementary reaction steps occur on the noble metal, when present. Of primary importance is the mechanism by which a metal site facilitates oxide reduction. When the OSC of metal impregnated oxides are compared to the supports, the metal catalysts exhibit a dramatic (300-400 K) decrease in the temperature required for oxide surface oxygen reduction,[82,83] with a corresponding increase in overall OSC.[43] Studies performed on ceria supported noble metal catalysts showed that bulk oxide reduction occurred at 727 K for Pd, Rh, Pt, Ru, and Ir catalysts.[84] These studies conclude that the oxygen lability increases dramatically upon addition of noble metals to ceria-zirconia catalyst. One goal of this research was to separate the elementary reaction steps occurring on the oxide and noble metal during redox catalysis on ceria-based oxides.

Chapters 5[85] and 6[86] present an investigation of the behavior of ceria and Pd/ceria during long time on stream reactions with CO using Raman and IR spectroscopy as well as high-resolution transmission electron microscopy (HRTEM). (Chapter 5 is a rapid communication and chapter 6 is the full article.) In order to clarify the location of carbon formation on the

catalyst, the rates of carbon formation on Pd/CeO_2 and the bare support were calculated based on spectroscopic evidence. At longer CO exposure times, the ceria support became active for the CO disproportionation. A mechanism for CO disproportionation on CeO_{2-x} involving aggregated oxygen vacancy sites was proposed.

The stability of carbonate species formed upon exposure of CO to Pd/CeO_2, $Pd/Ce_{0.75}Zr_{0.25}O_2$, Pd/ZrO_2, and the supports alone was investigated using FTIR in chapter 7.[87] On $Pd/Ce_{0.75}Zr_{0.25}O_2$ and the support alone, carbonates were less strongly bound after oxidation compared to reduction. The oxide-carbonate bond was destabilized upon oxidation of Ce^{3+} to Ce^{4+}, which indicates that the Ce^{4+} sites in $Ce_{0.75}Zr_{0.25}O_2$ were the active sites for carbonate destabilization. In contrast, the Ce^{4+} and Ce^{3+} sites in Pd/CeO_2 and CeO_2 stabilized carbonates to a similar degree, which indicated that site blocking by carbonates may play a role in the increased oxygen storage capacity of ceria-zirconia catalysts compared to ceria catalysts alone. The results of this study also assigned previously indistinct bands in the CO_3 out of plane bending region to monodentate, bidentate, and polydentate carbonate species on CeO_2 and $Ce_{0.75}Zr_{0.25}O_2$.

Finally, chapter 8 presents a summary of the major contributions of this work, along with recommendations for future studies in the field.

2.0 EXPERIMENTAL MATERIALS AND EQUIPMENT

Two complimentary spectroscopic techniques, Raman and FTIR, were used to conduct the molecular adsorption experiments on which this dissertation is based. Two separate systems were used, with individual gas delivery and sample cells. Details of specific experimental procedures are presented in relevant chapters of this dissertation, along with the accompanying results. Additionally, a variety of techniques including nitrogen adsorption, x-ray diffraction (XRD) and high-resolution transmission electron microscopy (HRTEM) were used to characterize the catalysts following various pretreatments.

2.1 CATALYST SYNTHESIS AND CHARACTERIZATION

2.1.1 Catalyst synthesis

Ceria (99.9%) and $Ce_{0.75}Zr_{0.25}O_2$ (99.9%) were supplied by Rhodia. Before use they were calcined in air at 823 K for 12 h. Zirconia was precipitated from a 1.5 M aqueous solution of $ZrO(NO_3)_2 \cdot 2H_2O$ (Alfa, 99.9%). Under vigorous stirring, ammonia solution (14.7 M) was added dropwise until the pH reached 10. The precipitate was aged in the supernatant solution for 24 h before filtering and repeated washing. The filtrate was then dried at 373 K for 12 h, followed by calcination in air at 773 K for 12 h.

Supports were loaded with 1% palladium, similar to other studies of model TWC.[88] The 1% Pd supported catalysts were prepared by wet impregnation of calcined CeO_2, $Ce_{0.75}Zr_{0.25}O_2$, and ZrO_2 with aqueous solutions of $Pd(NH_3)_4(NO_3)_2$ (Strem Chemicals, 99.9%) using the incipient wetness technique. First, the water absorption capacity of the oxide support was measured. Then the amount of Pd needed for 1% loading was calculated, and the necessary amount of a 5% solution of the $Pd(NH_3)_4(NO_3)_2$ was diluted with distilled water and mixed with the support. For example, the water absorption of the calcined CeO_2 was determined to be 0.554 mL water/ g CeO_2. To achieve 1% Pd impregnation, 8.06 g of calcined CeO_2 was added to a mixture of 1.5 mL of 5% $Pd(NH_3)_4(NO_3)_2$ solution and 2.8 mL distilled water. The wet catalyst mixture was equilibrated overnight, then dried and calcined. The 1% Pd/$Ce_{0.75}Zr_{0.25}O_2$ and 1% Pd/ZrO_2 catalysts were similarly impregnated, and all samples were dried at 373 K for 12 h and calcined in air at 823 K for 12 h.

2.1.2 Catalyst characterization

Following calcination, the specific surface area and pore volume distribution of the samples were determined by physisorption of N_2 at 77 K using a Micromeritics (ASAP 2010) volumetric sorption analyzer. The catalysts were evacuated at 673 K for 2 h prior to the measurements. Powder XRD data were obtained with a Philips XPERT diffractometer, using a standard Ni-filtered Cu Kα radiation source operating at 40 kV and 30 mA. All measurements were made in the thin film mode with a scan rate of 0.08 2θ˚/sec. The average crystalline size was calculated using the Scherrer equation based on the average broadening of the (111) and (220) XRD lines.

High resolution TEM images were obtained using a JEM2010 microscope operated at 200 kV with a maximum resolution of 0.14 nm. The samples for HRTEM study were dispersed

in ethanol by room temperature ultrasonication, and the emulsion thus obtained was deposited on a thin carbon film-covered copper grid. Following ethanol evaporation, the grid was mounted into the microscope.

2.2 EQUIPMENT

2.2.1 Raman Spectroscopy System

The system consisted of a Raman spectrometer with a temperature controlled *in situ* Raman cell in the laser focus; the cell was connected to a flow gas dosing system. The spectrometer was a Renishaw System 2000 confocal Raman spectrometer equipped with a Leica DMLM microscope and a 514.5-nm Ar^+ ion laser as the excitation source and a CCD detector. The laser power at the source was 5-25 mW, which caused minimal sample damage.[8] An Olympus ×50 objective was used to focus the unpolarized laser beam onto a <3 μm spot on the sample, and to collect the backscattered light. Ten scans were collected for each spectrum in the 100-4000 cm^{-1} range, using continuous grating mode, at a resolution of 4 cm^{-1}. Spectra were gathered using Wire software from Renishaw, with a BGrams interface. The spectrometer was calibrated daily using a silicon standard, with a strong primary band at 520 cm^{-1}.

Catalyst pellets were self-supported and prepared from powder. After grinding in an agate mortar, approximately 100 mg powder was pressed into a 10 mm pellet, which was mounted into the cell on a cover slip.

The cell was a THMS 600 Raman cell from Linkam Scientific, which was operated at atmospheric pressure. The window was water-cooled and the sample section was connected to

the treatment gases. The temperature controller (Linkam TMS 94) utilized a platinum resistive sensor on the cell's heating element. The cell working temperature range was 77 to 873 K. Product literature indicated temperature stability of <0.1 K for the cell temperature control system, in part because the sample cover slip rested directly on the silver heating element. The heating and cooling rate for these experiments was always 10 K/min. Fig. 5 shows a schematic of the Raman cell.

The reagent grade He (Air Products) was purified using zeolite and OxyTrap filters, both from Alltech. The CO (Praxair, >99.995%) was fitted with a Vista B γ-alumina trap, heated to 573 K, in order to remove metal carbonyl contaminants. The 10% O_2 in He (Praxair) was used without further purification. The gases (CO, He, and 10% O_2/He) were plumbed through Swagelok 2 μm filters in order to trap any remaining particulates. The desired flow rate of each gas was maintained within ± 1 cm^3/min using Brooks mass flow controllers (model 5850E), and the total gas flow rate was 100 cm^3/min for all Raman treatments and experiments. Fig. 6 shows a schematic of the Raman system.

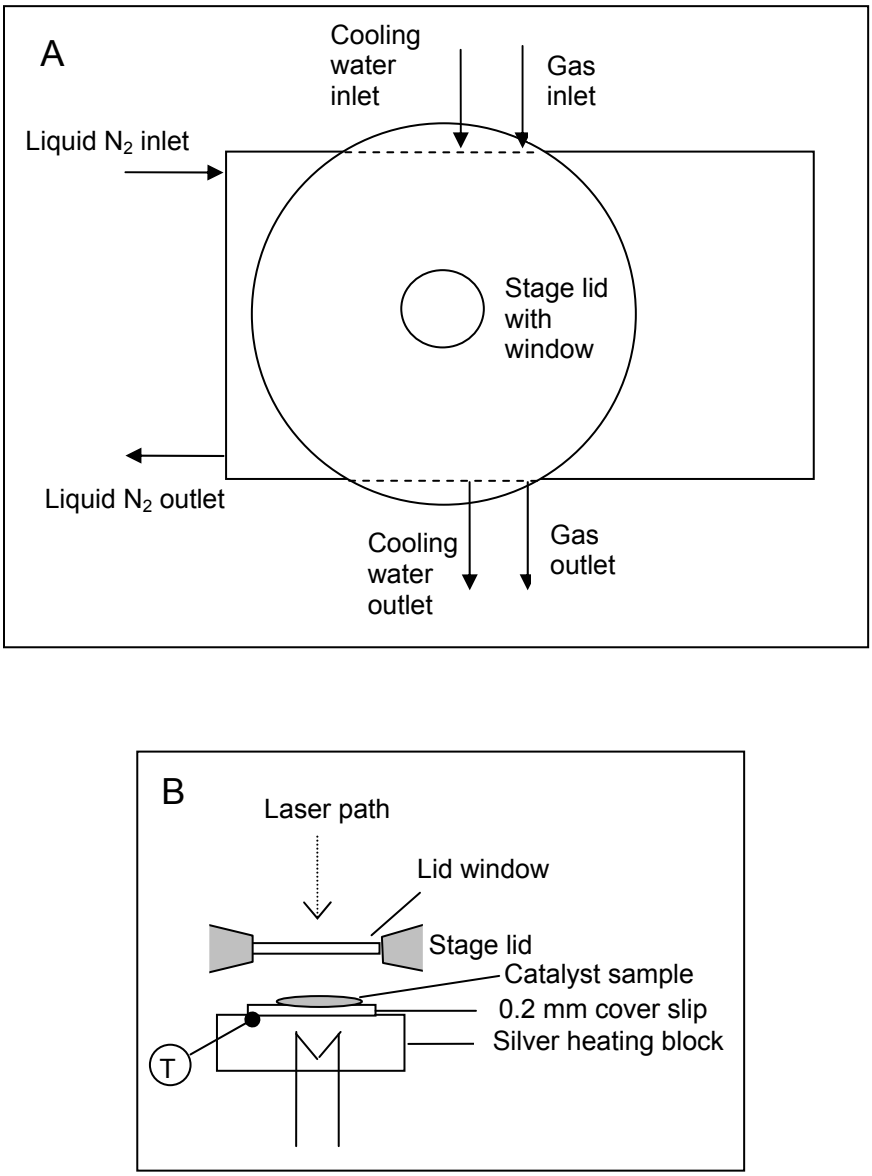

Figure 5. Raman spectroscopy cell. **.** (A) Top view of the Raman cell, (B) Cutaway side view of the cell showing sample and laser path

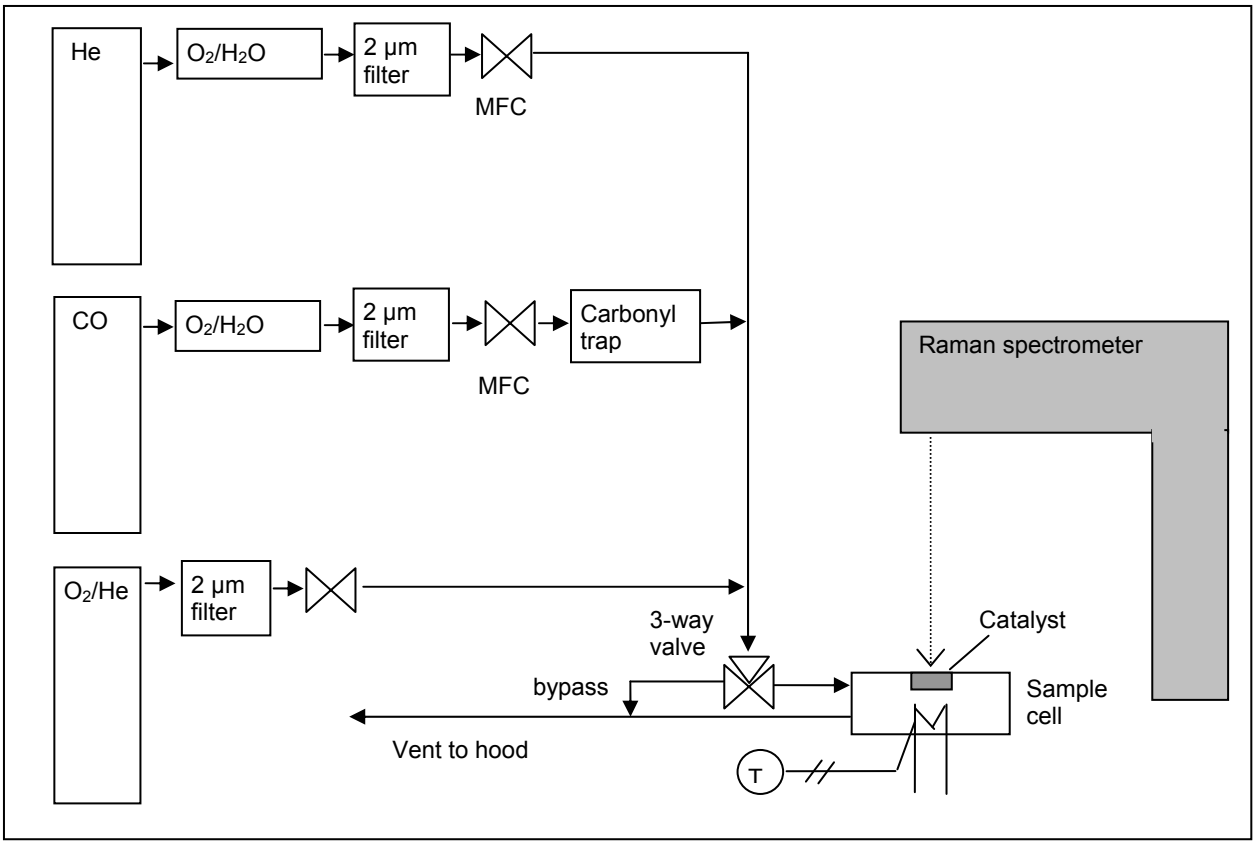

Figure 6. Raman spectroscopy system

2.2.2 FTIR Spectroscopy System

The FTIR system consisted of a spectrometer with a quartz IR cell in the beam path. The cell was connected to a vacuum and gas dosing system, and had a separate heating zone (capable of heating the sample over 723 K) and beam transmission zone.

The infrared spectrometer was a Mattson Research Series II equipped with a liquid N_2-cooled mercury-cadmium-telluride (MCT) detector. The instrument was operated in transmission mode at a resolution of 2 cm^{-1}, and 200 scans were accumulated per spectrum. Spectra were collected in the 400 – 4000 cm^{-1} range. In order to minimize the changes in atmospheric IR bands such as CO_2 and water vapor in the beam path, the bench was purged with dry N_2, which was metered using a needle valve attached to the vent portion of a liquid N_2 tank. Spectra were collected in single beam mode, converted to absorbance, and ratioed to a background spectrum, which was usually the pretreated catalyst. All spectra were collected and analyzed using WinFirst software from Mattson Instruments.

Catalyst pellets were self supported and prepared from powder. After grinding in an agate mortar, about 250 mg powdered catalyst was pressed in a 30 mm die. This resulted in a circular pellet with a density of 8-25 mg/cm^2, which was then trimmed with a blade to a rectangular shape, approximately 22 x 9 mm, for a good fit in the quartz sample holder. The sample support section of the sample holder consisted of two pieces of ~1 mm diameter quartz in a cage configuration, which left both surfaces of the pellet exposed to gas in the cell chamber.

The IR cell was constructed from quartz and included a heating zone above the beam path, and a sample holder with a magnetic end which allowed the sample to be raised into the heating zone and lowered to the beam path without perturbing the atmosphere or vacuum inside

the cell. The IR-transparent cell windows were made of potassium bromide. The cell heating zone consisted of a heating mantle encircling a cylindrical portion of the quartz cell. The sample temperature was measured outside the cell at a distance of 11 mm from the raised catalyst wafer using a type K Omega thermocouple. The temperature at the catalyst pellet was confirmed to remain within 5 K of the temperature at the thermocouple. An Omega temperature controller (model CN2011) was used to regulate the heating zone temperature. The top quartz section of the cell could be removed with an O-ring and clamp to allow exchange of catalyst samples. Fig. 7 shows a schematic of the FTIR cell.

Several gases were used without further purification, including O_2 (Praxair, >99.999%), 10% O_2 in He (Praxair, UHP), and H_2 (Air Products, >99.995%). The trace contaminants in CO (Air Products, >99.99%) and CO_2 (Praxair, >99.995%) were removed using a liquid N_2 cooled trap. Labeled $^{13}C^{16}O$ (Isotec, 99% ^{13}C) was used without further purification.

The high vacuum and gas dosing system was constructed of stainless steel and was capable of an ultimate vacuum of 2×10^{-6} Torr. The pumping system consisted of a turbomolecular pump (Pfeiffer) and a roughing pump (Edwards). The gases were dosed through two leak valves, and pressure in the system was monitored with two pressure transducers (MKS Instruments) with a range of 10^{-6} to 10^{-3} Torr, as well as an ion gauge for measuring vacuum in the range of 10^{-4} to 10^{-8} Torr. Fig. 8 shows a schematic of the FTIR system.

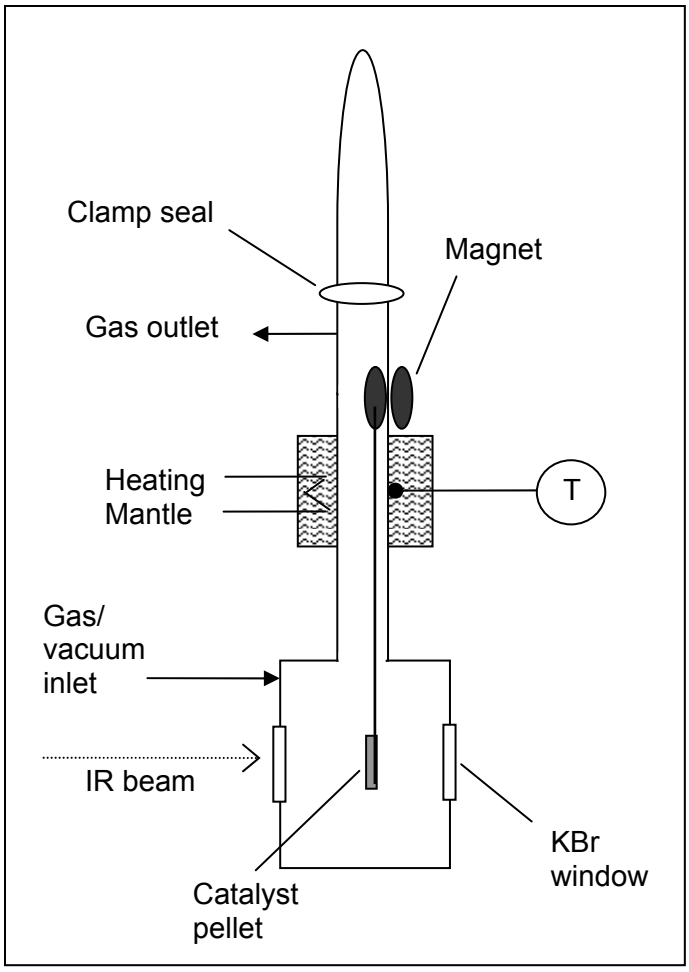

Figure 7. FTIR spectroscopy cell

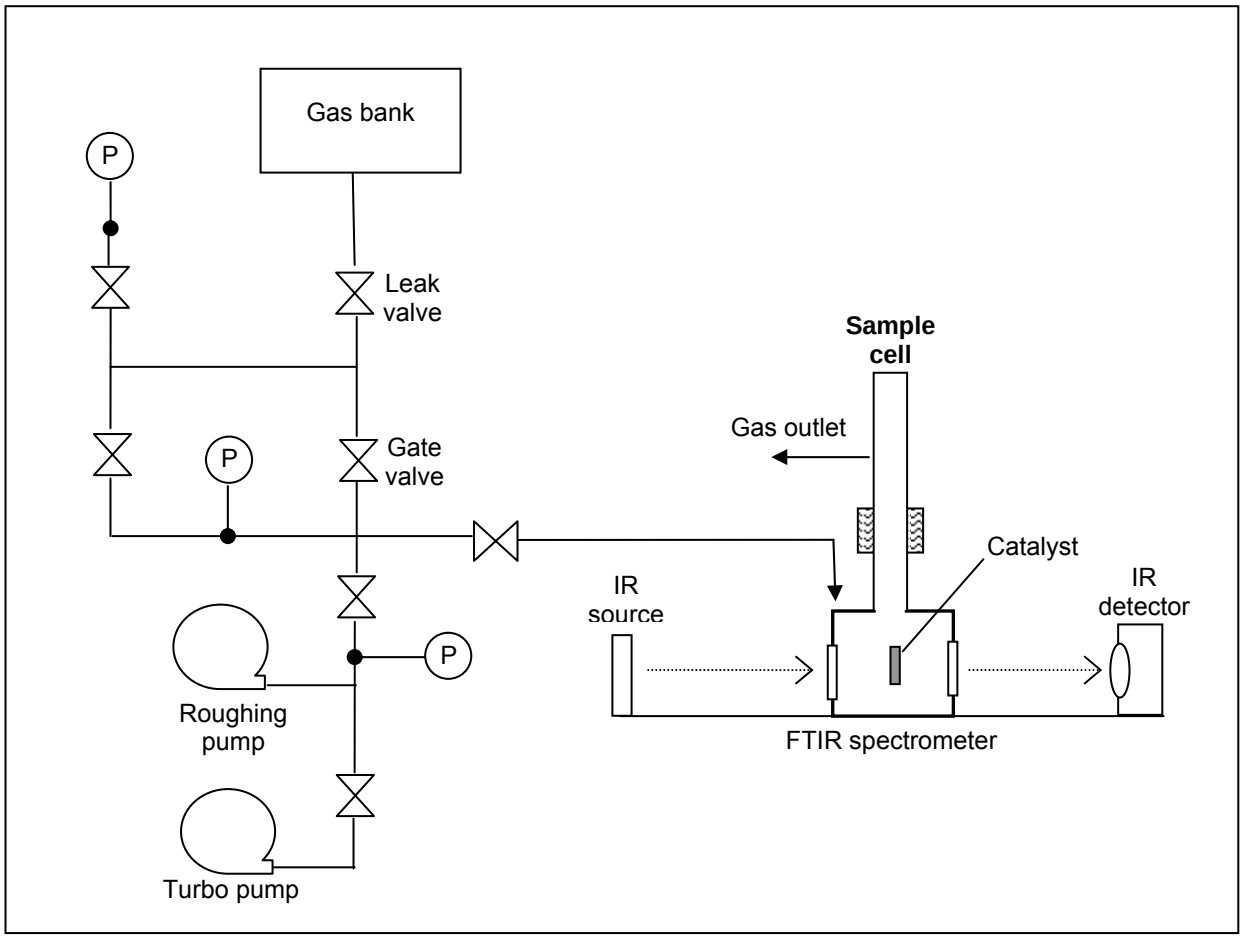

Figure 8. FTIR spectroscopy system

2.3 PROCEDURES

The experimental procedures used to obtain the spectroscopic data for this dissertation are detailed in the individual chapters. However, for clarity the gas dosing procedures for the Raman and FTIR systems will be introduced in this section and illustrated with schematics to show the time, temperature, and gas treatments used in this work.

For Raman studies performed in chapter 3 - 6 the sample pretreatment consisted of heating from room temperature to 673 K in 10% CO/He and maintaining these conditions for 1 h, followed by oxidation in 10% O_2/He for 1 h at 673 K. The pretreatment schematic is shown in Fig. 9.

In the CO exposure Raman experiments run in chapter 3 - 6, a spectrum was collected following pretreatment. Next, the sample was cooled to 623 K in the 10% O_2/He flow. Next, the sample was purged at 623 K with He to avoid a catalytic reaction between O_2 and CO, and then exposed to a 10% CO/He flow while spectra were collected as a function of increasing time. The schematic for the CO exposure experiments is shown in Fig. 10.

In another set of Raman experiments discussed in chapters 3, 4 and 6, the sample was pretreated as described above, except after 12 h CO exposure, the sample was cooled from 623 to 298 K in 10% CO/He and a spectrum was collected. Then, the gas flow was switched to 10% O_2/He and Raman spectra were collected as a function of increasing time. A schematic for the room temperature oxidation experiments is shown in Fig. 11.

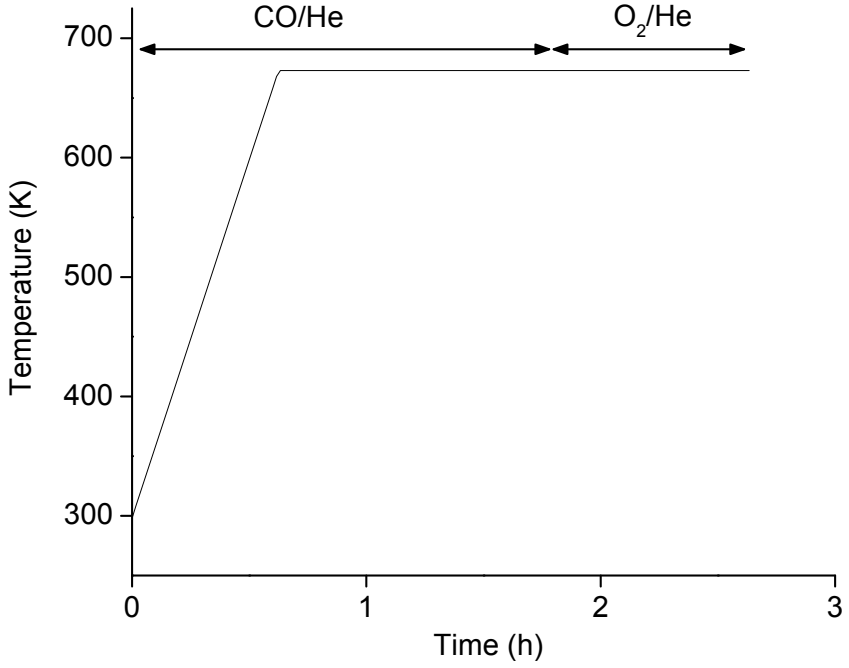

Figure 9. Pretreatment conditions for Raman experiments

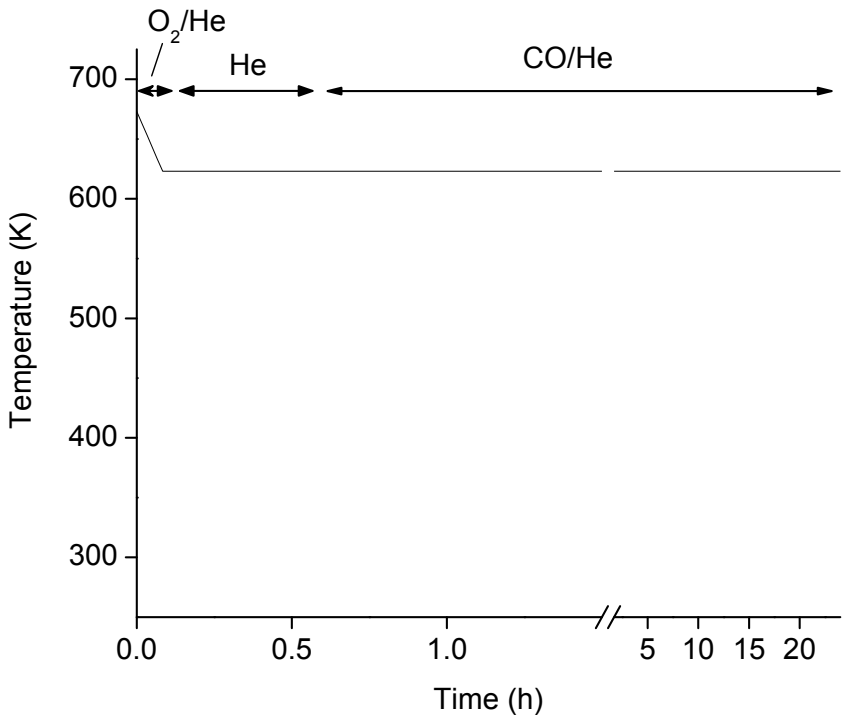

Figure 10. Procedure for CO exposure Raman experiments

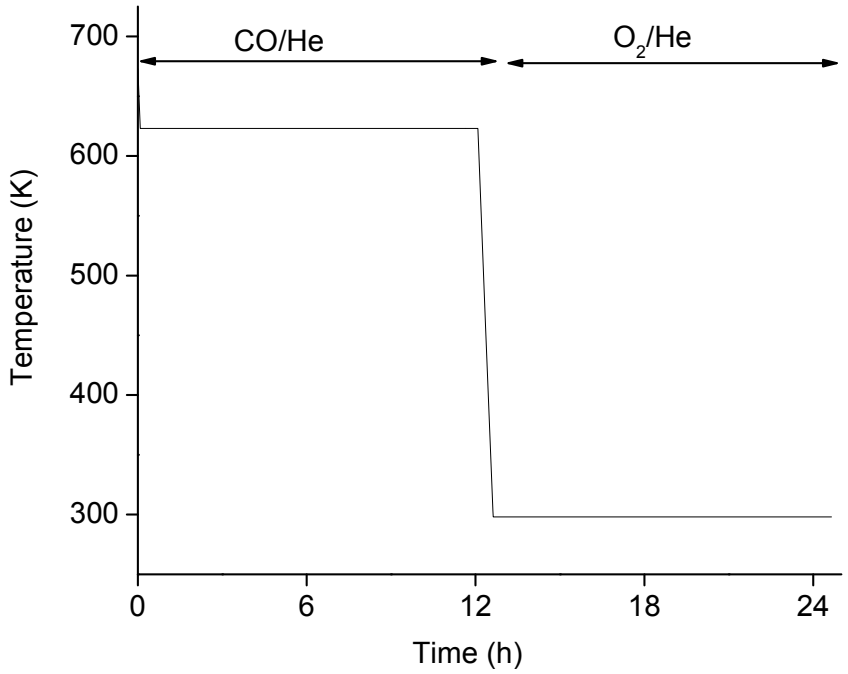

Figure 11. Procedure for room temperature oxidation Raman experiments (prior to CO exposure, the sample was cooled in 10% O_2/He and purged with He, not shown)

Experiments discussed in chapter 6 probed the interaction of CO with Pd/CeO_2 by examining the IR spectra of species formed after the catalyst was exposed to ^{13}CO. The Pd/CeO_2 was pretreated in flowing 10% O_2/He at 673 K for 1 h, followed by exposure to 50 Torr CO at 673 K, then 50 Torr O_2 at 673 K for 1 h. Next, the Pd/CeO_2 was exposed to 50 Torr ^{13}CO for 15 min and evacuated for 15 min at 623 K. The sample was then exposed to 50 Torr unlabeled CO_2 for 15 min at 923 K and evacuated for 15 min at 923 K, in order to exchange the carbon atoms of susceptible species. A schematic for the IR isotope experiment is shown in Fig. 12.

Also discussed in chapter 6, The FTIR band intensity of CO adsorbed on Pd was monitored as a function of reduction temperature on Pd/CeO_2. After pretreatment consisting of exposure to 50 Torr of CO at 673 K for 1 h followed by flowing a 10% O_2/He mixture at 673 K for 1 h, evacuation at 673 K 1 h, cooling to 623 K in flowing 10% O_2/He, and another evacuation at 623 K for 30 min, the Pd/CeO_2 was exposed to 5 Torr CO for 15 min at incremental temperatures from 293 to 623 K. The schematic for the temperature programmed CO adsorption is shown in Fig. 13.

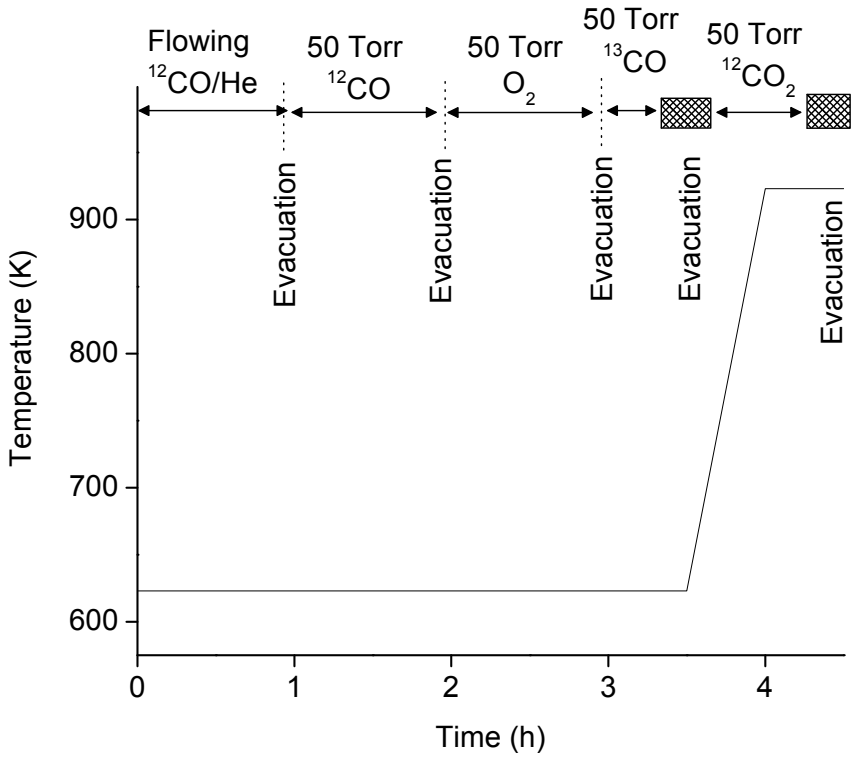

Figure 12. Procedure for FTIR isotope experiment discussed in chapter 6. Spectra were collected at 298 K; cooling for spectra collection is omitted from the figure.

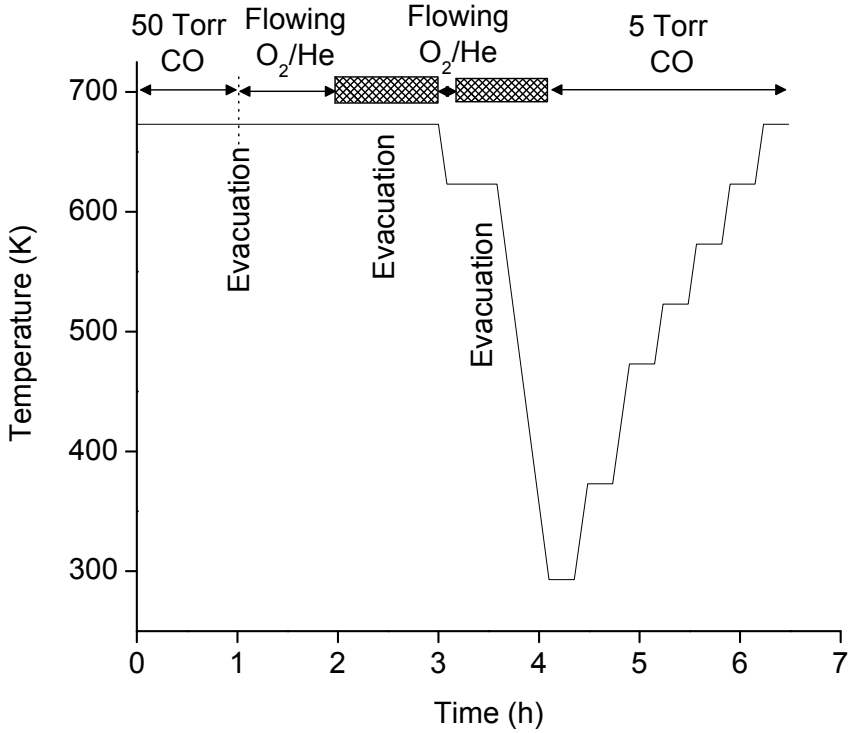

Figure 13. Procedure for FTIR temperature programmed CO adsorption experiment discussed in chapter 6. Spectra were collected at 298 K; cooling for spectra collection is omitted from the figure.

Additional carbon monoxide adsorption experiments carried out with FTIR were discussed in chapter 7. The standard sample pretreatment consisted of exposure to 50 Torr CO at 673 K for 1 h followed by exposure to flowing 10% O_2 in He at 673 K for 1 h, evacuation at 673 K for 1 h, cooling to 623 K in flowing 10% O_2/ He, and evacuation at 623 K for 30 min. A spectrum of the sample following pretreatment was acquired.

Next, spectra of the sample as well as the gas phase were acquired after each of the following gas treatments:

a) Exposure to 50 Torr CO at 298 K for 15 min

b) Exposure to 50 Torr CO at 623 K for 15 min

c) Evacuation at 623 K for 10 min

d) Exposure to 50 Torr O_2 at 623 K for 15 min

e) Evacuation at 623 K for 10 min

A schematic of the CO adsorption experiments is shown in Fig. 14.

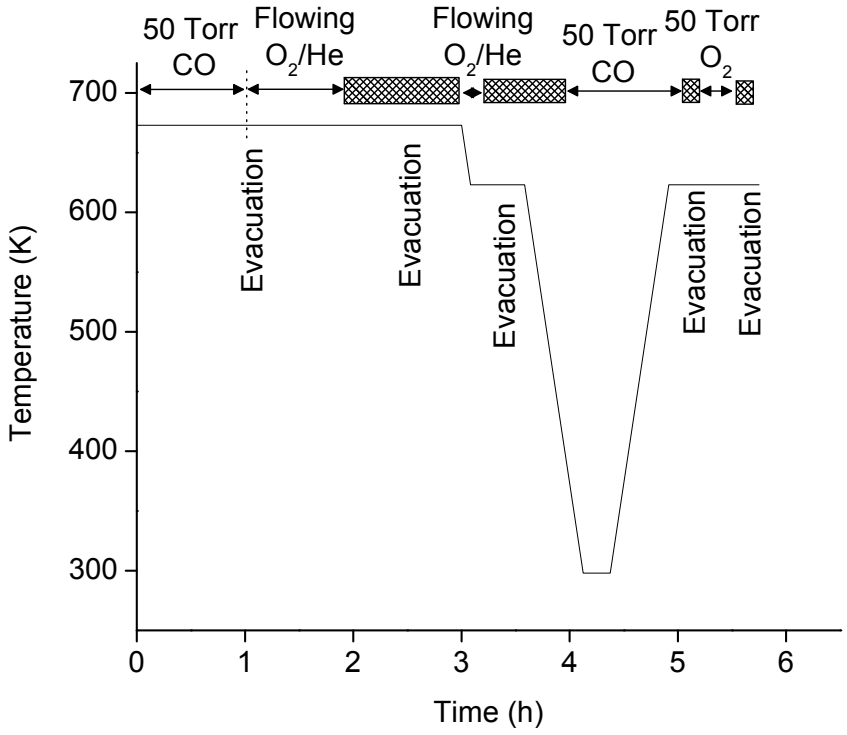

Figure 14. Procedure for FTIR CO adsorption experiments discussed in chapter 7. Spectra were collected at 298 K; cooling for spectra collection is omitted from the figure.

3.0 THE DYNAMIC SURFACE CHEMISTRY DURING THE INTERACTION OF CO WITH CERIA CAPTURED BY RAMAN SPECTROSCOPY

3.1 INTRODUCTION

Ceria is an essential component of the multi-oxide material used to support the noble metals in automotive three way catalysts (TWC). It inhibits thermal sintering of noble metals and promotes CO oxidation by water during fuel-rich excursions.[22] Moreover, because of the facile redox chemistry between the Ce^{3+} and Ce^{4+} oxidation states, ceria also acts as an oxygen buffering agent; viz., ceria has an oxygen storage capacity (OSC). Under oxidizing conditions, the Ce^{3+} ions are oxidized to Ce^{4+} by a stoichiometric reaction with gas phase oxygen. When the automotive emission stream is a reducing atmosphere, the ceria lattice oxygen is utilized to convert CO and hydrocarbons to CO_2, which results in the reduction of Ce^{4+} ions to Ce^{3+} ions. In essence, the oxygen buffering capacity of ceria dampens the oscillations of the engine air to fuel ratio. This improves the overall efficiency of the TWC with respect to oxidation of CO and hydrocarbon emission with simultaneous reduction of NO_x emissions.[22] On the average, the TWC containing ceria operates under conditions closer to optimum than a ceria-free TWC.

The OSC of a catalyst is a property that is measured and assessed in the context of determining the overall performance of a TWC. An established and widely utilized method for measuring the amount of stored oxygen is the pulse technique.[43,84] Typical sequences alternate

between O_2 pulses and CO pulses. The total number of O atoms removed from the oxide lattice via CO_2 formation from a single pulse of CO administered after a single pulse of O_2 is termed the OSC.[13] The total number of oxygen atoms removed from a completely oxidized sample during consecutive pulses of CO until CO_2 formation ceases is called the OSC complete (OSCC).[13] Clearly, the results of measurements to determine the oxygen storage capacity depend on reaction conditions: temperature, reactant partial pressures, and total pressure.[84] Videlicet, the OSC is the amount of labile lattice oxygen available for oxidation reactions under defined conditions. Common reaction conditions reported for OSC measurements are with 1-10% O_2 and 1-5% CO in an inert gas at 570-770 K and atmospheric pressure.[13,15,89,90]

The CO_2 evolved during the OSC measurement is formed via the abstractive reductive adsorption of CO. Oxygen abstraction from the ceria creates defects in the form of Ce^{3+} species and oxygen vacancies.[3,13,91] Additionally, ceria becomes an n-type semiconductor in reducing conditions, which facilitates sorption of electron acceptors.[92] The impact of these factors on the surface chemistry of carbon oxides on ceria remains unclear.

The research put forth in this investigation is directed at understanding the extent to which the interaction of CO with ceria is affected by the degree of ceria reduction. The type and nature of ceria surface species has been probed by *in situ* Raman spectroscopy. Of particular interest are reactions which may interfere with OSC measurements such as surface transformations of carbon oxide species and CO disproportionation to form CO_2 and carbon. Raman spectroscopy was chosen for this study because many vibrations of carbon oxide surface species are Raman active. As well, graphite and other carbonaceous moieties are good Raman scatterers with well-established spectra.[50,71-78]

3.2 EXPERIMENTAL

The CO_2 used in this investigation was supplied by Rhodia; the purity of the material exceeded 99.9%. The CeO_2 was calcined in air at 823 K for 12 h in a muffle furnace prior to any experimentation or characterization. Nitrogen physisorption measurements at 77 K were conducted using a Micromeritics ASAP 2010 volumetric sorption analyzer and the results were used to calculate the BET surface area (127 m^2 g^{-1}), the average pore diameter (4.8 nm), and the pore volume (0.20 cm^3 g^{-1}). An average ceria crystallite size of 9.7 nm was determined from the application of the Scherrer equation to the results of (111) and (220) XRD lines broadening experiments.

The Raman spectra were acquired using a system described earlier (Section 2.2.1 of this dissertation). The sample pretreatment consisted of heating from room temperature to 673 K in 10% CO/He and maintaining these conditions for 1 h, followed by oxidation in 10% O_2/He for 1 h at 673 K. In one set of experiments, the sample was exposed to 10% O_2/He at 673 K for 1 h, and then a spectrum was collected. Next, the sample was cooled to 623 K in the 10% O_2/He flow. Next, the sample was purged at 623 K with He to avoid a catalytic reaction between O_2 and CO, and then exposed to a 10% CO/He flow while Raman spectra were collected as a function of increasing time.

In another experiment, the sample was pretreated as described above, except after 12 h CO exposure, the sample was cooled from 623 to 298 K in 10% CO/He and a Raman spectrum was collected. Then, the gas flow was switched to 10% O_2/He and Raman spectra were collected as a function of increasing time.

3.3 RESULTS

The Raman spectrum of ceria after exposure to 10% O_2/He at 673 K consisted of a band at 1166 cm^{-1} attributed to a combination of A_{1g}, E_g, and, F_{2g} ceria lattice vibrational modes[49] and a band at 3634 cm^{-1} assigned to the O-H stretching mode of a ceria hydroxyl group vibration with bidentate coordination[43,93-95] (Fig. 15a). The two bands decreased in intensity by approximately a factor of 4 after exposure to CO at 623 K for 1 h (Fig. 15b). As well, new bands appeared at 2115 cm^{-1} and 1582 cm^{-1}, and a low-frequency shoulder formed on the 1166 cm^{-1} band at 1068 cm^{-1}. The 1068 cm^{-1} band has been assigned to a vibrational mode of cerium carbonate by several research groups.[46,47,92,94,96]

The dynamic nature of the surface chemistry associated with continued exposure to CO at 623 K was evident from the Raman spectra (Fig. 16). Twenty min exposure to CO marked the appearance of the 1068 cm^{-1} carbonate band on the shoulder of the 1166 cm^{-1} band and a band at 2115 cm^{-1}. After 3.4 h CO exposure time, bands at 1582, 1434, and 1331 cm^{-1} were observed (Fig. 16c), and the intensity of these three bands increased throughout the duration of the experiment (21.6 h). In comparison to the intensity increases observed for the 1582, 1434, and 1331 cm^{-1} bands, the intensity of the 3634 and 1166 cm^{-1} ceria bands and the 2115 and 1068 cm^{-1} bands did not change markedly with increasing CO exposure time. It should also be noted that after 17.3 h exposure to CO, a broad band centered at 2840 cm^{-1} was detectable (Fig. 16d), and it became more pronounced after 21.4 h exposure to CO (Fig. 16e).

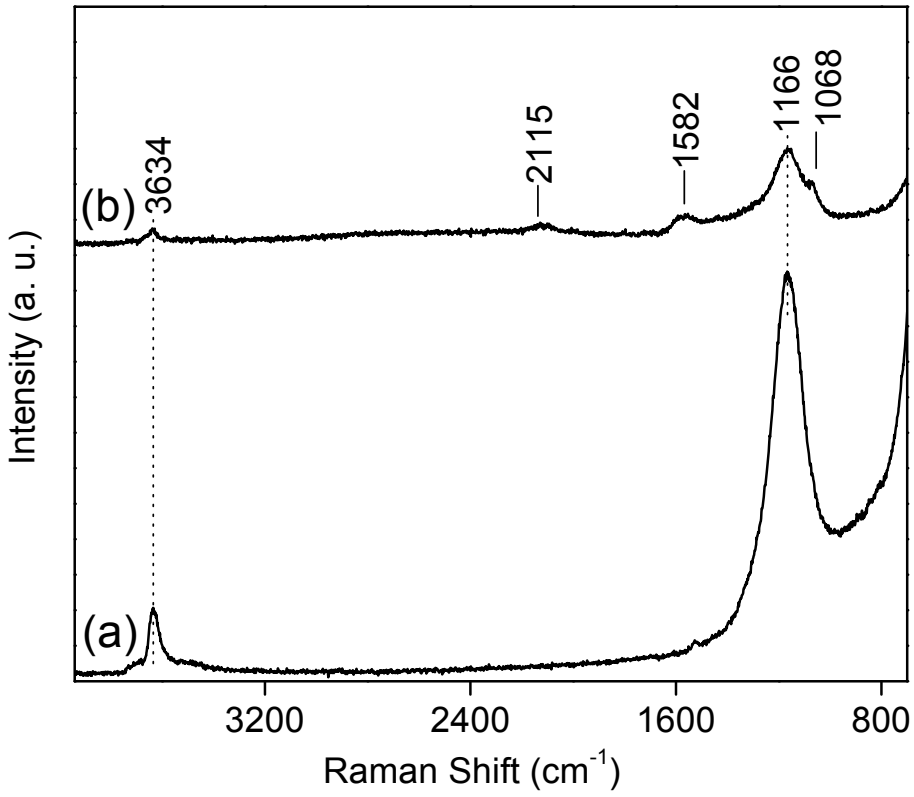

Figure 15. In situ Raman spectra of CeO_2 (a) after treatment in 10% O_2/He at 673 K for 1 h and (b) after exposure to 10% CO/He at 623 K for 1 h. All spectra were recorded at 623 K.

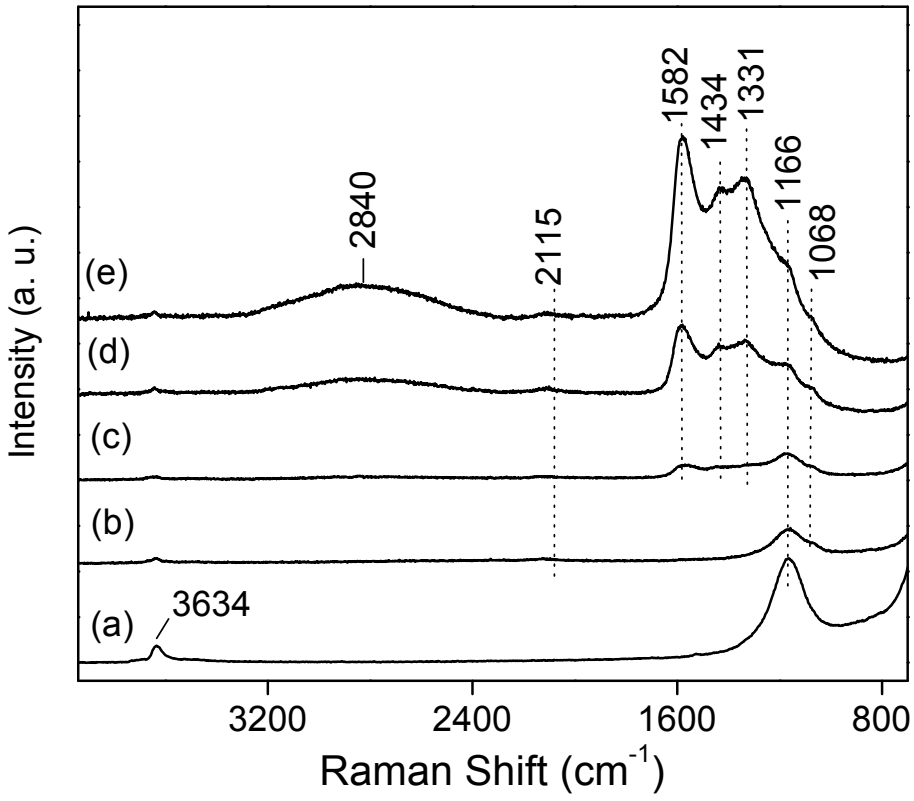

Figure 16. In situ Raman spectra of CeO_2 (a) after treatment in 10% O_2/He at 673 K for 1 h, then exposed to a flow of 10% CO/He at 623 K for: (b) 20 min, (c) 3.4 h, (d) 17.3 h, and (e) 21.6 h. All spectra were recorded at 623 K.

After exposing ceria to CO for 12 h at 623 K and cooling to room temperature, the position of the ceria lattice vibration was 1174 cm^{-1} (Fig. 17a),[97] in contrast to the spectra collected at 623 K in which the band was centered at 1166 cm^{-1} (Fig. 15 and 16). The shift to a higher frequency is attributed to the lattice thermal contraction; the accompanying increase in the bond energy caused a shift in the Raman mode.[97,98] Bands at 2115 and 3630 cm^{-1} were also present in the room temperature spectrum, as were bands at 1600 and 1340 cm^{-1} and the 1068 cm^{-1} carbonate band (Fig. 17a). The 1434 cm^{-1} band in Fig. 16c-e was obscured in the room temperature spectrum. The position of this vibrational band is consistent with a variety of surface species and vibrational modes. One speculative interpretation is that the 1434 cm^{-1} band is a carbon-cerium vibration.

Subsequent exposure to O_2 at room temperature for 30 min resulted in the disappearance of the 2115 cm^{-1} band and the appearance of a band at 831 cm^{-1}, which has been assigned to surface peroxide,[8,9,99,100] and bands at 2852 and 2935 cm^{-1} (Fig. 17b). The 2852 and 2935 cm^{-1} bands are formate modes. Specifically, the 2935 cm^{-1} is assigned to a C-H stretching mode[42,101] and the 2852 cm^{-1} band is assigned to a combination mode of the C-H bend and O-C-O asymmetric stretch.[42,43,101] Formate also exhibits strong infrared bands at 1599, 1553, and 1542 cm^{-1}, all assigned to the O-C-O asymmetric stretch.[42,101] Thus, a formate mode may be included in the collection of low intensity peaks in the vicinity of 1600 cm^{-1} after 12 h O_2 exposure (Fig. 17c).[42,101,102] Additionally, the position of the 1363 cm^{-1} band that appeared after 12 h O_2 exposure (Fig. 17c) agrees well with the 1362-1363 cm^{-1} which has been assigned to a formate asymmetric O-C-O stretching vibration,[101,102] or alternately, a formate C-H in plane vibration at 1369 cm^{-1}.[42]

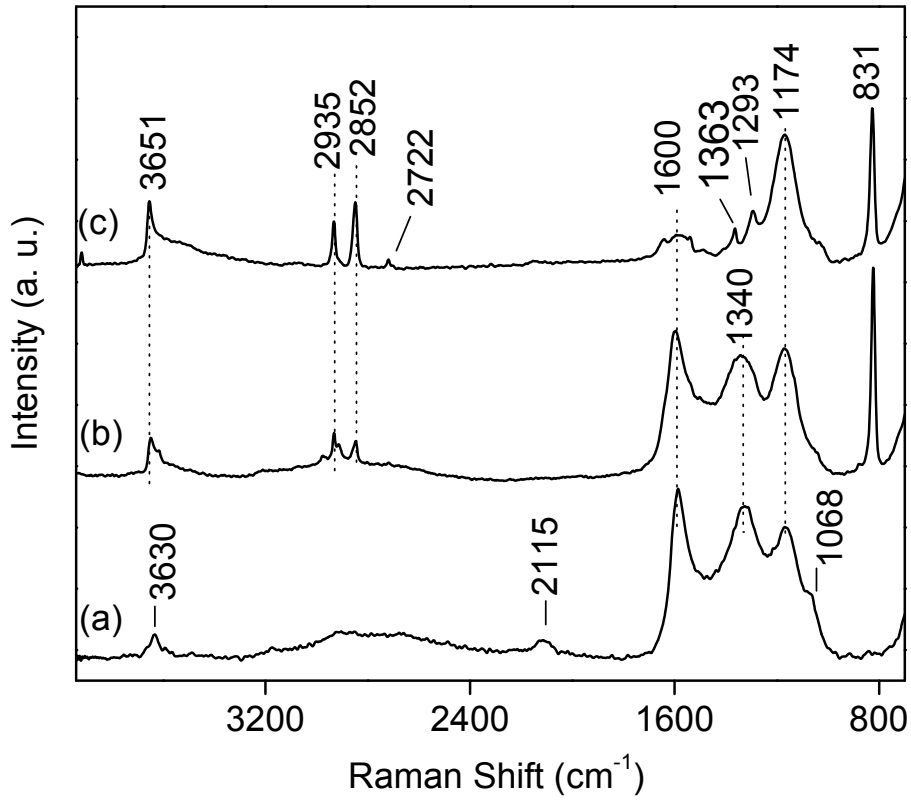

Figure 17. In situ Raman spectra of CeO_2 (a) treated in a flow of 10% CO/He at 623 K for 12 h, and after subsequent exposure to a flow of 10% O_2/ He at 298 K for (b) 30 min, and (c) 12 h. All spectra were recorded at 298 K.

The intensities of the bands at 1340 and 1600 cm^{-1} decreased substantially during 12 h exposure to O_2 at 298 K (Fig. 17c). The bands at 2852 and 2935 cm^{-1} increased in intensity during O_2 exposure, whereas the intensity of the 831 cm^{-1} band decreased. After 12 h exposure to O_2, bands were detected at 2722 cm^{-1} and 1363 cm^{-1}. The 2722 cm^{-1} band (Fig. 17c) was assigned previously in infrared spectra of ceria partially reduced in hydrogen at 673 K for 1 h to a formyl species.[42,101-103]

A band in the hydroxyl region at 3651 cm^{-1} was present after 12 h exposure to O_2; it was 21 cm^{-1} higher in frequency than the band present after 12 h exposure to CO. As well, a band at 1293 cm^{-1} was visible after 12 h O_2 exposure (Fig. 17c); assignment to a carbonate vibrational mode is viable,[43,46] yet speculative.

3.4 DISCUSSION

In 1994 Bozon-Verduraz and Bensalem pointed out that the propensity of ceria for non-stoichiometry contributed to significant uncertainty in our understanding of the nature of the species formed when carbon oxides interact with ceria based on IR spectroscopy investigations.[92] In other words, carbon oxides may interact with a fully oxidized surface or one that has reduced to sub-stoichiometric CeO_{2-x}. Indeed, the IR spectra of ceria exposed to carbon oxides consist of numerous overlapping bands in the C-O, C=O, and C=C vibrational region of 1050 - 1750 cm^{-1}.[42,96] Efforts to establish the frequencies of the variety of types of surface carbonate and carboxylate have been complicated by the complexity of the spectra – and the propensity of ceria for non-stoichiometry.

The results of this investigation show the increase in intensity of Raman bands at 1582-1600 and 1331-1340 cm^{-1} with increasing exposure time to flowing CO at 623 K (Fig. 15-17). The position of the bands are in line with reported, albeit generous, ranges for the two asymmetric vibrational modes of a surface carbonate, one high frequency and one low frequency in comparison to the doubly degenerate asymmetric CO stretching mode at 1415 cm^{-1} for a free carbonate ion.[44]

Additionally, the 1582-1600 and 1331-1340 cm^{-1} bands are in the range reported for the asymmetric and symmetric stretching modes of a carboxylate species, reported as 1510-1570 and 1310-1410 cm^{-1}, respectively.[46,48,104,105] The present research showed that the 1582 and 1331 cm^{-1} bands increased in intensity with continued exposure to CO at 623 K. Under these conditions, the abstractive reductive adsorption of CO to form CO_2 occurs with the concomitant formation of Ce^{3+} ions and oxygen vacancies.[3,22,91] Hence, it is reasonable to suggest that carboxylate formation would be favored as the ceria becomes more reduced and the number of oxygen vacancies increases. The formation of a carboxylate from CO requires only one ceria oxygen whereas formation of a carbonate requires two.

However, the more than 90% decrease the intensities of these two bands after exposure to flowing O_2 for 12 h at room temperature (Fig. 17) provides a strong driving force to consider alternative assignments to carbonate for the 1582-1600 and 1331-1340 cm^{-1} bands observed in this investigation, even though their formation under conditions similar to those used in the present work has been reported.[43,106] Carbonates of ceria are notoriously stable,[92] and no apparent change in the spectra of CO adsorbed on CeO_2 occurs after dosing O_2 on CeO_2 pre-adsorbed with CO according to Li et al.[46] In fact, the decomposition of the carbonates require a temperature of roughly 1000 K and an oxygen-free atmosphere.[46,92]

Carbon phonon modes are Raman active, and it is plausible that the 1582 and 1331 cm^{-1} bands are attributed to carbon-carbon vibrations. Specifically, the band position corresponds well with the 1575-1585 cm^{-1} band frequency of the doubly degenerate E_{2g} Raman-active phonon mode (G band) of sp^2 hybridized carbon materials such as graphite, charcoal and coke.[50,71,74,76,107,108] And the position of the band at 1331 cm^{-1} is comparable with the 1343-1360 cm^{-1} band position of a disorder-induced carbon A_{1g} phonon mode (D band) of graphitic and glassy carbons measured experimentally using a 514.5 nm excitation source,[71,76,78,109] as was used in this investigation. The broad band centered in the vicinity of 2840 cm^{-1} after prolonged exposure to CO at 623 K (Fig. 16d-e, Fig. 17a-b) is consistent with the assignment of the 1331-1340 cm^{-1} band to the D band of carbon, as it is in the position[71,74,77,110] and is of the shape[76,108] of a D band overtone.

The dissociation of CO must occur in order for surface carbon to form. To this end, it must be noted that the carbon-oxygen bonds of CO and CO_2 readily cleave on ceria at 673 K, as evidenced by isotope exchange experiments with $C^{18}O$ and $C^{18}O_2$.[43] In fact, the rate of exchange was faster on ceria than on Pt supported on ceria. Additionally, the band at 2115 cm^{-1} (Fig. 16 and 17) is characteristic of Ce^{3+} species. The band has been assigned to the CO stretching mode of a CO-Ce^{3+} species[111] (although earlier investigations assigned it to the symmetry-forbidden $^2F_{5/2} \rightarrow {}^2F_{7/2}$ electronic transition of Ce^{3+}.[47,92] In contrast to CO adsorbed on Ce^{4+} in which the CO vibrational frequency is 5-24 cm^{-1} higher than gas phase CO,[112] the frequency of CO adsorbed on Ce^{3+} is 28 cm^{-1} lower in frequency than the gas phase. A donation of electron density from the Ce^{3+} ion to the CO is consistent with the shift, as is the interpretation that the reduced cerium cations sites favor CO dissociation.

Formation of surface formate species was observed upon room temperature O_2 exposure to ceria that was previously treated in CO at 623 K (2852 and 2935 cm^{-1} bands in Fig. 17b-c). One possible mechanism to account for formate formation is the reaction of a dioxygen surface species with carbon followed by a reaction with a hydroxyl group. A type of reactive dioxygen species, surface peroxide, was observed on the ceria upon addition of O_2, as evidenced by the 831 cm^{-1} band (Fig. 17).

It may be inferred from the presence of a D band of carbon (1331-1340 cm^{-1}) in addition to a G band (1582-1600 cm^{-1}) that the carbon is highly reactive. The presence of the D band demonstrates that the carbon particle size is small. An empirical relationship has been established in the literature relating the ratio of the carbon band intensities (I_G/I_D) to the graphite particle size as measured by XRD; the relationship for a 514 nm Raman laser is $I_G/I_D = 44$ Å$/L_a$, where L_a is the crystalline size of the graphite plane.[50,76] The integrated band intensities have been obtained using the deconvolution and peak fitting method described by Nistor et al.[113] Using this method in the current work, the average carbon particle size was calculated as 1.7 nm. Though this value is smaller than the 2 nm experimentally verified lower limit[51] of the empirical relationship for disordered carbon spectra, it may nevertheless be surmised that the carbon in the current work has a small particle size, less than 2 nm, and therefore exhibits a high degree of disorder. Most importantly, the surface of such small particles is comprised largely of carbon atoms that are coordinatively unsaturated. Thus, the interaction of coordinatively unsaturated carbon sites with surface peroxides is a viable model for room temperature carbon oxidation.

3.5 CONCLUSION

Prolonged exposure of ceria to CO at 623 K generates reactive lattice defects and carbon-containing surface species. It may be inferred from the increase in intensity of the vibrational bands at 1582-1600 and 1331-1340 cm^{-1} with continuing CO exposure that accumulation of one or more surface species occurs. Although carbonates and carboxylates remain viable species to which the bands may be assigned, the band positions are also in line with carbon phonon modes. It has been suggested that carbon may form by CO disproportionation, and this suggestion is supported by the formation of formates upon subsequent exposure to O_2 at room temperature.

4.0 A MECHANISTIC INVESTIGATION OF FORMATE FORMATION ON CERIA BASED OXIDES

4.1 INTRODUCTION

The interaction of carbon monoxide with metal oxide supported catalysts to form chemisorbed species and reaction products is essential to the study of various catalytic reactions, including water gas shift, CO oxidation, and NO reduction by CO. Carbon monoxide is also commonly used as a probe molecule for surface science studies.

Various surface species result from the reaction of CO with oxide supports containing hydroxyl species. These include oxidation of the CO by surface oxygen to form CO_2 [1], interaction of the product CO_2 with the oxide surface to form carbonates [2], or CO disproportionation [3]. Near a hydroxyl, surface formate species may form [4]. Surface formates are a suspected intermediate in the water gas shift reaction [5].

$$CO + O_s \rightarrow CO_2 \quad [1]$$

$$CO_2 + O_s^{2-} \rightarrow CO_3^{2-} \quad [2]$$

$$2CO \rightarrow C_s + CO_2 \quad [3]$$

$$CO + OH_s \rightarrow COOH_s \quad [4]$$

$$COOH_s \rightarrow CO_2 + \tfrac{1}{2} H_2 \quad [5]$$

This study used *in situ* Raman spectroscopy to examine the interaction of CO with CeO_2 based catalysts. The major industrial use of CeO_2 is as an oxygen storage component (OSC) in automotive emissions three way catalysts (TWC).[114] The facile conversion of the cation from Ce^{3+} to Ce^{4+} enables the TWC oxidize hydrocarbons and CO during fuel rich excursions.[115] Understanding of the interaction of CO with ceria based catalysts is important because the quantitative oxidation of CO by TWC has been used as a measure of the OSC of ceria-containing catalyst formulations.[13]

4.2 EXPERIMENTAL

4.2.1 Materials

Ceria (99.9%) and $Ce_{0.75}Zr_{0.25}O_2$, (99.9%) were provided by Rhodia and calcined in air at 823 K for 12 h prior to use. Zirconia was precipitated from an aqueous solution of $ZrO(NO_3)_2$ (Alfa, 99.9%) with aqueous ammonia at pH 10. The precipitate was aged in the supernatant liquid for 24 h before filtering, washing, and drying at 373 K for 12 h; it was then calcined in air at 773 K for 12 h. The 1% Pd supported catalysts were prepared by impregnation of CeO_2, $Ce_{0.75}Zr_{0.25}O_2$, and ZrO_2 with aqueous solutions of $Pd(NH_3)_4(NO_3)_2$ (Strem Chemicals, 99.9%). The impregnated samples were dried at 373 K for 12 h and then calcined in air at 823 K for 12 h.

The reagent grade He (Air Products, 99.998%) and CO (Praxair, 99.995%) were purified of trace oxygen and water using zeolite and OxyTrap filters, both from Alltech. Additionally, the CO was fitted with a Vista B γ-alumina trap, heated to 573 K, in order to remove metal carbonyl contaminants. The 10% O_2 in He (Praxair) was used without further purification.

The sample pretreatment, if not otherwise specified, consisted of heating the sample from room temperature to 673 K in 10% CO/He, and maintaining these conditions for 1 h. Subsequently, the flow was changed to 10% O_2/He at 673 K for 1 h. Experimental conditions were chosen to represent typical pretreatment prior to OSC measurements,[18,88] and the treatment described above will be referred to as the "standard" pretreatment.

4.2.2 Catalyst characterization

The specific surface area and pore volume distribution of the calcined samples were determined by physisorption of N_2 at 77 K using a Micromeritics (ASAP 2010) volumetric sorption analyzer. Prior to the measurements the catalyst samples were degassed by evacuation at 673 K for 2 h. The average crystalline size was calculated using the Scherrer equation based on the average broadening of the (111) and (220) lines in the X-ray diffraction (XRD) spectra of the catalyst powders obtained with a Philips XPERT diffractometer, using a standard Ni-filtered Cu Kα radiation source operating at 40 kV and 30 mA. All measurements were made in the thin film mode with a scan rate of 0.08 2θ˚/sec. The catalyst characteristics are shown in Table 1.

Table 1. Catalyst textural characteristics

Sample	Surface area (m^2/g)	Pore volume (cm^3/g)	Pore diameter (nm)
CeO_2	127	0.199	4.8
$Ce_{0.75}Zr_{0.25}O_2$	106	0.287	9.3
ZrO_2	51	0.117	7.5
1% Pd/CeO_2	133	0.195	4.8
1% Pd/$Ce_{0.75}Zr_{0.25}O_2$	114	0.288	9.0
1% Pd/ZrO_2	49	0.103	8.0

4.2.3 Raman studies

The *in situ* Raman spectra were acquired using a system described earlier.[80] (Section 2.2.1 in this dissertation.) All samples were pretreated by heating from room temperature to 673 K in 10% CO/He and maintaining these conditions for 1 h. Probing studies were performed on all six catalysts to explore surface species formed after 1 h CO exposure. Following standard pretreatment, the sample was cooled to 623 K in 10% O_2/He, a spectrum was taken, and then the cell was purged with pure He for 15 min at 623 K. Next the gas flow was switched to 10% CO/He for 1 h and a second spectrum was recorded. Additional experiments were conduced on CeO_2 and Pd/CeO_2 to determine the effects of room temperature oxidation following CO exposure. Following standard pretreatment, the sample was reduced in 10% CO/He at 623 K for 12 h. It was then cooled to room temperature in 10% CO/He, and subsequently the flow was changed to 10% O_2/He for 30 min, after which a spectrum was recorded.

4.3 RESULTS

The effect of CO exposure to pretreated catalysts at 623 K was observed using Raman spectroscopy. The pretreated CeO_2 sample exhibited one Raman band at 1166 cm^{-1} which has been assigned to a mixing of the A_{1g}, E_g, and F_{2g} ceria lattice mode vibrations,[49] as well as a Raman band in the hydroxyl region at 3634 cm^{-1} (Fig. 18A spec. 1). After exposure to CO for 1 h at 623 K, three new bands appeared, at 2115, 1582, and 1068 cm^{-1} (Fig. 18A spec. 2). The 2115 cm^{-1} band may be attributed to the formation of Ce^{3+}. This band is consistent with the CO stretching mode of CO-Ce^{3+}, but has alternately been assigned to the symmetry-forbidden $^2F_{5/2}$

$\rightarrow {}^2F_{7/2}$ electronic transition of Ce^{3+};[47,92,112] in either case, the band at 2115 cm^{-1} is indicative of reduced ceria cations on the sample surface. The band formed at 1068 cm^{-1} after 1 h CO exposure may be assigned to carbonate species. The Raman spectrum of stoichiometric cerium (III) carbonate exhibited a strong doublet at 1086 and 1077 cm^{-1} (not shown). Studies have attributed a band in the 1073-1062 cm^{-1} region to bulk cerium carbonate.[46,47,92,94,96]

Following pretreatment, the Pd/CeO_2 spectra showed the same features, at 3634 and 1166 cm^{-1}, as the CeO_2 sample (Fig. 18B spec. 1). After Pd/CeO_2 exposure to CO, three new bands were observed at 1582, 1331, and 1068 cm^{-1} (Fig. 18B spec. 2); the band at 1068 cm^{-1} may be assigned to cerium carbonate species.

The Raman spectrum of ZrO_2 at 623 K in 10% O_2/He exhibited one band in the hydroxyl region at 3667 cm^{-1} (Fig. 19A spec. 1). Subsequent exposure of the sample to CO at 623 K for 1 h resulted in the appearance of four new bands: 1385, 1561, 2872, and 2979 cm^{-1} (Fig. 19A spec. 2). The four band positions are consistent with an assignment of surface formate species. The bands at 1561 cm^{-1} and 1385 cm^{-1} are assigned to the C-H bending and O-C-O stretching vibrations,[116-118] respectively. The 2872 cm^{-1} band is attributed to the formate C-H stretch,[116-118] and the 2979 cm^{-1} band is assigned to a combination[116-118] of the 1561 and 1385 cm^{-1} bands.[101] The spectrum of Pd/ZrO_2 at 623K after 1 h exposure to CO contained only bands at 1582 cm^{-1} and 1331 cm^{-1} (Fig. 19B spec. 2). No hydroxyl band was detected; however, the band(s) may be obscured by the strong fluorescence in the region of 2000 – 4000 cm^{-1}.

With $Ce_{0.75}Zr_{0.25}O_2$ at 623 K in 10% O_2/He, two bands were observed (Fig. 20A spec. 1). One band at 3654 cm^{-1} is in the hydroxyl region. The other band at 1206 cm^{-1} is consistent with the oxide lattice vibrations. Prior Raman studies of $Ce_xZr_{1-x}O_2$ did not present spectra above 1000 cm^{-1}.[35,119-121] However, CeO_2 exhibits a band at 1166 cm^{-1} assigned to a combination of

the A_{1g}, E_g, and F_{2g} vibrational modes of the ceria lattice,[49] and both the CeO_2 and the $Ce_xZr_{1-x}O_2$ have a cubic fluorite crystal structure.[122] One would expect that the 1166 cm^{-1} lattice vibration of CeO_2 shifted to 1206 cm^{-1} in $Ce_{0.75}Zr_{0.25}O_2$ because the smaller ionic radius of the Zr cations, compared to the Ce cations, results in a contraction of the lattice.[33,122] Such a lattice contraction manifests itself in the Raman spectra as a shift of the lattice vibrational bands to higher wavenumbers.[97,98]

Exposure of the $Ce_{0.75}Zr_{0.25}O_2$ to CO resulted in the appearance of four new bands: 2847, 2115, 1582, and 1068 cm^{-1} (Fig. 20A spec. 2). The presence of a low intensity band at 2958 cm^{-1} cannot be ruled out despite the poor signal to noise ratio. As well, a low intensity band at 1331 cm^{-1} cannot be ruled out because it may be obscured by the broad band at 1206 cm^{-1}. In accordance with the band assignment for ZrO_2, the 2958 and 2847 cm^{-1} bands observed with $Ce_{0.75}Zr_{0.25}O_2$ are attributed to formate species.[101] The band at 1068 cm^{-1} has been assigned to carbonate species.[46,47,92,94,96]

The bands observed with $Pd/Ce_{0.75}Zr_{0.25}O_2$ at 623 K in 10% O_2/He were similar to those obtained with $Ce_{0.75}Zr_{0.25}O_2$ under the same condition: a hydroxyl vibration at 3654 cm^{-1} and a lattice vibration at 1206 cm^{-1} (Fig. 20B spec. 1). After exposure of $Pd/Ce_{0.75}Zr_{0.25}O_2$ to CO at 623 K for 1 h, a distinct band appeared at 1582 cm^{-1}, with a shoulder peak in the vicinity of 1331 cm^{-1} (Fig. 20B spec. 2). As well, formate bands at 2930 and 2847 cm^{-1} were observed, which is not surprising for zirconia-containing materials; such species have been reported to be stable at high temperatures.[123,124]

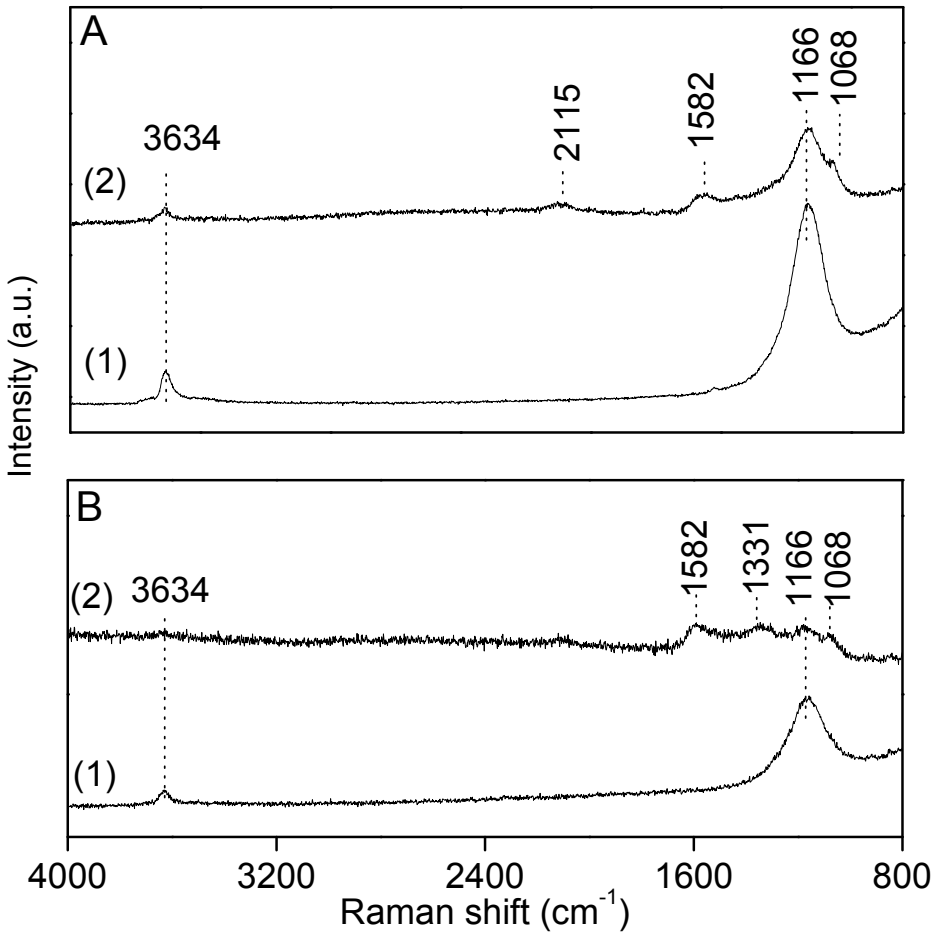

Figure 18. *In situ* Raman spectra of CeO_2 (A) and 1% Pd/CeO_2 (B) after pretreatment in 10% O_2/He at 673 K for 1 h (Intensity X 0.5) (1) and after exposure to 10% CO/He at 623 K for 1 h (2). All spectra were collected at 623 K.

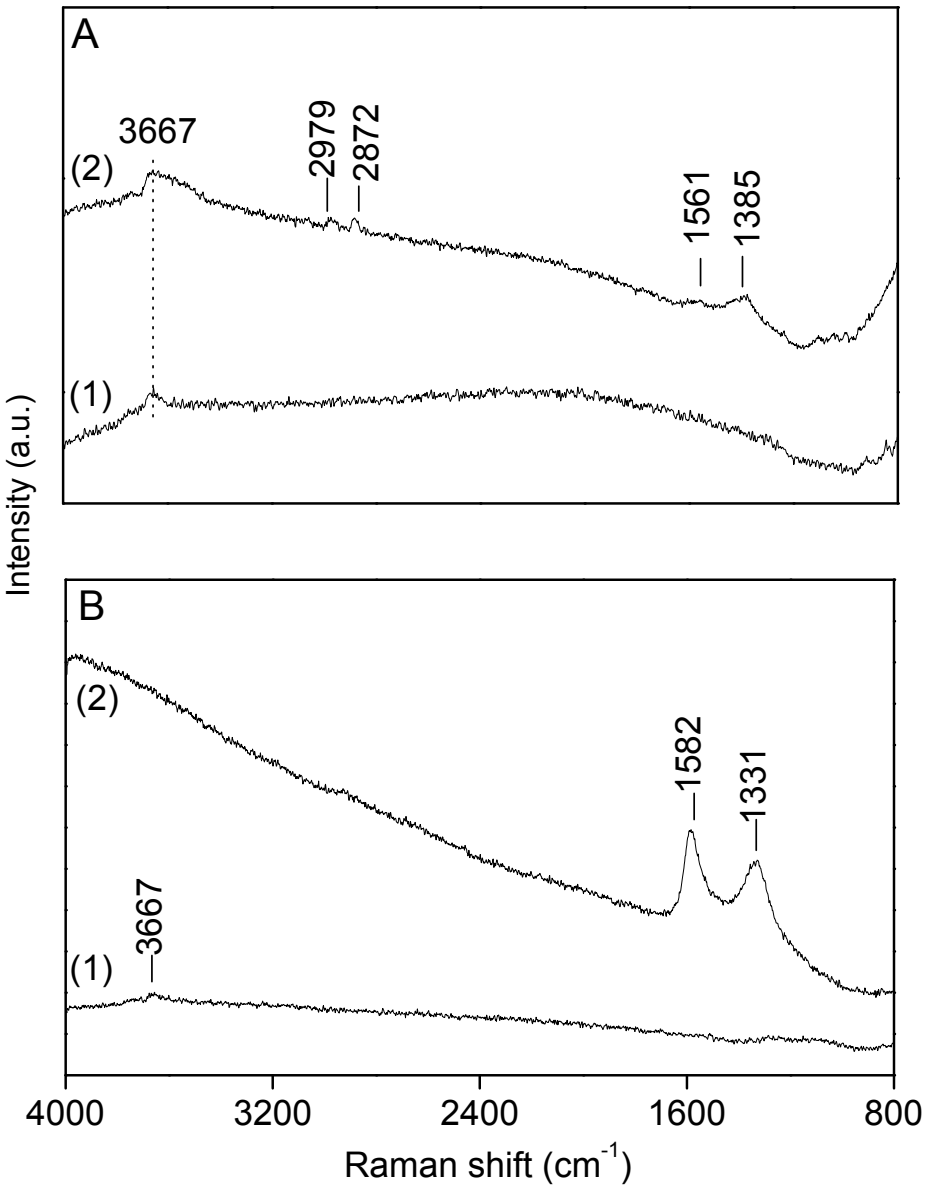

Figure 19. *In situ* Raman spectra of ZrO_2 (A) and 1% Pd/ZrO_2 (B) after pretreatment in 10% O_2/He at 673 K for 1 h (1) and after exposure to 10% CO/He at 623 K for 1 h (2). All spectra were collected at 623 K.

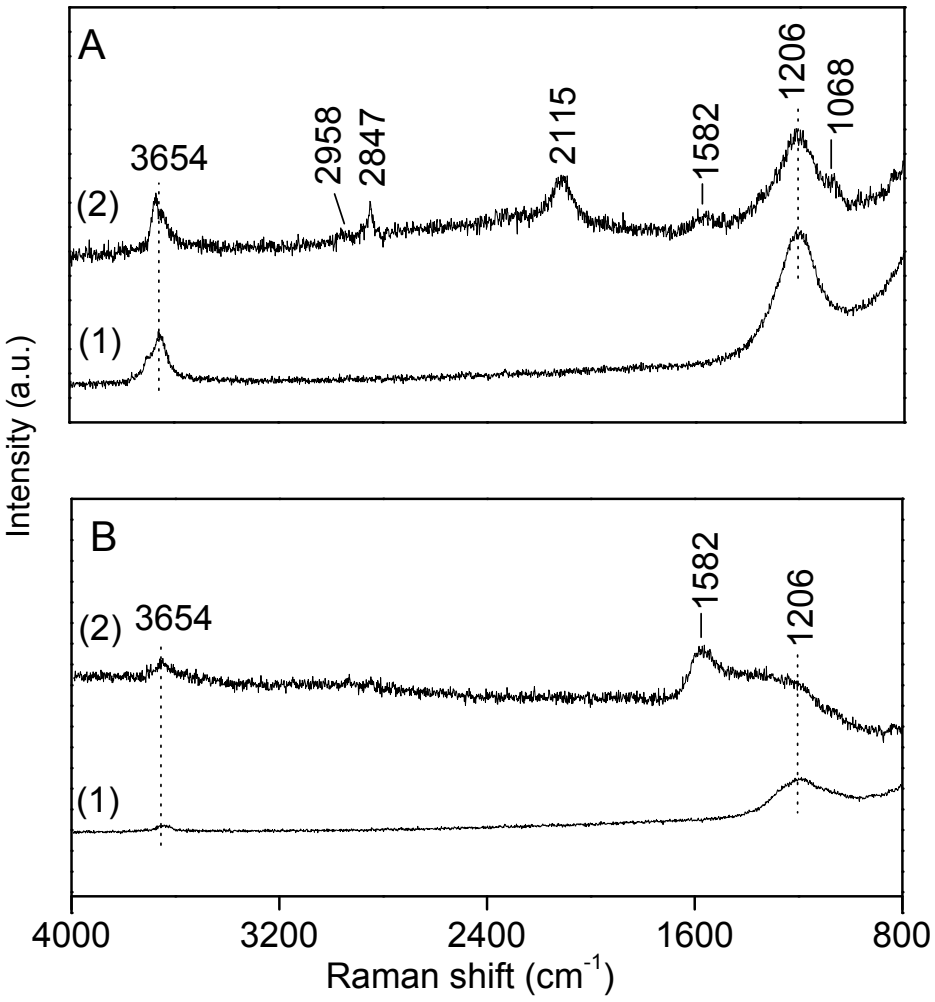

Figure 20. *In situ* Raman spectra of $Ce_{0.75}Zr_{0.25}O_2$ (A) and 1% $Pd/Ce_{0.75}Zr_{0.25}O_2$ (B) after pretreatment in 10% O_2/He at 673 K for 1 h (Intensity X 0.5) (1) and after exposure to 10% CO/He at 623 K for 1 h (2). All spectra were collected at 623 K.

The stability of the species formed on CeO_2 and Pd/CeO_2 after 12 h CO exposure was investigated under mild oxidizing conditions (Fig. 21). On CeO_2, new bands at 2935 and 2852 cm^{-1}, which appeared after O_2 exposure, may be assigned to surface formates. The bands have been assigned to the C-H stretching mode,[42,101] and a combination of the C-H bending mode and O-C-O asymmetric stretching mode[42,43,101] of surface formate, respectively. New bands which appeared at 858 and 831 cm^{-1} after O_2 exposure to CeO_2 and at 831 cm^{-1} on Pd/CeO_2 may be assigned to peroxide species.[8,9,99,100] The bands at 1600 and 1340 cm^{-1} did not change significantly after CeO_2 was exposed to O_2 for 30 min (Fig. 21A). Conversely, the intensity of the Pd/CeO_2 band at 1590 cm^{-1} (Fig. 21B) decreased dramatically after O_2 exposure. No formate bands were detected after O_2 exposure to Pd/CeO_2.

4.4 DISCUSSION

Previous investigations have put forth spectroscopic evidence for the occurrence of CO disproportionation on ceria. Raman studies in the current work demonstrate unambiguous evidence for CO disproportionation on CeO_2, $Ce_{0.75}Zr_{0.25}O_2$, and all the Pd catalysts, namely, the appearance of carbon bands[71,74,77,110] at 1582 and 1331 cm^{-1} on those catalysts following exposure to CO at 623 K (Fig. 10, 12). It is reasonable that the reduced Ce^{3+} are the active sites for the reaction, because CO disproportionation was observed on the reducible oxides only.

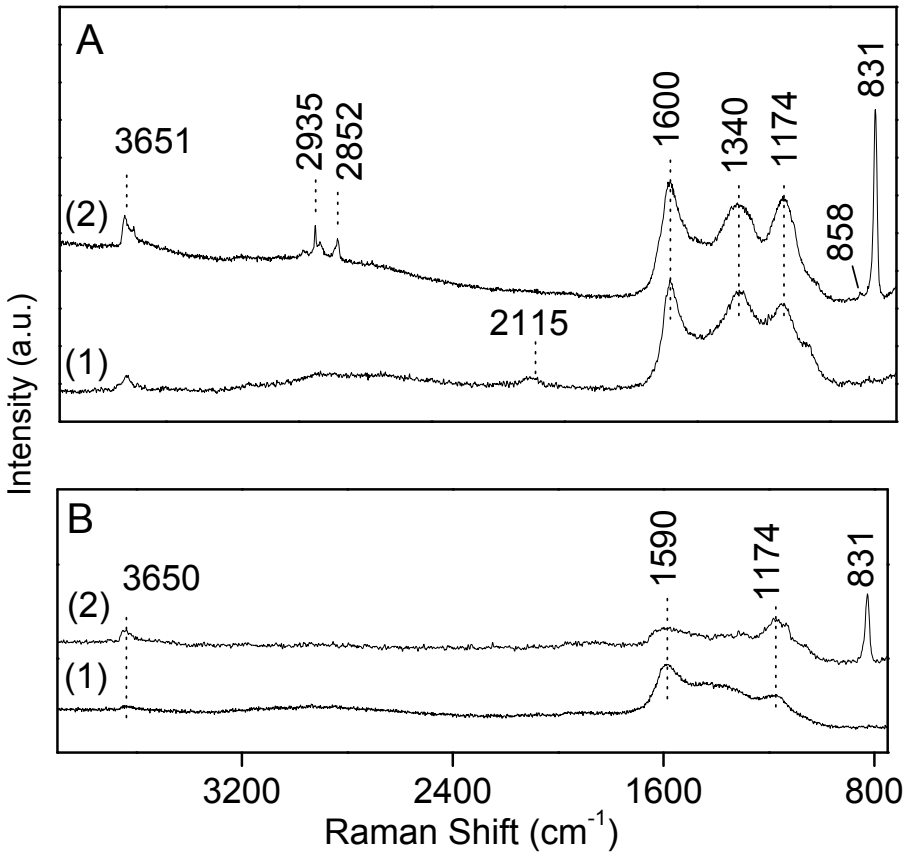

Figure 21. *In situ* Raman spectra of CeO_2 (A) and 1% Pd/CeO_2 (B) pretreated in a flow of 10% CO/He at 623 K for 12 h (1) and after subsequent exposure to a flow of 10% O_2/He at 298 K for 30 min (2). All spectra were recorded at 298 K.

The bands at 1582 and 1331 cm^{-1} are in the same position as the bands tentatively assigned to carbonaceous deposits on CeO_2[80] upon exposure to CO after pre-oxidation.[50,71,73-78,109] Graphite and other sp^2 hybridized carbons exhibit strong Raman bands in these positions - namely, there is a Raman active E_{2g} carbon-carbon stretching mode at 1582 cm^{-1},[50,71,73-77] and a Raman active breathing mode of a sp^2 hybridized carbon with A_{1g} symmetry in the vicinity of 1331 cm^{-1}.[50,74-76,78,109] The A_{1g} breathing mode is forbidden in large perfect crystals, but becomes Raman active in small crystallites.

Further evidence for the assignment of bands at 1582 and 1331 cm^{-1} to carbonaceous deposits is the presence of bands in those positions on Pd/CeO_2, Pd/ZrO_2 and $Pd/Ce_{0.75}Zr_{0.25}O_2$ under the same conditions. Prior research has established that Pd is active as a CO disproportionation catalyst.[63-65] Cerium carbonates and/or carboxylates form after pre-oxidation and subsequent exposure to CO.[41,46,92] However, assignment of the bands to cerium carbonate/carboxylate may be rejected because of their appearance on Pd/ZrO_2, and the bands cannot be assigned to zirconium carbonates/carboxylates, as they are thermally unstable at 623 K.[123,124] In addition, the band positions are inconsistent with formate species as observed on metal free ZrO_2 (Fig. 19B), and the bands cannot be attributed to a formate species on ceria. Only traces of formates have been detected on ceria exposed to CO after oxidation; pre-reduction with H_2 prior to CO exposure is necessary to obtain appreciable amounts of formates.[41,42]

However, ceria formate species were observed in this study following oxidation of carbonaceous deposits (Fig. 21A). Scheme 4 shows one viable path for the observed formation of formate species from the reaction of carbonaceous deposits with adsorbed peroxide. Lack of observed formate species on Pd/CeO_2 following oxidation of carbonaceous species (Fig. 21B)

indicates that the metal catalyzes formate decomposition in an oxidative environment. This conclusion is supported by a previous study of a similar catalyst, 3% Pt supported on high surface area ceria. In that study, formate formation was observed using IR spectroscopy after 3.8 Torr CO exposure at room temperature and subsequent evacuation.[43] Thus, formates are expected to be stable on the 1% Pd/CeO_2 used in the current work under a CO atmosphere or vacuum; the fact that they are not observed in 10% O_2/He demonstrates that the species may be oxidized at this temperature.

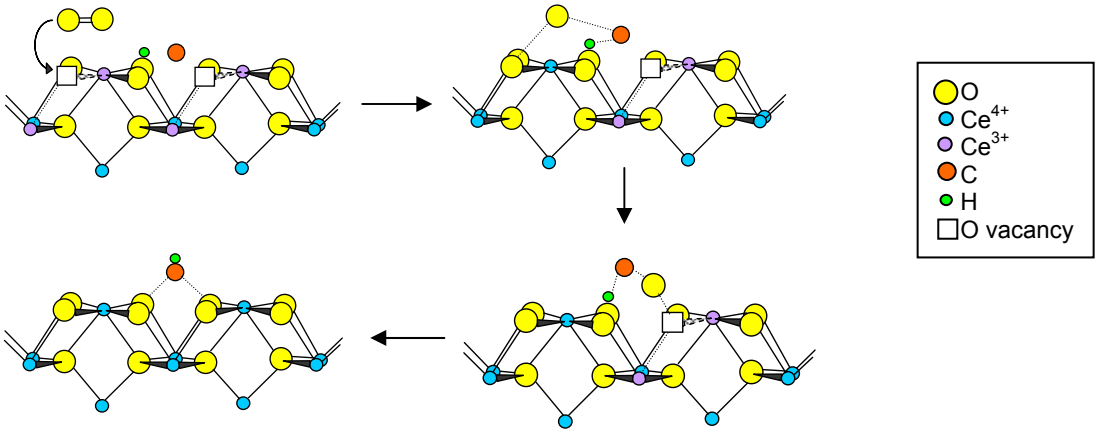

Scheme 4. Formate formation from carbon deposits on CeO_2

In 1989, Li et.al.[42] investigated the formation of formates on partially reduced ceria after exposure to CO at room temperature. They proposed a mechanism for formate formation whereby the carbon atom of CO fills an oxygen vacancy and thereby interacts with a Ce^{3+} cation. The chemisorption of CO to metals[125] and metal oxides[105] is commonly modeled as a bond between the 5σ orbital of CO, located on the C atom, and the metal or metal cation, for example

M^{x+}-C=O. However, this work for the first time shows that the interaction of reduced ceria with CO may occur through the oxygen end of the molecule, such as Ce^{3+}-O=C. Scheme 4 shows the dioxygen species peroxide (O_2^{2-}) filling the oxygen vacancies in ceria, and interacting with a ceria hydroxyl and elemental carbon on the surface.

The mechanism of formate oxidation (Scheme 4) can be used to elucidate the mechanism of the reverse reaction, formate formation, by the principle of microscopic reversibility. This principle takes into account the fact that the transition state for a reaction is the same for the forward and reverse reaction. The ratio of the rates of change in the rotational, vibrational, and electronic states of the forward to reverse reactions reduces to the equilibrium constant, K_{eq}.[126] Therefore the principle of microscopic reversibility illustrates that for any reaction at equilibrium, the forward and reverse reactions occur at the same rate.[126]

Scheme 4 shows that one reaction intermediate for formate decomposition is an oxygen atom simultaneously bound to a oxygen vacancy and carbon. Applying the concept of microscopic reversibility to the current work indicates that formate formation through CO interaction with reduced ceria occurs through the reverse of the process shown in Scheme 4. Therefore formate formation must also occur through a similar intermediate, which can only be realized if the oxygen end of CO interacts with an oxygen vacancy, prior to rearrangement with a nearby hydroxyl.

This study provides unambiguous evidence for CO disproportionation on CeO_2 and $Ce_{0.75}Zr_{0.25}O_2$, likely through active Ce^{3+} sites. In addition, this study reports the interaction of CO with a reduced oxide through the oxygen end of the molecule, as concluded by the principle of microscopic reversibility.

5.0 WHEN CO OXIDIZES A METAL OXIDE

The reduction of metal oxides by CO is well-established for oxides containing metal cations with multiple oxidation states. An oxygen atom is abstracted from the lattice by CO to form CO_2, leaving behind a two-electron vacancy. According to recent theoretical investigations of point vacancies on CeO_2, the electrons are localized on adjacent cerium cations such that each cation essentially possess a 3+ oxidation state.[6,127] This work will show that at an aggregated vacancy, the degree of electron localization controls the rates at which CO acts as an electron donor or acceptor to form an energetically activated complex.

We provide evidence that CO acts as both an electron acceptor and an electron donor when interacting with CeO_{2-x}. Specifically, we conducted *in situ* Raman spectroscopy investigations of CO exposure to CeO_{2-x} and Pd/CeO_{2-x}. When oxidized, CeO_2 is reduced by CO via the abstractive reduction pathway, with CO acting as the electron donor. On the other hand, carbon formation on the pure oxide mandates that CO serves as the electron acceptor in order for the bond to cleave homolytically through the CO disproportionation reaction. By following the signature carbon G and D Raman bands for sp^2 hybridized microcrystalline carbon,[51] it is apparent that no carbon is detected for CeO_{2-x} during the first 0.3 h exposure to CO (Fig. 22A). Carbon on CeO_{2-x} is detected after 0.8 h exposure to CO at a rate that remains relatively constant through 14 h. In contrast, for the Pd/CeO_{2-x} both carbon bands are present at 0.3 h (Fig. 22B),

which is expected because the Pd catalyzes CO disproportionation. The rate of this reaction decreases rapidly as the carbon blocks the Pd surface sites and by 8 h is essentially the same as the rate on CeO_{2-x} (Fig. 22C).

However, the most intriguing aspect of these results is the increasing rate of carbon formation on both CeO_{2-x} and Pd/CeO_{2-x} after 14 h. This behavior relates to changes in the CeO_{2-x} surface by prolonged exposure to CO. Surprisingly, the formation of carbon becomes autocatalytic (product-catalyzed) on both CeO_{2-x} and Pd/CeO_{2-x} after 14 h, as evidenced by the increase in the reaction rate. Thus, the reaction must occur on the support for Pd/CeO_{2-x}.

It is reasonable to speculate that the O surface atom formed from CO bond dissociation is the reactive product that drives the autocatalytic reaction. At later CO exposure times, the increasing rate of carbon formation is consistent with formation of new active sites with delocalized electron density. The experimental work of Esch et al. and Fukui et al. showed aggregate oxygen vacancy cluster formation on ceria[6,7] Presumably, the aggregate electron density is more delocalized compared to point defect electron density; however, no literature regarding this topic exists. The CO bond cleavage yields elemental carbon and an oxygen species interacting with the aggregate vacancy cluster.

By definition, a reaction in which the reaction rate increases is autocatalytic, videlicet product-catalyzed. Therefore the active site must be regenerated by oxidation of additional CO by ceria lattice oxygens adjacent to the aggregated vacancy. Though we have no direct evidence that O atoms are abstracted adjacent to the aggregated vacancy, it is a reasonable conclusion from the rate data shown.

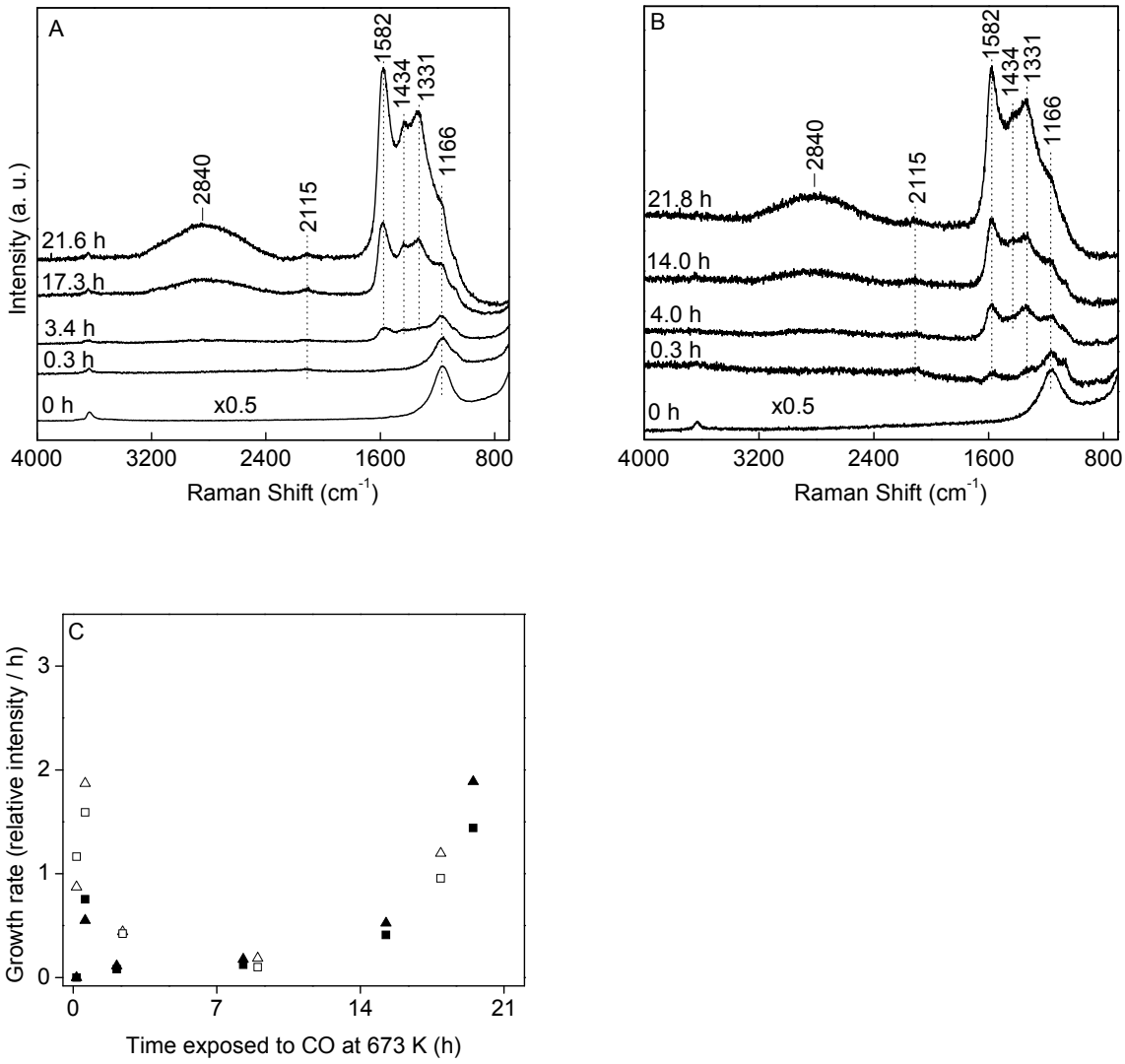

Figure 22. In situ Raman spectra of CeO_2 (A) and 1% Pd/CeO_2 (B) after pretreatment and following exposure to 10% CO/He at 623 K for time (hours) as listed. All spectra were recorded at 623 K. Relative growth rates (C) of the 1582 (▲,Δ) and 1331 cm^{-1} (■,□) Raman bands observed on CeO_2 (▲,■) and Pd/CeO_2 (Δ,□) upon exposure to 10% CO/He at 623 K, as a function of exposure time. Intensities were normalized to 1166 cm^{-1} ceria lattice mode.

6.0 RELATIVE RATES FOR CO DISPROPORTIONATION ON PALLADIUM AND CERIA: IS CERIA THE BETTER CATALYST?

6.1 INTRODUCTION

Oxidation reactions on metal oxide catalysts often require labile oxygen species on the surface.[5] For example, the Mars van Krevelen oxidation mechanism involves reduction and re-oxidation of the catalyst.[128] Along these lines, research has focused on the utilization and development of metal oxides with abundant labile oxygen species, in other words the ability to store and release oxygen depending on O_2 partial pressure.[3,15,30,91]

Ceria is widely used as a component of catalyst supports because of the easy transition for cerium to change between Ce^{4+} and Ce^{3+}.[3] The difference in the oxygen content of oxidized ceria with cerium nearly all as Ce^{4+}, and ceria reduced under specific conditions with some cerium as Ce^{3+}, has been termed the oxygen storage capacity (OSC). Because of this OSC, ceria included in the support of automotive catalytic converters improves their effectiveness to oxidize CO and hydrocarbons while simultaneously reducing NO_x under oscillating rich-lean emission conditions.[13] Ceria also promotes the water-gas shift reaction, which oxidizes CO with water under fuel rich excursions.[22] Recent studies[112,129-135] have focused on the use of Pd in

automotive catalysts because of compatibility with low-sulfur fuels and low price compared to Pt.[1] It should also be noted that ceria-supported noble metals exhibit dramatically improved OSC compared to ceria alone.[1]

An important factor in automotive three way catalyst (TWC) performance, therefore, is the catalyst's OSC. Ongoing development of improved TWCs relies on the accurate determination of OSC. While no standard method has been established, widely used OSC procedures involve exposing the catalyst to alternating pulses of oxidant and reductant, the most common of which are O_2 and CO.[18,43,84] The amount of CO_2 produced by a single pulse of CO is a measure of the OSC.[13] On the other hand, the *total* amount of oxygen a material will supply under operating conditions is typically measured by exposing the oxidized catalyst to consecutive pulses of CO until the production of CO_2 ceases; the total amount of CO_2 produced is a measure of the OSC complete (OSCC).[13] Typically, OSC measurements are carried out at 570-770 K with 1-10% O_2 or 1-5% CO, with the balance an inert gas.[13,90]

Besides the reaction of CO with labile surface oxygen, any side reaction that affects the CO and CO_2 exit stream concentrations will impact the accuracy of OSC measurements. Carbon from CO may be stored on the surface as carbonates or graphitic carbonaceous deposits; the formation of both species is generally neglected during OSC measurements.[14,16,18,90,136,137] Carbonates form from the interaction of surface oxygen species with CO to form the adsorbed CO_3 moiety. Another possible reaction, carbon monoxide disproportionation, may result in the overestimation of OSC since the reaction forms CO_2 without participation of labile surface O species.

The CO disproportionation reaction is thermodynamically possible at temperatures below 1000 K, but kinetically insignificant in the absence of a catalyst.[53] The rate of CO

disproportionation is appreciable on Ni,[54-58] Fe,[59,60] Co,[56,60,61] Pt,[62] Pd,[63-65] Ru,[66] and Rh[67] metal deposited on various supports. Some metal oxides, such as MgO[68] and Fe_3O_4,[69] have also been found to catalyze CO disproportionation. Regarding CeO_2, indirect evidence of CO disproportionation was obtained by observing the FTIR spectra of adsorbed species following CO exposure to reduced CeO_2.[70] Since several bands were identical to those formed after CO_2 exposure, and CO could not have been oxidized by the reduced ceria surface, CO disproportionation was inferred. Additionally, Raman spectroscopy results from this laboratory indicate that CO disproportionation on CeO_2 and ceria based oxides does occur.[80,81]

Thus, the interaction of ceria catalysts with CO is of interest because oxidation of CO is a common measure of the OSC of automotive TWC; as well CO adsorption is often used to probe catalyst surface site chemistry. The primary objective of the present study is to investigate the interaction of CO with CeO_2 and Pd/CeO_2 catalysts using Raman and IR spectroscopy. In order to probe disproportionation on these catalysts, Raman is an appropriate tool for detection of carbon, since graphite and disordered carbon are good Raman scatterers.[50,51,76]

6.2 EXPERIMENTAL

6.2.1 Materials

Cerium dioxide, CeO_2 (99.9%) was supplied by Rhodia and calcined in air at 823 K for 12 h before use. The 1% Pd/CeO_2 was prepared by impregnation of the support with an aqueous solution of $Pd(NH_3)_4(NO_3)_2$ (Strem Chemicals, 99.9%). The impregnated sample was dried at 373 K for 12 h, and then calcined in air at 823 K for 12 h.

The reagent grade He (Air Products, 99.998%) and CO (Praxair, 99.995%) were purified of trace oxygen and water using zeolite and OxyTrap filters, both from Alltech. Additionally, the CO was fitted with a Vista B γ-alumina trap, heated to 573 K, in order to remove metal carbonyl contaminants. The 10% O_2 in He (Praxair) was used without further purification. For the static isotopic IR study, CO and CO_2 (Praxair, 99.995%) were run through a liquid N_2 cooled trap to remove trace contaminants. Labeled $^{13}C^{16}O$ (Isotec, 99% ^{13}C) was used without further purification.

The sample pretreatment, if not otherwise specified, consisted of heating the sample from room temperature to 673 K in 10% CO/He, and maintaining these conditions for 1 h. Subsequently, the flow was changed to 10% O_2/He at 673 K for 1 h. Experimental conditions were chosen to represent typical pretreatment prior to OSC measurements,[18,88] and the treatment described above will be referred to as the "standard" pretreatment.

6.2.2 Catalyst characterization

The catalysts were characterized in an earlier study.[81] (Section 4.2.2 and Table 1 of this dissertation.)

6.2.3 Infrared studies

Infrared spectra were collected with a Mattson Research Series II Fourier transform spectrometer using a liquid N_2 cooled MCT detector. The catalyst sample was pressed into a self-supported disc (8-25 mg/cm^2 thick) which was mounted into a sample holder and placed into the quartz IR cell, described elsewhere.[138] The cell was attached to a vacuum system with an ultimate

vacuum of 2×10^{-6} Torr achieved using a turbomolecular pump. Data were obtained at 2 cm^{-1} resolution, and 200 scans were averaged for each spectrum collected. All IR spectra were acquired after the sample had cooled to room temperature.

6.2.4 Raman studies

The Raman spectra were acquired using a system described earlier.[80] (Section 2.2.1 of this dissertation.)

6.2.5 Electron microscopy

High resolution transmission microscopy (HRTEM) images were obtained using a JEOL JEM2010 instrument with a lattice resolution of 1.4 Å and an accelerating voltage of 200 kV. Selected area diffraction (SAD) was used for the phase identification.

The samples for HRTEM study were prepared in air by grinding the catalyst in an agate mortar with ethanol, followed by suspending the powder in ethanol using ultrasonication ($\leq$ 5 W/cm^2). Then the resulting aerosol was deposited on thin, holey amorphous carbon films with a depth of 100-200 Å supported on the standard gold grids.

6.3 RESULTS

6.3.1 Infrared studies

The interaction of CO with Pd/CeO_2 was probed by examining the IR spectra of species formed after the catalyst was exposed to ^{13}CO. The Pd/CeO_2 was pretreated in flowing 10% O_2/He at 673 K for 1 h, followed by exposure to 50 Torr CO at 673 K, then 50 Torr O_2 at 673 K for 1 h. Next, the Pd/CeO_2 was exposed to 50 Torr ^{13}CO for 15 min and evacuated for 15 min at 623 K. The sample was then exposed to 50 Torr unlabeled CO_2 for 15 min at 923 K and evacuated for 15 min at 923 K, in order to exchange the carbon atoms of susceptible species. At this point a spectrum was taken, shown in Fig. 23 (spec. 1). Low-intensity bands were observed in the carbonate and carboxylate regions at 1700-1200 cm^{-1}, consistent with previously observed ^{12}C carbonate/carboxylate[41,43,45-47,92] species. After the surface species were re-oxidized in O_2, bands in the carbonate region dramatically increased in intensity and red-shifted approximately 30-50 cm^{-1} (Fig. 23 spec. 2). The largest shift was 1581 – 1537 cm^{-1}, which has been assigned to a bidendate carbonate.[46] This shift is similar to the frequency shift of the ^{13}CO molecule, which is predicted to be 47 cm^{-1}.[48] Other ^{13}C carbonate bands are consistent with those observed previously.[43,46,47] Concurrent with ^{13}C carbonate formation, gas phase $^{13}CO_2$ was detected after oxidation of the surface species, with characteristic bands at 2294 and 2275 cm^{-1} (Fig. 23 spec. 3).

The FTIR band intensity of CO adsorbed on Pd was monitored as a function of reduction temperature on Pd/CeO_2. After pretreatment consisting of exposure to 50 Torr of CO at 673 K for 1 h followed by flowing a 10% O_2/He mixture at 673 K for 1 h, evacuation at 673 K 1 h, cooling to 623 K in flowing 10% O_2/He, and another evacuation at 623 K for 30 min, the

Pd/CeO_2 was exposed to 5 Torr CO for 15 min at 293 - 623 K as shown (Fig. 24). The interaction of Pd with CO, as shown by the Pd-CO stretching band intensities, decreased with increasing reduction temperature. Linear Pd-CO bands [46,92,112,139] at 2067 cm^{-1} and 2092 cm^{-1} were observed at 293 K, but only one linear species was present above 373 K, with a band at 2087 cm^{-1}. A band at 1973 cm^{-1}, which can be attributed to bridged Pd-CO,[46,92,112,139] was also observed.

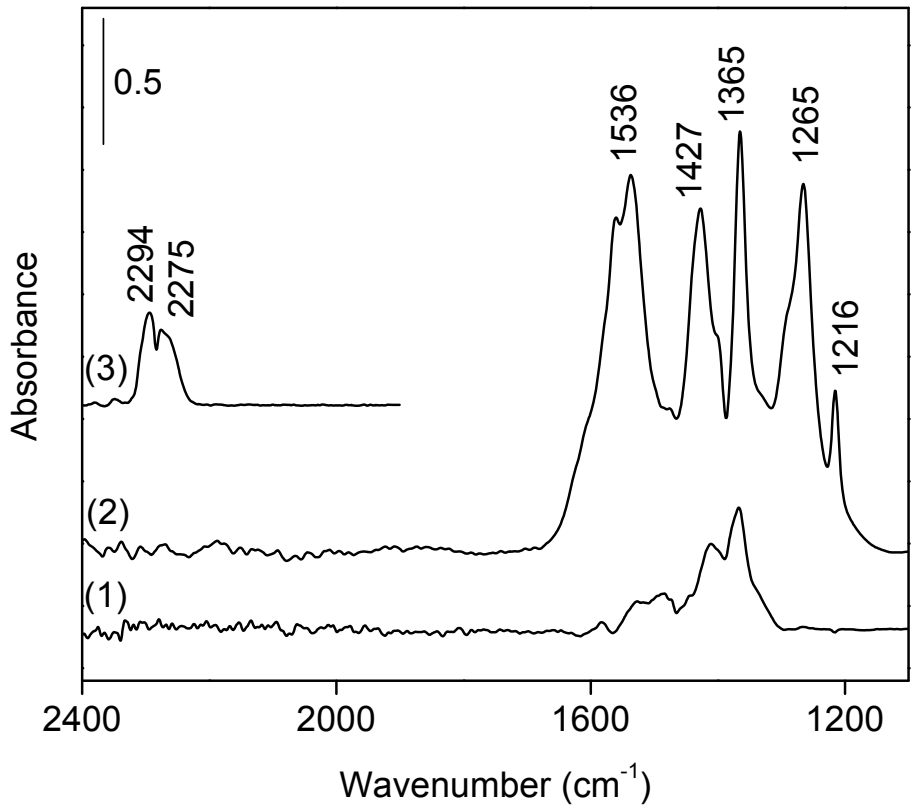

Figure 23. FTIR spectra of 1% Pd/CeO_2 after reduction by ^{13}CO (50 Torr) at 623 K for 15 min followed by evacuation at 623 K for 15 min, reaction of the sample with $^{12}CO_2$ (50 Torr) at 923 K for 15 min and evacuation at 923 K for 15 min (1) and after subsequent reoxidation by O_2 (50 Torr) at 623 K for 15 min (2). Spectrum (3) is the gas phase after reoxidation (Intensity X 20). All spectra were collected at 298 K.

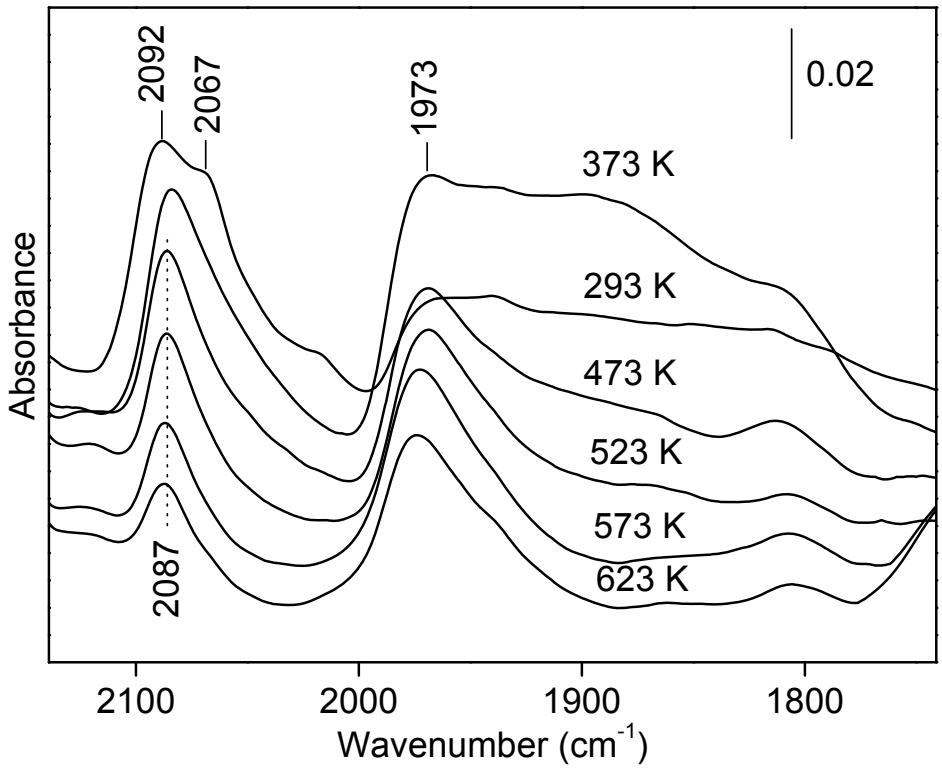

Figure 24. FTIR spectra of CO adsorption on 1% Pd/CeO_2 after reduction of the catalyst wafer by 5 Torr CO for 15 min at different temperatures, as shown. All spectra were collected at 298 K.

6.3.2 Raman studies

The temporal effect of CO exposure to pretreated catalysts at 623 K was observed using Raman spectroscopy. After standard pretreatment, the sample was cooled to 623 K in 10% CO/He, and these conditions were maintained for 24 h, recording spectra periodically. The pretreated CeO_2 sample exhibited one Raman band at 1166 cm^{-1} which has been assigned to a mixing of the A_{1g}, E_g, and F_{2g} ceria lattice mode vibrations,[49] as well as a Raman band in the hydroxyl region at 3634 cm^{-1} (Fig. 25). After exposure to CO for 0.3 h at 623 K, bands appeared on CeO_2 at 2115 cm^{-1} and at 1068 cm^{-1} as a low-frequency shoulder of the 1166 cm^{-1} band (Fig. 25). The 2115 cm^{-1} band may be attributed to the formation of Ce^{3+}. This band is consistent with the CO stretching mode of CO-Ce^{3+}, but has alternately been assigned to the symmetry-forbidden $^2F_{5/2} \rightarrow {}^2F_{7/2}$ electronic transition of Ce^{3+};[47,92,112] in either case, the band at 2115 cm^{-1} is indicative of reduced ceria cations on the sample surface. The band formed at 1068 cm^{-1} after 0.3 h CO exposure may be assigned to carbonate species. The Raman spectrum of stoichiometric cerium (III) carbonate exhibited a strong doublet at 1086 and 1077 cm^{-1} (not shown). Studies have attributed a band in the 1073-1062 cm^{-1} region to bulk cerium carbonate.[46,47,92,94,96] Bands at 1582, 1434, and 1331 cm^{-1} also appeared after 0.8 h and their intensities continued to increase during CO exposure (Fig. 25). After 17 h CO exposure, a broad band appeared at 2840 cm^{-1} and increased in intensity up to 22 h.

Following pretreatment, the Pd/CeO_2 spectra showed the same features, at 3634 and 1166 cm^{-1}, as the CeO_2 sample (Fig. 26). After 0.3 h exposure to CO, new bands were observed at 1582, 1331, and 1068 cm^{-1}; the band at 1068 cm^{-1} may be assigned to cerium carbonate species. Similar to CeO_2, a broad band at 2840 cm^{-1} formed after 14 h CO exposure.

The relative intensities and growth rates of the bands at 1582, 1434, and 1331 cm^{-1} over time are compared for Pd/CeO_2 and CeO_2 (Fig. 27). The bands were normalized to the ceria lattice mode at 1166 cm^{-1} in each spectrum. The spectra could not all be deconvoluted because of baseline artifacts, especially at low exposure times. For the purposes of this research, it is sufficient to compare the intensities over time on the same sample. Even with this restriction, it is apparent that the main difference between the bands on these samples was the high initial rate of band growth on Pd/CeO_2 compared to CeO_2 (Fig. 27B).

The surface microstructure of CeO_2 and Pd/CeO_2 previously exposed to CO were investigated using HRTEM (Fig. 28). Crystalline carbon was observed on both CeO_2 and Pd/CeO_2. Separation of the 002 plane lattice fringes was measured by locating areas on the carbon with several consecutive lattice fringes, measuring the total perpendicular length and dividing by the number of contrasting fringes. The plane separation was measured as 0.48 nm for carbon formed on ceria, and 0.45 and 0.48 nm for carbon formed on Pd/CeO_2. This is slightly larger than the 0.35 nm separation between graphite planes,[140] and indicates the planes in the crystalline carbon in this work are misaligned.

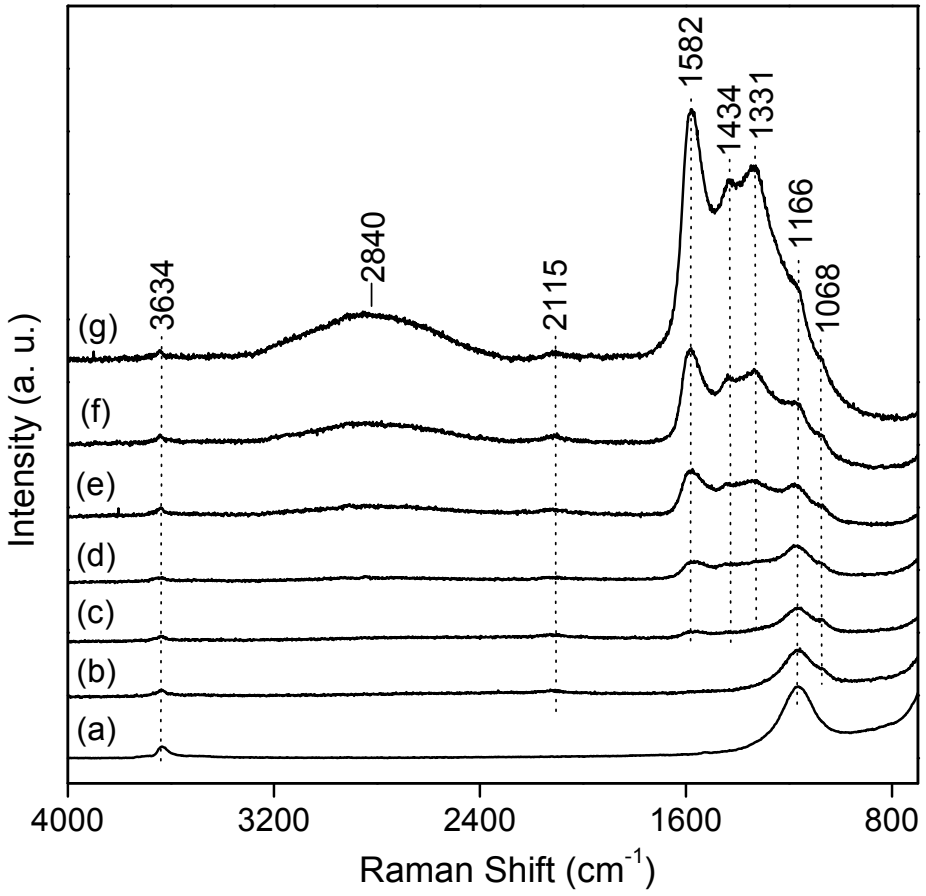

Figure 25. *In situ* Raman spectra of CeO_2 (a) after pretreatment and following exposure to 10% CO/He at 623 K for (b) 0.3 h (Intensity X 0.5), (c) 0.8 h, (d) 3.4 h, (e) 13.2 h, (f) 17.3 h, and (g) 21.7 h. All spectra were recorded at 623 K.

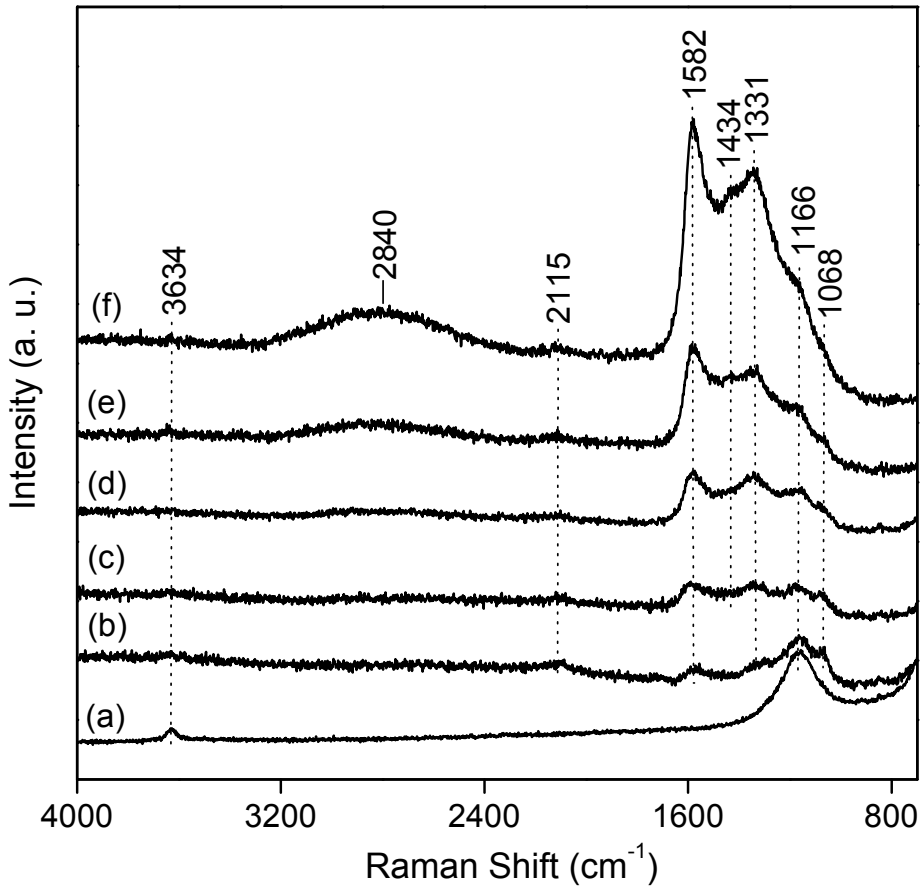

Figure 26. *In situ* Raman spectra of 1% Pd/CeO_2 (a) after pretreatment and following exposure to 10% CO/He at 623 K for (b) 0.3 h (Intensity X 0.5), (c) 0.8 h, (d) 4.0 h, (e) 14.0 h, and (f) 21.8 h. All spectra were recorded at 623 K.

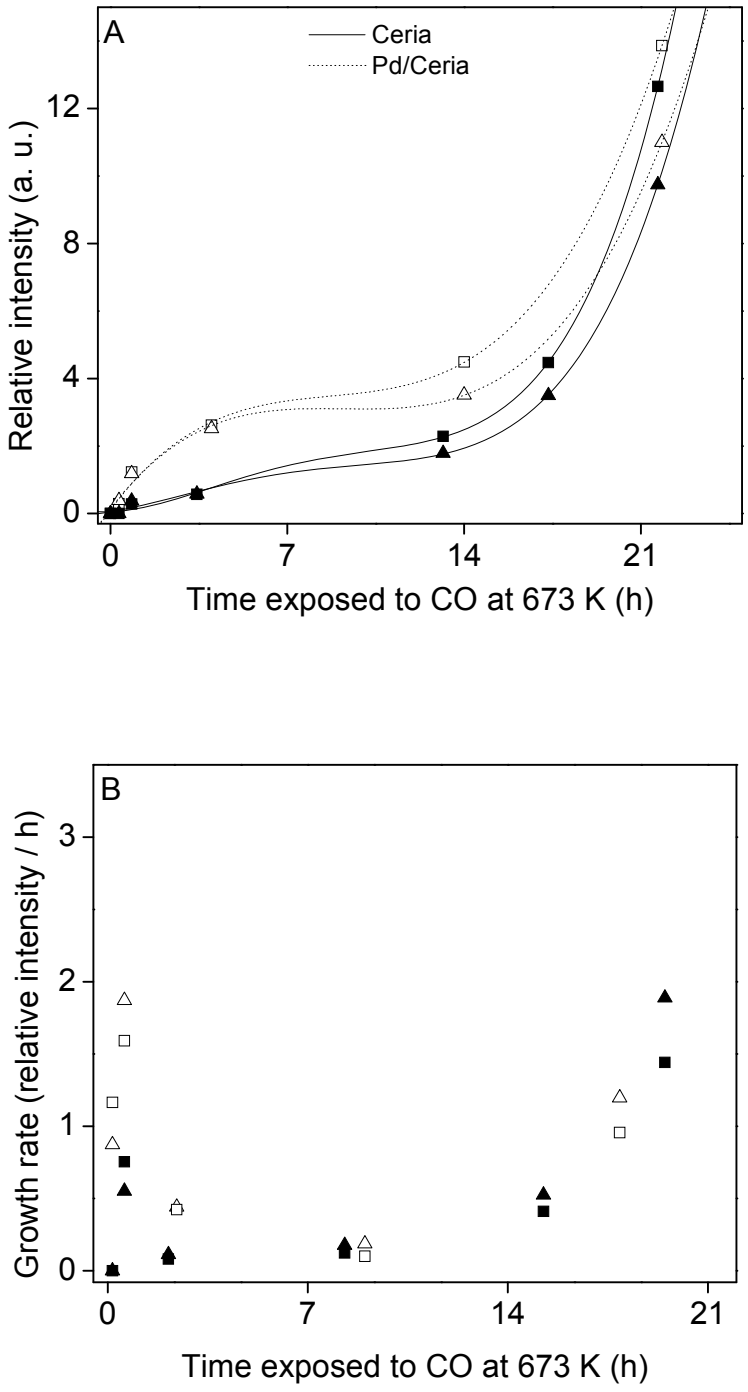

Figure 27. Relative intensities (A) and growth rates (B) of the 1582 (▲,Δ) and 1331 cm^{-1} (■,□). Raman bands observed on CeO_2 (▲,■) and Pd/CeO_2 (Δ,□) upon exposure to 10% CO/He at 623 K, as a function of exposure time. Intensities were normalized to 1166 cm^{-1} ceria lattice mode, and the lines in (A) have no physical significance.

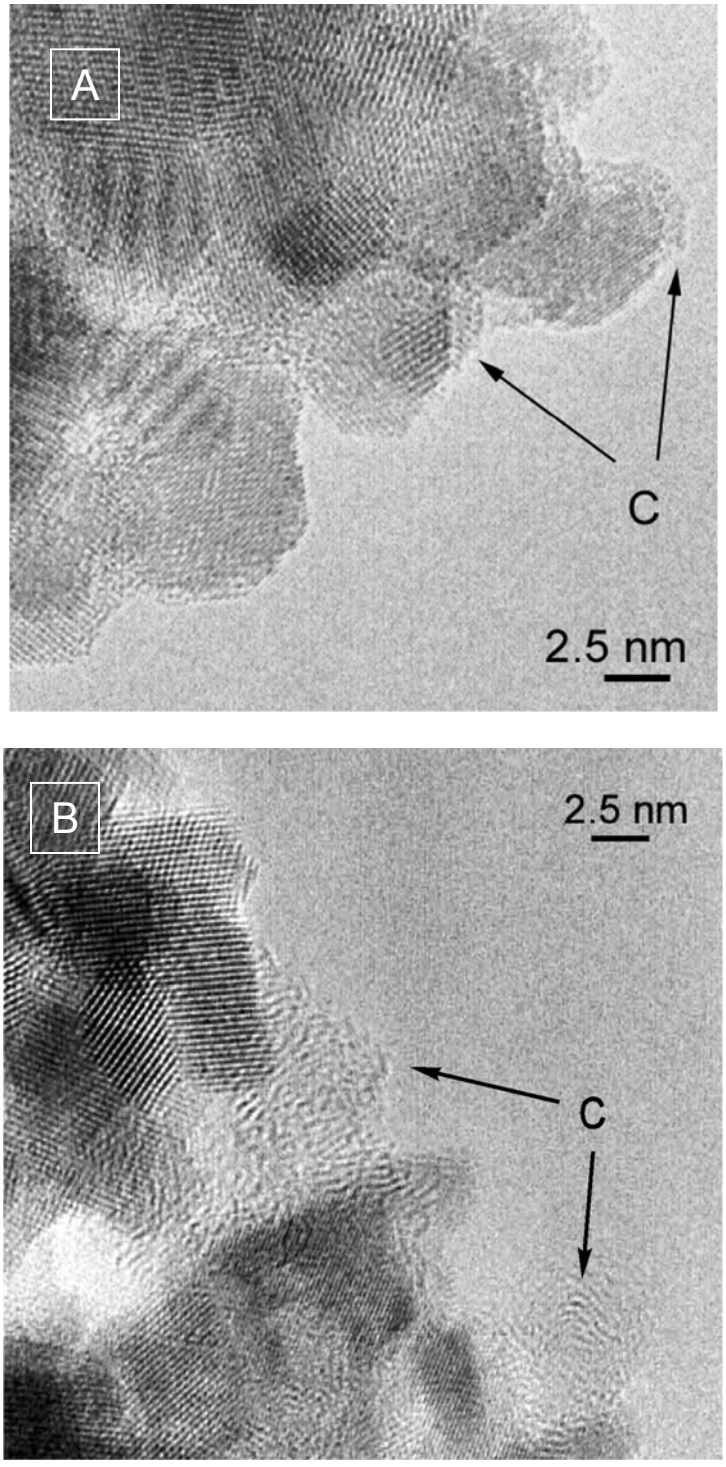

Figure 28. HRTEM image of CeO_2 (A) and 1% Pd/CeO_2 (B), pretreated in a flow of 10% CO in He at 623 K for 12 h

6.4 DISCUSSION

Previous investigations have put forth spectroscopic evidence for the occurrence of CO disproportionation on ceria.[70,80] Raman studies in the current work confirm the appearance of carbon bands[71,74,77,110] at 2840, 1582, and 1331 cm^{-1} on CeO_2 and Pd/CeO_2 following exposure to CO at 623 K (Fig. 25, 26).

For Pd/CeO_2, certainty in the 1331, 1582, and 2840 cm^{-1} band assignments is obtained from the FTIR CO isotope exchange results (Fig. 23 and Scheme 5). The ^{13}C forms on the Pd/CeO_2 through ^{13}CO disproportionation at 623 K, and ^{13}carbonate/^{13}carboxylates also form. Both types of species are stable towards evacuation.[41,46,92] Yet, the concentration of surface ^{13}carbonates/^{13}carboxylates decreases by a substitution reaction with $^{12}CO_2$ (Fig. 23 spec. 1), while the ^{13}C deposits are unaffected. Evacuation of the gas phase and subsequent exposure to O_2 oxidizes the ^{13}C deposits, as evidenced by the presence of gas-phase $^{13}CO_2$ (Fig. 23 spec. 3) and labeled carbonate species (Fig. 23 spec. 2). Labeled carbon dioxide in the gas phase would not result from carbonate decomposition, because ceria surface carbonates are stable in O_2 at 623 K.[92] This interpretation is supported by the HRTEM images of carbon deposits on CeO_2 and Pd/CeO_2 following exposure to CO (Fig. 28).

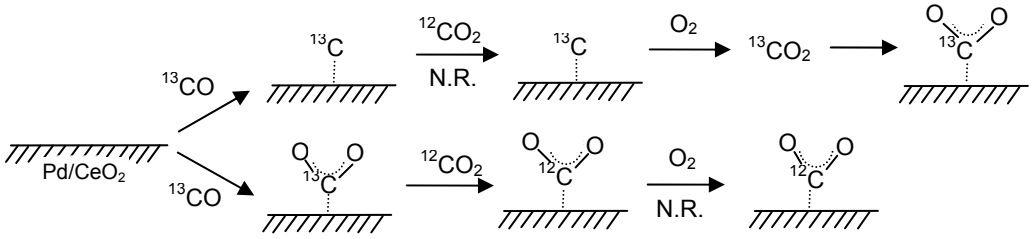

Scheme 5. Possible surface chemistry occurring in Fig. 23. The pathways illustrate surface species only and not the bonding geometry. No reaction is abbreviated N.R.

Carbon deposition is ongoing during CO exposure with both the Pd/CeO_2 and CeO_2 (Fig. 25, 26). The differences in the relative carbon band intensities with time for Pd/CeO_2 and CeO_2 suggest different mechanisms of carbon formation for the two samples. However, it should be noted the spectra were similar at CO contact times exceeding 7 h.

Palladium surface atoms participating as reaction sites for CO disproportionation surely may explain the differences of the Pd/CeO_2 and CeO_2 spectra during early exposure times. The CO disproportionation rate on Pd/CeO_2 is higher during the first 4 h, as evidenced by the greater intensity of bands at 1582 and 1331 cm^{-1}. Yet, the number of exposed Pd atoms available to disproportionate CO decreases over time due to site blocking by carbon. The site blocking chemistry is well illustrated by the decrease in Pd-CO bands as a function of CO reduction temperature, monitored by FTIR (Fig. 24).

Yet, as noted earlier, the differences between the Pd/CeO_2 and CeO_2 spectra diminish at CO contact times exceeding roughly 7 h. This behavior may be understood by considering the relative rate of carbon formation on the two catalysts during the experiment (Fig. 27). The initially higher rate of carbon formation on Pd/CeO_2 is attributed to CO disproportionation on Pd, and the rate decreases during the first 7 h due to Pd site blocking. Between roughly 7 and 10

h, the rates were approximately constant and minimal on both catalysts. Surprisingly, at times longer than 10 h the carbon deposition rate increases similarly on both CeO_2 and Pd/CeO_2. Clearly, sites on the ceria must be responsible for the increasing rate, and a change in the nature and/or type of the sites occurs after the first 10 h of CO exposure.

The overall CO disproportionation reaction, $2\ CO \rightarrow CO_2 + C_{(s)}$, may be divided into two steps (Scheme 6). The reduction step involves CO_2 formation by abstractive reduction of CeO_2 by CO. Most likely, abstraction of a lattice oxygen to make a two electron oxygen vacancy forms a site for the next step of CO disproportionation, oxidation. The electrons are localized on the neighboring cerium ions, as evidenced by the presence of a Ce^{3+}-CO vibration at 2115 cm^{-1} (Fig. 25, 26). Similar to CeO_2 oxidation by dioxygen,[141] the oxygen of CO is attracted by the localized electrostatic field of the vacancy.[6,127] The CO bond cleaves homolytically and the vacancy is eliminated by the oxidative incorporation of the oxygen atom of CO to an O^{2-} lattice species, while elemental carbon forms.

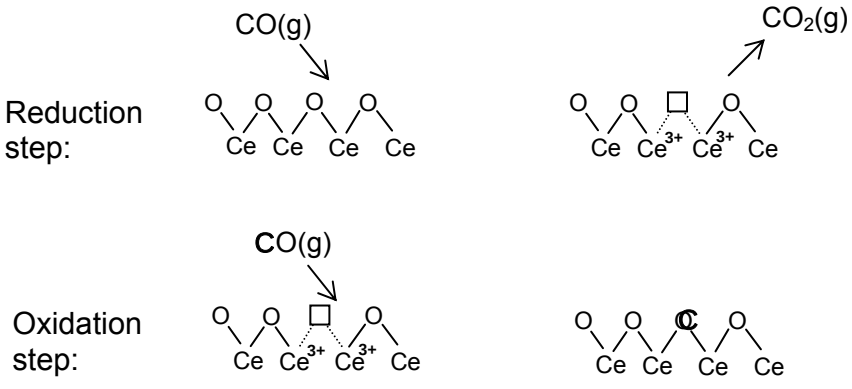

Scheme 6. CO reaction pathway to carbon

However, the chemistry depicted in Scheme 6 does not account for the increase in the rate of carbon formation after roughly 7 h that occurs both for the Pd/ CeO_2 and the CeO_2. One plausible explanation is simply an increase in the number of vacancy sites with increasing time of CO exposure. However, the number of these sites would need to increase progressively over the duration of the CO exposure, and this is not observed (Fig. 27). Rather, the rate abruptly increases after 10 h. The observed behavior is better described by a different type of reaction site, one that forms after prolonged reduction of the surface by CO. The increasing rate of the CO disproportionation reaction also indicates that the reaction is autocatalytic (product catalyzed) at reaction times longer than 10 h.

Vacancy clusters form when oxygen atoms adjacent to an existing vacancy are abstracted. Dimers, trimers, lines, and larger aggregate vacancies on single crystal surfaces of ceria have been imaged by STM and AFM.[6,7] Such vacancies on polycrystalline ceria have also been inferred from Raman investigations using dioxygen as a probe molecule. In that study, three different types of surface peroxides formed upon O_2 adsorption on partially reduced ceria: peroxides on aggregate vacancies, peroxides on line vacancies, and peroxides on point vacancies.[8] The thermal stability of peroxide species followed the trend of aggregate < line < point.[8] In other words, the aggregate vacancies are most reactive for cleavage of the O-O peroxide bond, which fills two vacancies and thus re-oxidizes the ceria.

The factors that make aggregate vacancies more reactive than line and point vacancies for peroxide bond cleavage also make them more reactive for CO bond cleavage. Indeed, as shown in a previous investigation, oxygen exposure to CeO_2 after the 12 h reaction with CO resulted in negligible Raman band intensity for peroxides on aggregate vacancies (877 cm^{-1}) or peroxides on line vacancies (858 cm^{-1}).[80] (Fig. 17 in this dissertation) These bands were essentially absent

because they form in vacancies which are the more reactive sites for CO disproportionation. The disproportionation of CO fills oxygen vacancies; the most reactive sites fill preferentially and thus large vacancies are transformed into small/point vacancies. Reaction with gas phase dioxygen or room temperature lattice diffusion[83,142] should not play a role in vacancy annilihation.[143]

The reactivity trend of aggregate > line > point for CO bond cleavage may be understood in terms of the extent to which the electron density may be considered delocalized in the vicinity of the vacancy. Recent theoretical calculations have suggested that the electrons from the oxygen point vacancy are localized on the nearest cerium cations.[6] An aggregate vacancy site may be viewed as a finite space in which these electrons are delocalized because of the concentration of Ce cations with the associated oxygen vacancy electrons. In other words, aggregate vacancy sites exhibit metallic behavior in comparison to isolated vacancies. Thus the aggregate vacancies may be thought of as nano-domains of metallic Ce^{3+}, which provide electron density to the CO surface species with which they are interacting. The extent to which the electron density is delocalized impacts the rate at which CO acts as an electron donor or acceptor.

At early CO exposure times, CO acts as an electron donor while reducing the oxide surface, forming O vacancies and CO_2. Carbon is formed through CO disproportionation with CO as the electron acceptor, but at a slow rate because only point vacancies, with localized electron density, are available as active sites. At later CO exposure times, the aggregated vacancies provide more electron density to the CO surface species with which they are interacting. As an electron acceptor, the CO bond cleaves to yields elemental carbon and an

oxygen species interacting with the aggregate vacancy cluster. At intermediate times of 5 – 14 h, oxygen vacancies on the surface are aggregating but have not formed the minimum size to donate electron density to CO.

By definition, a reaction in which the reaction rate increases is autocatalytic, videlicet product-catalyzed. Therefore the active site must be regenerated by oxidation of additional CO by ceria lattice oxygens adjacent to the aggregated vacancy. When the reaction rate is low, oxygen vacancies are forming but have not aggregated to the extent required for the reaction to become autocatalytic. At times after 14 h, the disproportionation of CO on CeO_2 is an autocatalytic reaction. Although we have no direct evidence that O atoms are abstracted adjacent to the aggregated vacancy, it is a reasonable conclusion from the rate evidence.

7.0 CARBONATE FORMATION AND STABILITY ON CERIA-ZIRCONIA SUPPORTED PALLADIUM CATALYSTS

7.1 INTRODUCTION

In the current multi-oxide material used to support automotive exhaust three-way catalysts, ceria-zirconia solid solutions confer oxygen storage capacity (OSC) to the catalyst and improve textural properties.[15,144] The OSC behavior is possible as a result of the facile redox chemistry between the Ce^{3+} and Ce^{4+} oxidation states. OSC is often measured using pulse techniques to titrate the oxygen available in the catalyst using a reductant, commonly CO.[13,43,84] Obviously the measured OSC will change depending on the temperature, pressure, and reductant/oxidant concentrations chosen for the test. Common reaction conditions reported for OSC measurements are with 1-10% O_2 and 1-5% CO in an inert gas at 570-770 K and atmospheric pressure.[13,15,89,90] Therefore, residual carbon in the form of carbonates or microcrystalline carbon formed from CO disproportionation may interfere with the accuracy of OSC measurements.

This work uses IR spectroscopy to examine the interaction of CO and O_2 with Pd/CeO_2, $Pd/Ce_{0.75}Zr_{0.25}O_2$, Pd/ZrO_2, and the supports alone. The surface species on the catalysts and supports under realistic OSC conditions were examined. This work compares the reactivity of the separate components of the ceria-zirconia supported noble metal catalysts presently used for automotive three way catalysts for carbonate formation. Carbonate species are the focus of this

study because microcrystalline carbonaceous species are not IR active. The ZrO_2 and Pd/ZrO_2 catalyst were included in order to characterize the behavior of a non-reducible support, compared to the ceria and ceria-zirconia supported reducible oxide catalysts.

7.2 EXPERIMENTAL

7.2.1 Materials

Ceria (99.9%) and $Ce_{0.75}Zr_{0.25}O_2$, (99.9%) were provided by Rhodia and calcined in air at 823 K for 12 h prior to use. Zirconia was precipitated from an aqueous solution of $ZrO(NO_3)_2$ (Alfa, 99.9%) with aqueous ammonia at pH 10. The precipitate was aged in the supernatant liquid for 24 h before filtering, washing, and drying at 373 K for 12 h; it was then calcined in air at 773 K for 12 h. The 1% Pd supported catalysts were prepared by impregnation of CeO_2, $Ce_{0.75}Zr_{0.25}O_2$, and ZrO_2 with aqueous solutions of $Pd(NH_3)_4(NO_3)_2$ (Strem Chemicals, 99.9%). The impregnated samples were dried at 373 K for 12 h and then calcined in air at 823 K for 12 h.

The O_2 (Praxair, 99.999%) and 10% O_2/He (Praxair, UHP) were used without purification. The trace contaminants in CO (Air Products, 99.99%) were removed using a liquid N_2 cooled trap.

7.2.2 Catalyst characterization

The catalysts were characterized earlier.[81] (Section 4.2.2 and Table 1 of this dissertation).

7.2.3 Infrared studies

Infrared spectra were recorded using a Mattson Research Series II Fourier-transform spectrometer using a liquid N_2 cooled MCT detector. The instrument was operated at a resolution of 2 cm^{-1} and 200 scans were accumulated per spectrum. The catalyst sample was pressed into a self-supporting disk (15 mg/cm^{-2} thick), mounted into the sample holder and placed into the quartz IR cell, described elsewhere.[138] The cell was connected to a vacuum system with an ultimate vacuum of 2×10^{-6} Torr achieved using a turbomolecular pump. All spectra were acquired after the sample had cooled to room temperature.

The standard sample pretreatment consisted of exposure to 50 Torr CO at 673 K for 1 h followed by exposure to flowing 10% O_2 in He (60 cc/min) at 673 K for 1 h, evacuation at 673 K for 1 h, cooling to 623 K in flowing 10% O_2/ He, and evacuation at 623 K for 30 min. A spectrum of the sample following pretreatment was acquired.

Next, spectra of the sample as well as the gas phase were acquired after each of the following gas treatments:

a) Exposure to 50 Torr CO at 298 K for 15 min

b) Exposure to 50 Torr CO at 623 K for 15 min

c) Evacuation at 623 K for 10 min

d) Exposure to 50 Torr O_2 at 623 K for 15 min

e) Evacuation at 623 K for 10 min

The experimental cycle was repeated 3 - 4 times with the same pellet; for all samples the difference in peak intensities measured between the first and the last repetition did not exceed 10%. The spectra were processed using WinFirst software (Mattson). The spectra presented are the difference spectra for each treated pellet, from which the gas phase background and standard pretreated pellet spectra have been subtracted.

7.3 RESULTS

7.3.1 Ceria

After room temperature adsorption of CO on ceria (Fig. 29a), hydrogen carbonate CO_3 stretching [$\nu(CO_3)$] bands were observed at 1602, 1399, and 1045 cm^{-1}, with the corresponding OH bending mode [$\delta(OH)$] at 1218 cm^{-1} and CO_3 out of plane wagging mode [$\pi(CO_3)$] at 824 cm^{-1}.[41] Bands observed at 1570, 1290, and 1006 cm^{-1} may be attributed to $\nu(CO_3)$ of bidentate carbonate, with the $\pi(CO_3)$ at 855 cm^{-1}.[45] The monodentate and polydentate bands appear in similar positions, so assignments may be ambiguous.[45] However, given the relative stability under various treatments, the 1503, 1362, and 1045 cm^{-1} bands may be attributed to monodentate carbonates, and the 1468, 1362, 1045, and 855 cm^{-1} bands are best assigned to polydentate carbonates.[45] Note the 1362 and 1054 cm^{-1} bands are attributed to both species. Carboxylate bands, which would appear at 1510-1518 and 1279 cm^{-1},[42] were not observed in Fig 29a; neither were bridged carbonate bands, which have been reported at 1736 and 1135 cm^{-1}.[45]. The band observed at 2347 cm^{-1} in Fig. 29a is the same frequency as the C-O stretching mode of gas phase CO_2, but

may be attributed to adsorbed CO_2.[45] The CO_2 in Fig. 29a indicates room temperature oxidation of CO to CO_2. For reference, carbonate and related surface species are illustrated in Scheme 7.

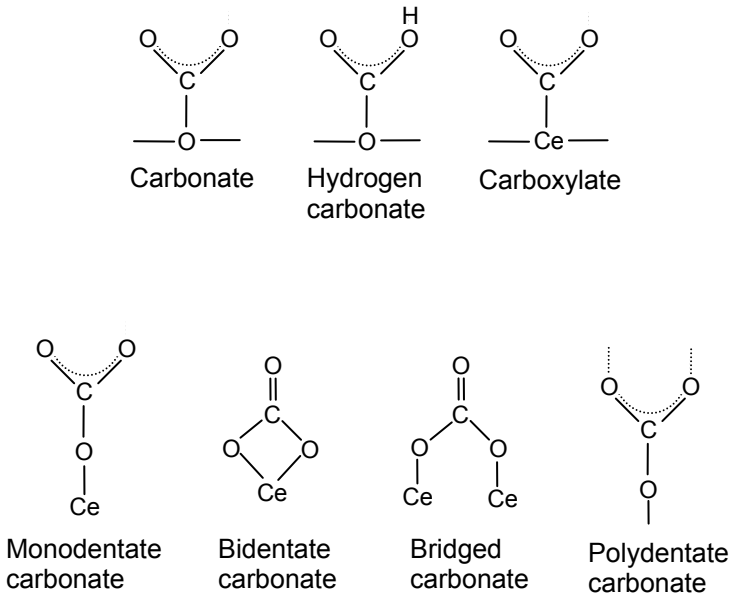

Scheme 7. Carbonate/carboxylate surface species.

Upon heating ceria to 623 K (Fig. 29b), the CO_3 carbonate stretching band intensities decreased slightly but lost definition, possibly because the baseline in the 1600 – 1200 cm^{-1} region increased. A weak band at 2113 cm^{-1}, which has been associated with to CO adsorbed on Ce^{3+},[92] was observed. The hydrogen carbonate band at 1218 cm^{-1} disappeared upon heating. Because the hydrogen carbonate band at 1602 cm^{-1} increased intensity, it may be assigned to a second type of hydrogen carbonate.[45] The CO_2 band shifted to 2354 cm^{-1} in Fig. 29b, which is consistent with the stretching mode of linearly adsorbed CO_2.[45]

When the heated ceria sample was evacuated, bands attributed to adsorbed CO_2, bidentate carbonate, and hydrogen carbonate (1602 cm^{-1} band) decreased in intensity. (Fig. 29c). After

oxidation by O_2 for 15 min, the spectrum in the carbonate region (Fig. 29d) returned to similar band intensities and definition as the sample originally exposed to CO at 298 K. The hydrogen carbonate band at 1218 cm^{-1} re-appeared after O_2 exposure. The appearance of gas phase CO_2 in Fig. 29d indicates some carbonate decomposition occurred in O_2 at 623 K. Upon evacuation, the only band that disappeared was gas phase CO_2 at 2349 cm^{-1}; all carbonate species appeared stable to 10 min evacuation at 623 K (Fig. 29e).

7.3.2 Pd/Ceria

The spectrum following Pd/CeO_2 exposure to CO at room temperature (Fig. 30a) was similar to the spectrum on ceria. Hydrogen carbonate $\nu(CO_3)$ bands were observed at 1601, 1400 and 1045 cm^{-1}, and the δ(OH) band was at 1218 cm^{-1}.[41] Bidentate carbonate $\nu(CO_3)$ bands were observed at 1570, 1299 and 1008 cm^{-1}, along with a $\pi(CO_3)$ band at 861 cm^{-1}.[45] A band at 1476 cm^{-1} was assigned to the $\nu(CO_3)$ of monodentate carbonate; as well, a band at 1371 cm^{-1} was assigned to the $\nu(CO_3)$ of both monodentate and polydentate carbonates Carbon dioxide linearly adsorbed on CeO_2 was observed at 2354 cm^{-1}. As was also observed on ceria, the CO_2 in Fig. 30a may indicate room temperature oxidation of CO to CO_2. Additionally, bands attributed to the C-O stretching mode of CO adsorbed on Pd were observed at 2099 and 2068 cm^{-1}, which can be assigned to linear species singly and multiply coordinated, respectively.[145,146]

After heating to 623 K (Fig. 30b), the bridged carbonate band at 1570 cm^{-1} disappeared; as well, the hydrogen carbonate band at 1218 cm^{-1} was not thermally stable. The adsorbed CO_2 band at 2354 cm^{-1} increased, similar to behavior on ceria under the same conditions.

Following evacuation of the heated Pd/CeO_2 sample, only a monodentate carbonate band at 1384 cm^{-1} remained in the carbonate region, along with an ill-defined band at 1446 cm^{-1} which may be assigned to polydentate carbonate (Fig. 30c).

After oxidation in O_2 at 623 K, the intensity of the polydentate carbonate bands decreased and bands attributed to additional types of carbonate species, such as monodentate, bidentate and hydrogen carbonate species, re-appeared on Pd/CeO_2; the re-oxidized spectra was qualitatively similar to the original room temperature CO exposed sample. The appearance of gas phase CO_2 in Fig. 30d indicates some carbonate decomposition occurred in O_2 at 623 K. After evacuation at 623 K, the monodentate carbonates remained and other carbonate species decreased in intensity (Fig. 30e).

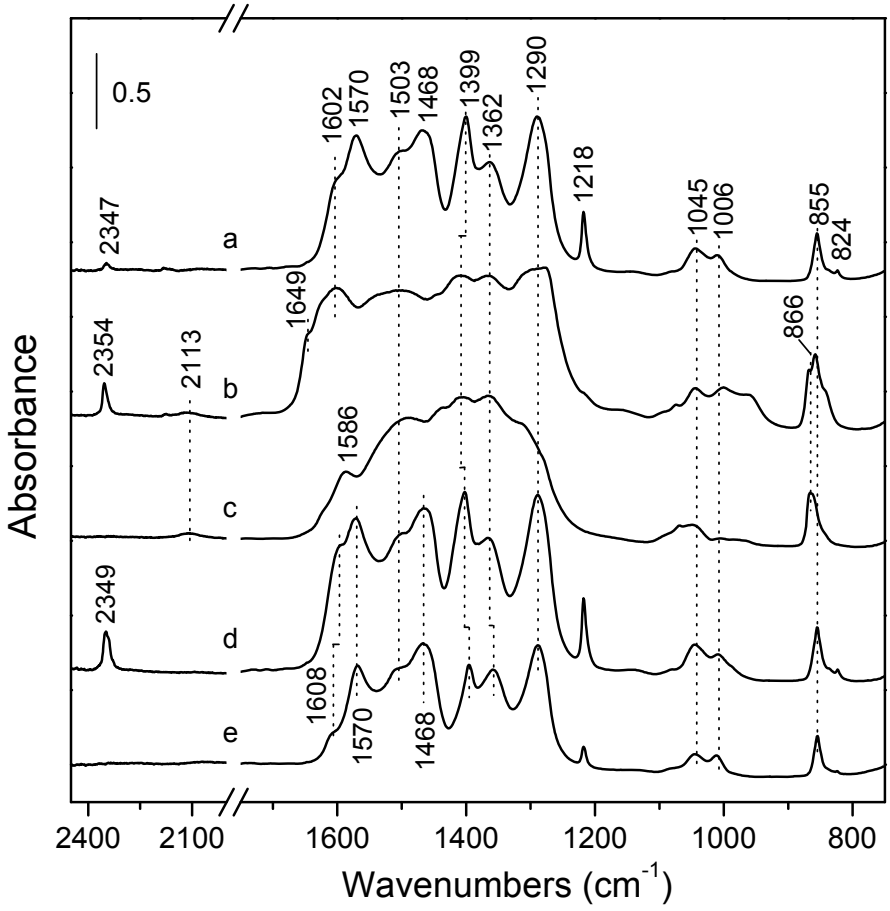

Figure 29. FTIR spectra of CeO_2 after adsorption of CO (50 Torr) for 15 min at 298 K (a), exposure to CO (50 Torr) for 15 min at 623 K (b), followed by evacuation for 10 min at 623 K (c), subsequent oxidation by O_2 (50 Torr) for 15 min at 623 K (d), followed by evacuation for 10 min at 623 K (e). All spectra were recorded at 298 K.

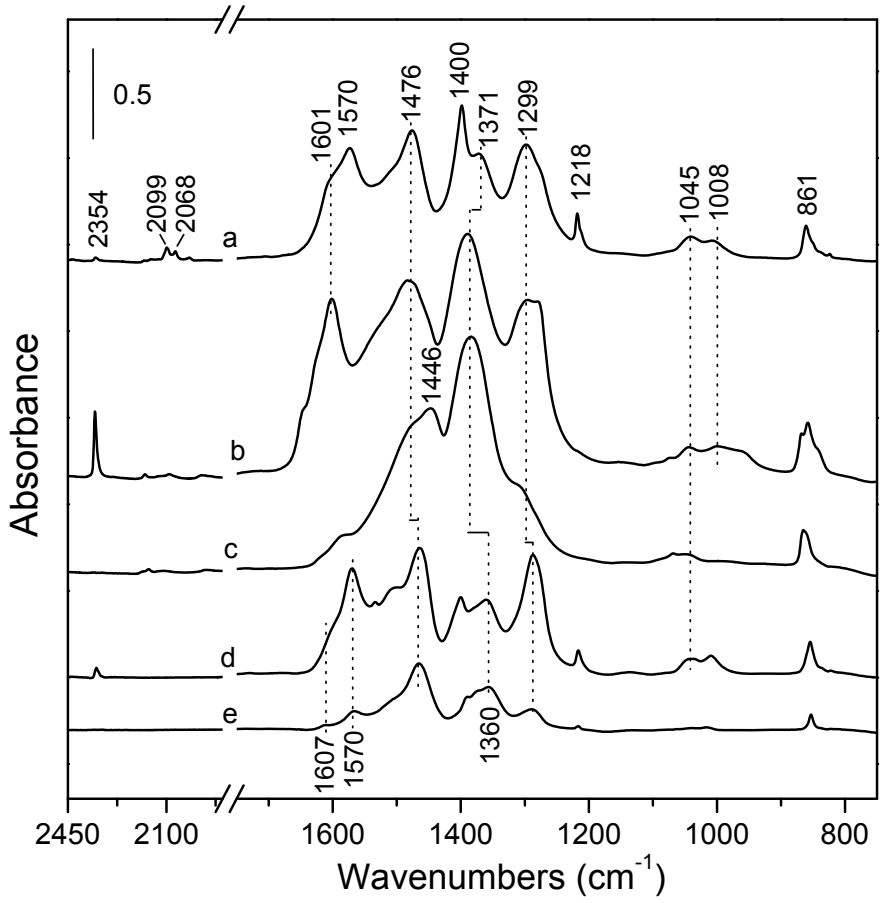

Figure 30. FTIR spectra of 1% Pd/CeO_2 after adsorption of CO (50 Torr) for 15 min at 298 K (a), exposure to CO (50 Torr) for 15 min at 623 K (b), followed by evacuation for 10 min at 623 K (c), subsequent oxidation by O_2 (50 Torr) for 15 min at 623 K (d), followed by evacuation for 10 min at 623 K (e). All spectra were recorded at 298 K.

7.3.3 Zirconia

The carbonate bands observed on ZrO_2 following CO exposure were lower in intensity than those observed on CeO_2. After exposure to CO at room temperature, bands attributed to carbonate species were observed on ZrO_2 (Fig. 31a). Bands at 1566 and 1325 cm^{-1} may be assigned to the $\nu(CO_3)$ of bidentate carbonate,[147,148] and bands at 1623 and 1431 can be attributed to the $\nu(CO_3)$ of hydrogen carbonate, with the corresponding δ(OH) at 1223 cm^{-1}.[124]

Upon heating (Fig. 31b), the carbonate band intensities changed little, and bands attributable to formate species were observed in the ν(CO) region at 1566 and 1370 cm^{-1}, as well as in the ν(CH) region at 2971 and 2890 cm^{-1} (not shown).[117,124,147,148] A weak band at 2349 cm^{-1} is consistent with adsorbed CO_2, and the band observed at 2187 cm^{-1} has been assigned to CO adsorbed on Zr^{4+}.[147-149] The band at 1050 cm^{-1} has been attributed to the $\nu(CO_3)$ of carbonate species.[147]

Adsorption of all species on ZrO_2 decreased dramatically following evacuation (Fig. 31c), and the little remaining carbonate bands disappeared after O_2 exposure at 623 K (Fig 31d). Following evacuation at 623 K (Fig. 31e), carbonate bands at 1556, 1428, and 1314 cm^{-1} increased slightly.

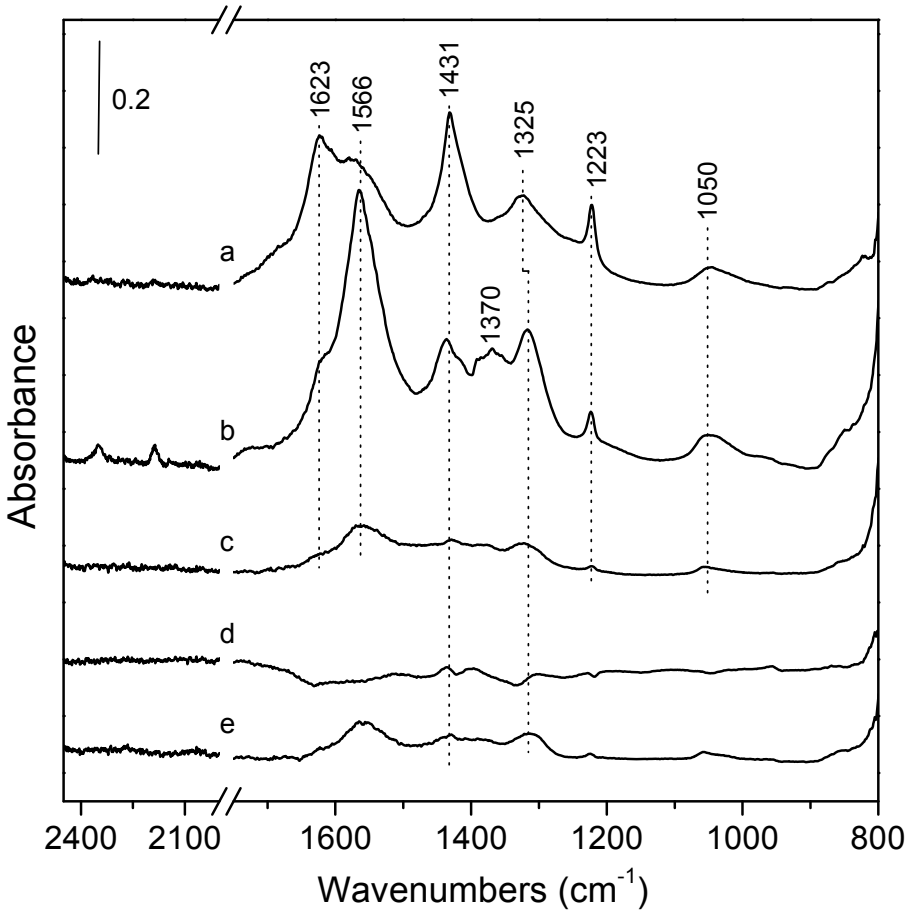

Figure 31. FTIR spectra of ZrO_2 after adsorption of CO (50 Torr) for 15 min at 298 K (a), exposure to CO (50 Torr) for 15 min at 623 K (b), followed by evacuation for 10 min at 623 K (c), subsequent oxidation by O_2 (50 Torr) for 15 min at 623 K (d), followed by evacuation for 10 min at 623 K (e). All spectra were recorded at 298 K.

7.3.4 Pd/Zirconia

In reducing environments, carbonate formation on Pd/ZrO_2 was similar to that on ZrO_2. The main difference in the two catalysts was the formation of well-defined carbonate and formate species on Pd/ZrO_2 following oxidation. After room temperature CO adsorption on Pd/ZrO_2, (Fig. 32a) carbonate band assignments were similar to those on ZrO_2. Bands at 1560 and 1315 cm^{-1} may be assigned to the $\nu(CO_3)$ of bidentate carbonate,[147,148] and bands at 1600 and 1440 can be attributed to the $\nu(CO_3)$ of hydrogen carbonate, with the corresponding δ(OH) at 1221 cm^{-1}.[124] The band at 2101 cm^{-1} has previously been assigned to CO linearly adsorbed on Pd,[150] and the 2199 cm^{-1} band may be attributed to CO adsorbed on Zr^{4+}.[147-149] A weak band at 2352 cm^{-1} is consistent with adsorbed CO_2.

Upon heating (Fig. 32b), formate bands increased in the ν(CO) region at 1560 and 1370 cm^{-1}. Bands were discernable in significant noise in the formate ν(CH) region at 2971 and 2890 cm^{-1} (not shown).[117,124,147,148] The linearly adsorbed Pd-CO band at 2101 cm^{-1} decreased, the Zr^{4+}-CO band at 2190 cm^{-1} retained its intensity, and the adsorbed CO_2 band at 2352 cm^{-1} increased intensity.

Bands for all adsorbed species decreased significantly upon subsequent evacuation (Fig. 32c). After oxidation at 623 K bidentate carbonate and hydrogen carbonate bands re-appeared (Fig. 32d). When the sample was evacuated, the bands for adsorbed species all decreased significantly in intensity (Fig. 32e).

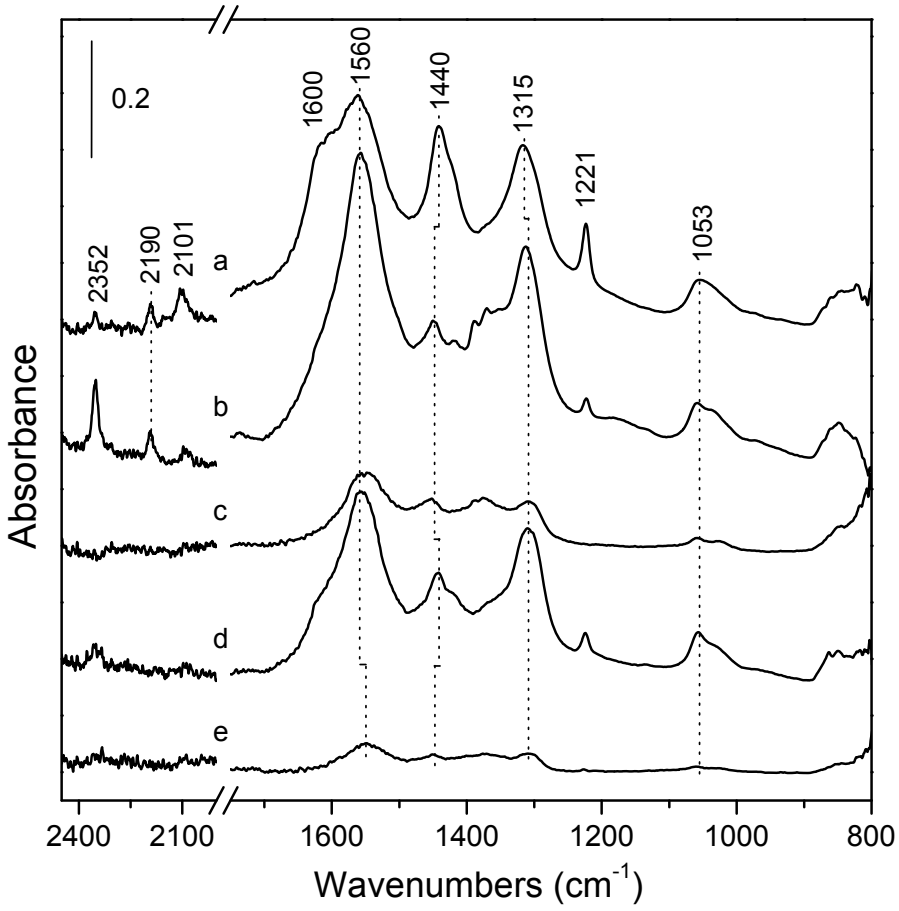

Figure 32. FTIR spectra of 1% Pd/ZrO_2 after adsorption of CO (50 Torr) for 15 min at 298 K (a), exposure to CO (50 Torr) for 15 min at 623 K (b), followed by evacuation for 10 min at 623 K (c), subsequent oxidation by O_2 (50 Torr) for 15 min at 623 K (d), followed by evacuation for 10 min at 623 K (e). All spectra were recorded at 298 K.

7.3.5 Ceria-zirconia

After exposure of $Ce_{0.75}Zr_{0.25}O_2$ to CO, several bands similar to ceria carbonate species were observed. Indeed, results from previous research indicate that IR carbonate band locations on ceria-zirconia mixed oxides are within 5 cm^{-1} of the carbonate band locations for pure ceria up to zirconia concentrations of about 50%.[151,152] After room temperature CO exposure (Fig. 33a), hydrogen carbonate $\nu(CO_3)$ bands were observed at 1603 and 1400 cm^{-1}, with the corresponding $\delta(OH)$ at 1218 cm^{-1}. Bidentate carbonate $\nu(CO_3)$ bands were present at 1330 and 1290 cm^{-1}. A band attributed to $\nu(CO_3)$ of monodentate carbonate was observed at 1512 cm^{-1}. The band at 2353 cm^{-1} may be assigned to CO_2 adsorbed on the support.

Bands attributed to formate species appeared upon heating at 1480, 1381 and 2892 cm^{-1} (not shown), while hydrogen carbonate bands decreased (Fig. 33b).

After the $Ce_{0.75}Zr_{0.25}O_2$ was evacuated (Fig. 33c), bidentate and hydrogen carbonate bands decreased in intensity, while polydentate and monodentate carbonate species remained on the surface. The adsorbed CO_2 disappeared upon evacuation.

Following exposure to O_2 (Fig. 33d), some hydrogen carbonate species formed as evidenced by the bands at 1407 and 1218 cm^{-1}. As well, the zirconia bidentate carbonate band re-appeared at 1326 cm^{-1}. The surface species were all susceptible to desorption upon evacuation (Fig. 33e).

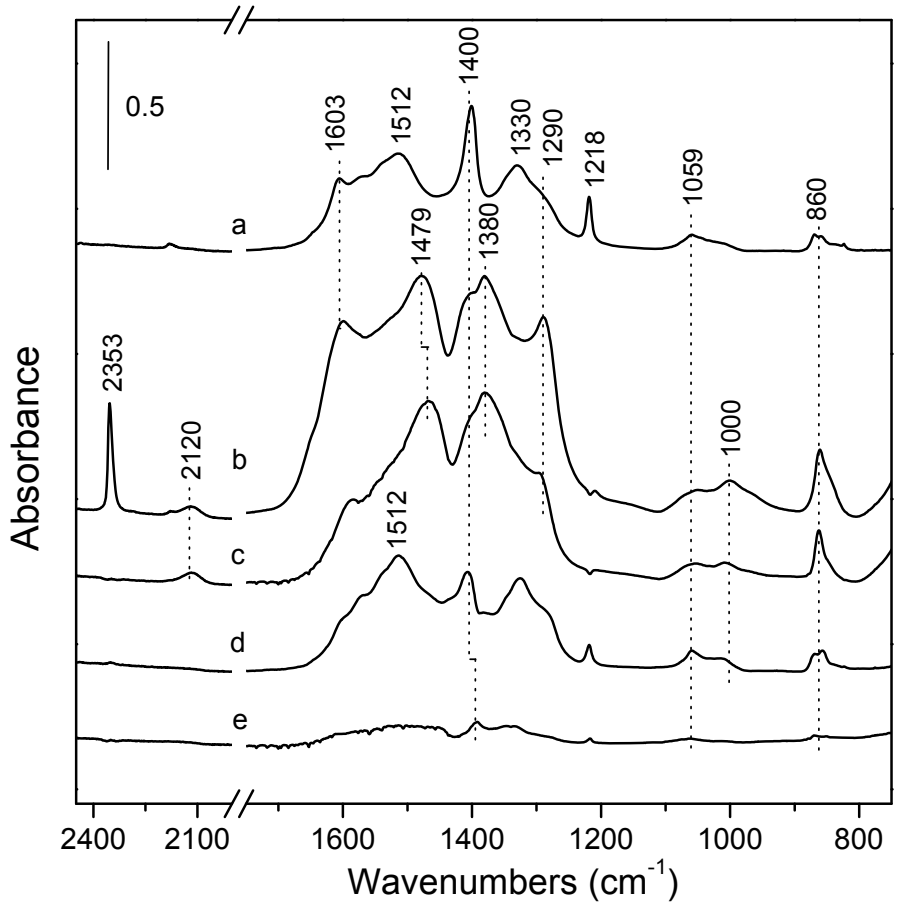

Figure 33. FTIR spectra of $Ce_{0.75}Zr_{0.25}O_2$ after adsorption of CO (50 Torr) for 15 min at 298 K (a), exposure to CO (50 Torr) for 15 min at 623 K (b), followed by evacuation for 10 min at 623 K (c), subsequent oxidation by O_2 (50 Torr) for 15 min at 623 K (d), followed by evacuation for 10 min at 623 K (e). All spectra were recorded at 298 K.

7.3.6 Pd/Ceria-zirconia

The behavior of $Pd/Ce_{0.75}Zr_{0.25}O_2$ following the experimental treatments was qualitatively similar to $Ce_{0.75}Zr_{0.25}O_2$, except for the presence of CO adsorbed on Pd. After room temperature CO exposure (Fig. 34a), hydrogen carbonate $\nu(CO_3)$ bands were observed at 1594 and 1408 cm^{-1}, and the $\delta(OH)$ band was at 1218 cm^{-1}. Bands assigned to $\nu(CO_3)$ of bidentate carbonate (1328 and 1298 cm^{-1}) and monodentate carbonate (1516 cm^{-1}) were observed. The band at 2013 cm^{-1} may be assigned to CO linearly adsorbed on Pd[145,146] and the band at 2353 cm^{-1} may be assigned to adsorbed CO_2.

The hydrogen carbonate bands decreased upon heating (Fig. 34b), while bands arose at 1479, 1380 and 2892 cm^{-1} (not shown), which may be assigned to formate species.

After the $Pd/Ce_{0.75}Zr_{0.25}O_2$ was evacuated (Fig. 34c), bidentate and hydrogen carbonate bands decreased in intensity, while polydentate and monodentate carbonate and formate species remained on the surface. The adsorbed CO_2 disappeared upon evacuation.

Following exposure to O_2 (Fig. 34d), some hydrogen carbonate species formed as evidenced by the bands at 1407 and 1218 cm^{-1}. As well, the zirconia bidentate carbonate band re-appeared at 1326 cm^{-1}. Nearly all the surface species were susceptible to evacuation (Fig. 34e).

The assignments for the carbonate and formate bands observed at wavenumbers greater than 1000 cm^{-1} are summarized in Table 2.

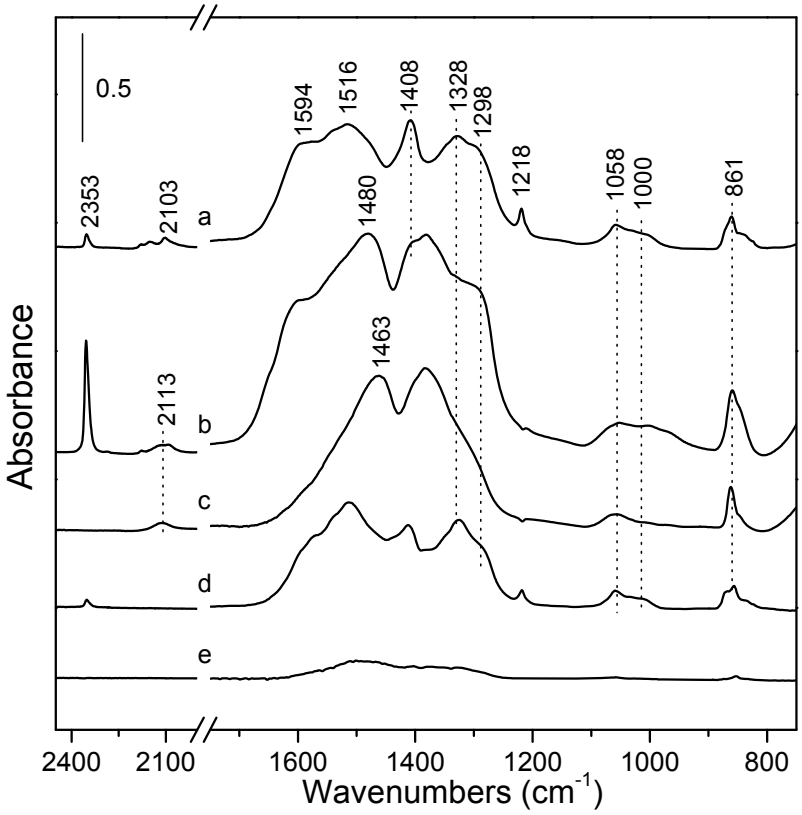

Figure 34. FTIR spectra of 1% Pd/ $Ce_{0.75}Zr_{0.25}O_2$ after adsorption of CO (50 Torr) for 15 min at 298 K (a), exposure to CO (50 Torr) for 15 min at 623 K (b), followed by evacuation for 10 min at 623 K (c), subsequent oxidation by O_2 (50 Torr) for 15 min at 623 K (d), followed by evacuation for 10 min at 623 K (e). All spectra were recorded at 298 K.

Table 2. Band positions (cm^{-1}) for selected species observed after CO exposure

Sample	CO_2 $\nu(CO_2)$	Pd-CO $\nu(CO)$	Hydrogen carbonate $\nu(CO_3)$	Hydrogen carbonate $\delta(OH)$	Bidentate carbonate $\nu(CO_3)$	Monodentate carbonate $\nu(CO_3)$	Polydentate carbonate $\nu(CO_3)$
CeO_2	2347	--	1602	1218	1570	1503	1468
			1399		1290	1362	1362
			1045		1006	1045	1045
Pd/CeO_2	2345	2099	1601	1218	1570	1476	1446
		2068	1400		1299	1371	1371
			1045		1008	1045	1045
ZrO_2	2349	--	1623	1223	1566	--	--
			1431		1325		
			1050		1050		
Pd/ZrO_2	2352	2101	1600	1221	1560	--	--
			1440		1315		
			1053		1053		
$Ce_{0.75}Zr_{0.25}O_2$	2353	--	1603	1218	1330	1512	1059
			1400		1290	1059	
			1059		1000		
$Pd/Ce_{0.75}Zr_{0.25}O_2$	2353	2013	1594	1218	1328	1516	1058
			1408		1298	1058	
			1000		1058		

7.3.7 Results in $\pi(CO_3)$ out of plane bending region

In order to clarify the carbonate behavior on the ceria based catalysts without involving the drifting baseline and poorly defined bands in the carbonate $\nu(CO_3)$ region, the carbonate $\pi(CO_3)$ out of plane bending region was examined in detail.

On CeO_2, the major band present at room temperature in CO was at 855 cm^{-1}, and a low intensity band at 823 cm^{-1} was also observed (Fig. 35A, spec. a). After heating to 623 K, new bands at 868 and 840 cm^{-1} appeared, the 855 cm^{-1} band redshifted, and the band at 823 cm^{-1} disappeared (Fig. 35A, spec. b). Upon evacuation, the band at 840 cm^{-1} decreased intensity (Fig. 35A, spec. c). After exposure to O_2, the low intensity band at 823 cm^{-1} reappeared (Fig. 35A, spec. d), but disappeared upon subsequent evacuation (Fig. 35A, spec. e). On Pd/CeO_2, the results were similar except the main band at 861 cm^{-1} blueshifted upon heating (Fig. 35B).

The trends for the band intensities on both CeO_2 and Pd/CeO_2 are shown in the insets in Fig. 35. The trends for CeO_2 and Pd/CeO_2 were qualitatively similar, indicating that all detected carbonate species were interacting with the ceria support. The intensities are relative to the baseline value at 900 cm^{-1}, and are normalized to the greatest intensity observed on each catalyst. The carbonates at 840, 855, and 868 cm^{-1} (assignments on CeO_2) were most stable in CO at 623 K. After subsequent evacuation, the carbonate at 868 cm^{-1} had the smallest decrease in intensity. This carbonate was also the most easily oxidized. The carbonate band at 840 cm^{-1} shows similar behavior to 855 cm^{-1} but entirely desorbs upon evacuation. The carbonate band at 823 cm^{-1} was the only band that did not increase intensity upon CO exposure at room temperature or 623 K, and in fact, the band markedly increased under oxidizing conditions.

On $Ce_{0.75}Zr_{0.25}O_2$, low intensity bands were observed at 870, 859, 849, 840, and 823 cm^{-1} after room temperature CO exposure (Fig. 36A, spec. a). Upon heating, all bands increased intensity, with the 859 cm^{-1} band redshifting and becoming the most intense, while a new band appeared at 878 cm^{-1} (Fig. 36A, spec b). The carbonate bands were little affected by evacuation (Fig. 36A, spec. c), and all bands decreased intensity after O_2 exposure except for the band at 823 cm^{-1} (Fig. 36A, spec. d). All bands significantly lost intensity upon evacuation following O_2 exposure (Fig. 36A, spec. e). On $Pd/Ce_{0.75}Zr_{0.25}O_2$, the band at 861 cm^{-1} was the most intense band after room temperature CO exposure, but the other band intensity changes with treatments were qualitatively similar to those on $Ce_{0.75}Zr_{0.25}O_2$ (Fig. 36B).

The quantitative trends of the band intensities with treatment on both $Ce_{0.75}Zr_{0.25}O_2$ and $Pd/Ce_{0.75}Zr_{0.25}O_2$ are shown in the insets in Fig. 36. Upon examination, some trends are similar to those observed on CeO_2 catalysts (Fig. 35), but there are several differences. The behavior of the carbonate band at 823 cm^{-1} is similar to that on CeO_2 catalysts; it was stable under oxidizing conditions. The carbonate band at 870 cm^{-1} also increased upon oxidation. However, a key difference between the carbonate behavior on the mixed oxide and pure ceria was the presence of a carbonate band at 878 cm^{-1}. This band was low intensity and qualitatively similar to the 870 cm^{-1} band. Additional differences included the behavior of the carbonate band at 859 cm^{-1}; in the mixed oxide this band decreased intensity upon evacuation whereas on CeO_2 catalysts it increased slightly. The band at 849 cm^{-1} on the mixed oxide was qualitatively similar to the band at 855 cm^{-1} on CeO_2. The band at 840 cm^{-1} showed a slight increase upon oxidation with both Pd catalysts, but not the bare oxides.

It should be noted that because ceria is a basic oxide, carbonate species formation is favored on ceria based oxide surfaces when CO or CO_2 impurities are present, i.e., ambient

conditions. Because of the high stability of surface carbonate species on ceria based oxides, the catalyst surfaces in this work were not "cleaned" of carbonate contamination before the start of the experiment, because the pretreatment conditions were not severe enough. Other researchers[41,42,47] found it was necessary to perform high temperature outgassing (1000 K) and/or oxygen treatments (873 K) prior to their spectroscopic studies of ceria, particularly to remove tenacious bulk polydendate carbonates. Therefore, it should be expected that several types of surface carbonates were present on the ceria surface prior to the first treatment, exposure to 50 Torr CO at room temperature. However, it is assumed in the analysis that no remaining "core" carbonates, as observed by Bozon-Verduraz et. al.,[92] should have interfered with the difference spectra because the pretreatment temperature of 673 K was more severe than the highest experimental temperature of 623 K. Similar to the pretreatment used in this work, Sharma et. al.[88] performed IR studies on Pd/ceria without first "cleaning" the surface of carbonates.

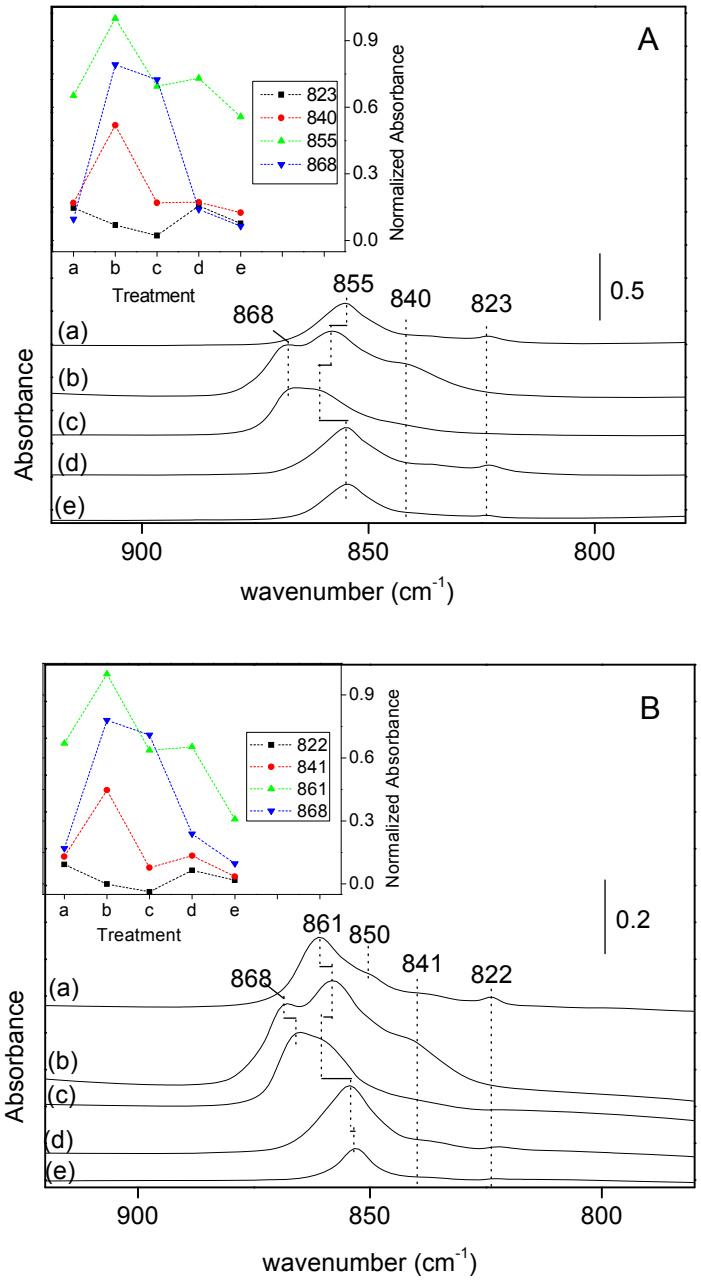

Figure 35. FTIR spectra of the out of plane π (CO_3) bending region of CeO_2 (A) and Pd/CeO_2 (B) after adsorption of CO (50 Torr) for 15 min at 298 K (a), exposure to CO (50 Torr) for 15 min at 623 K (b), followed by evacuation for 10 min at 623 K (c), subsequent oxidation by O_2 (50 Torr) for 15 min at 623 K (d), followed by evacuation for 10 min at 623 K (e). All spectra were recorded at 298 K. Dynamics of the normalized absorbance are shown in the inset.

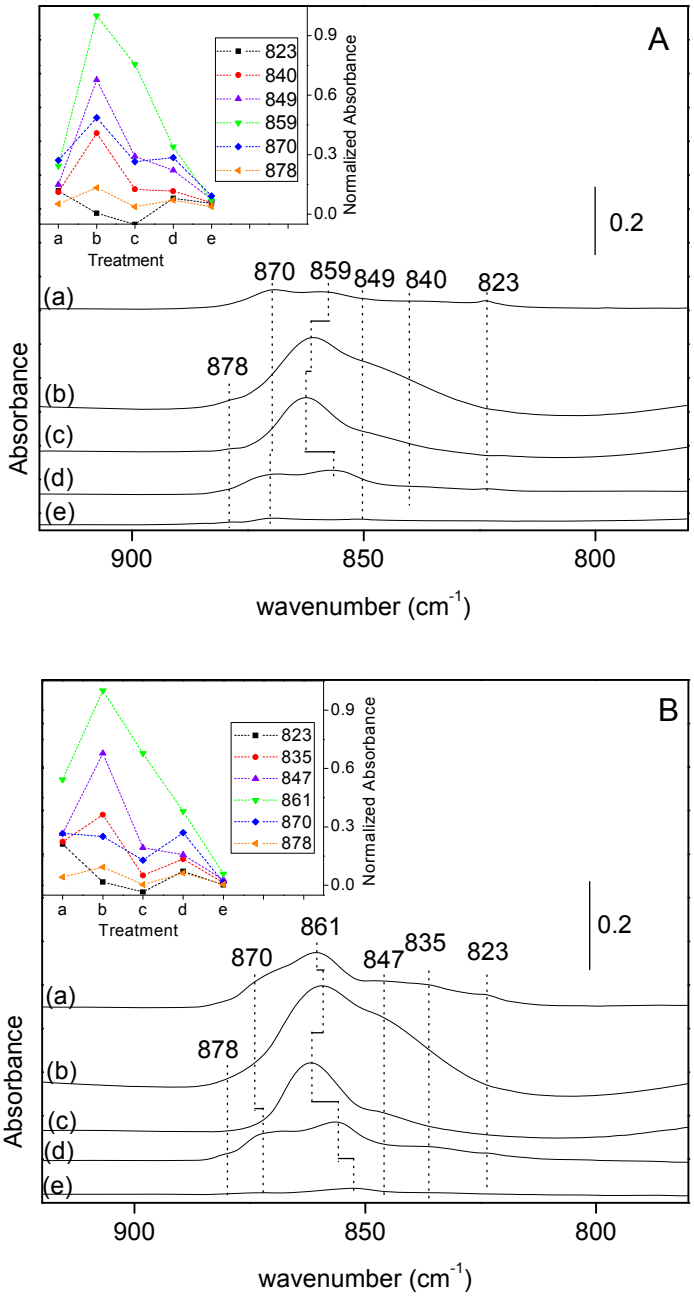

Figure 36. FTIR spectra of the out of plane π (CO_3) bending region of $Ce_{0.75}Zr_{0.25}O_2$ (A) and $Pd/Ce_{0.75}Zr_{0.25}O_2$ (B) after adsorption of CO (50 Torr) for 15 min at 298 K (a), exposure to CO (50 Torr) for 15 min at 623 K (b), followed by evacuation for 10 min at 623 K (c), subsequent oxidation by O_2 (50 Torr) for 15 min at 623 K (d), followed by evacuation for 10 min at 623 K (e). All spectra were recorded at 298 K. Dynamics of the normalized absorbance are shown in the inset.

7.4 DISCUSSION

Although there is a general consensus that the addition of zirconia to ceria enhances the oxide oxygen storage capacity, the mechanism for increased OSC is still a matter of debate. Unlike ceria, pure zirconia has only one stable oxidation state and thus does not release and accept oxygen via a redox mechanism. Yet, upon addition of ZrO_2 in amounts of approximately 15-50%, significant improvements in ceria oxygen storage capacity have been reported.[18,24]

The substitution of a Ce^{4+} cation by a Zr^{4+} cation eliminates a redox site on the oxide. Thus, the increase in labile oxygen species obtained by addition of Zr^{4+} must more than compensate for the loss in cerium redox sites; indeed several scenarios have been put forth to explain the observed macroscopic behavior. The role of zirconia addition in the oxygen storage capacity enhancement has been attributed to electronic effects, such as the localization of electrons on Ce^{3+} near oxygen vacancies.[6] However, the most accepted explanations for the increased OSC of the mixed oxide involve geometric effects; for example, lattice relaxation may be induced by the smaller size of the Zr^{4+} cation than the Ce^{3+} cation. It is speculated that the smaller radius of zirconia reduces the lattice strain during Ce^{4+} reduction, thereby enhancing the stability of oxygen defects.[34]

Carbonate formation on ceria and related oxides is facile at conditions of interest for many applications; for instance, heat treatment at 1000 K in oxygen or vacuum is commonly used to remove all traces of carbonates from the ceria surface.[24,41,42,92] This study investigated the interaction of surface carbonate species with ceria based oxides under conditions relevant to automotive applications.

The current investigation has shown that the carbonates present on $Ce_{0.75}Zr_{0.25}O_2$ are less strongly bound after oxidation compared to reduction. As shown in Fig. 33c and 34e, evacuation

more pronouncedly decreased the intensity of the carbonate bands after oxidation than after reduction. In contrast, evacuation equally affected the carbonates on ceria during evacuation following O_2 exposure and CO exposure (Fig. 29c, 29e). The addition of the metal did not alter the qualitative behavior observed for each oxide catalyst (Fig. 30c, 30e, 34c, 34e), indicating the chemistry occurring on the oxides remains relevant when examining the metal loaded systems. It should be noted that the bands associated with carbonates on Pd/CeO_2 were less intense following O_2 exposure compared to CO exposure; however, no carbonates bands remained on $Pd/Ce_{0.75}Zr_{0.25}O_2$ following O_2 exposure.

In order to account for the decrease in $Ce_{0.75}Zr_{0.25}O_2$ carbonate stability following dioxygen exposure, it is reasonable to consider that upon oxidation of Ce^{3+} to Ce^{4+}, the oxide-carbonate bonds were destabilized. The destabilized carbonates were subsequently desorbed by evacuation. In this case, the Ce^{4+} sites in $Ce_{0.75}Zr_{0.25}O_2$ were the active sites for carbonate destabilization. This interpretation is supported by previous studies which observed the interaction of dioxygen with ceria surface carbonates and showed the dioxygen preferentially reoxidized the surface, with no observed isotopic scrambling with oxygen in the carbonate species.[153]

In contrast to the mixed oxide, in this study the carbonates on CeO_2 exhibited similar stability during evacuation following oxidation and reduction. This indicates that under the conditions of the current research, the Ce^{4+} and Ce^{3+} sites in CeO_2 stabilize carbonates to a similar degree following each treatment. Because IR is a quantitative technique, it is reasonable to conclude that the Ce^{4+} sites in $Ce_{0.75}Zr_{0.25}O_2$ were more active for carbonate destabilization than Ce^{4+} sites on CeO_2. The lesser stability of carbonates on the mixed oxide compared to the

ceria is manifested on the macroscopic level by the increased oxygen storage capacity. However, the chemistry is more appropriately visualized as a decrease in site blocking by carbonates.

As oxygen removal progresses, more Ce^{3+} sites are formed. These Ce^{3+} sites are stronger bases than the Ce^{4+} site. Hence, the corresponding salt that forms by reaction with CO_2 is more stable, and indeed Ce(III) forms stable bulk carbonate salt, $Ce_2(CO_3)_3$. Such stable species may be considered as annihilated sites with respect to oxygen uptake and release chemistry. The results of the present work are in agreement with the interpretation presented in a previous study of oxygen release/storage and CO_2 adsorption on ceria catalysts, which concluded that carbonate species adsorbed on the reduced Ce^{3+} sites.[154] Carbonate species formation was inferred from the oxygen and carbon balances calculated during O_2, CO, and CO_2 pulse experiments carried out at 723 K. However, the conditions for the current work were able to show a difference between the activity of the Ce^{4+} sites in CeO_2 and $Ce_{0.75}Zr_{0.25}O_2$ for carbonate destabilization, whereas the cited prior study investigated only ceria catalysts.

The bands in the out of plane CO_3 wagging region may be assigned based on the band stability under the conditions used in this work. On CeO_2 and Pd/CeO_2, the band at 823 cm^{-1} has previously been assigned to hydrogen carbonate.[41,45] After hydrogen carbonate, the bidentate carbonate species were the least stable. The band at 840 cm^{-1} is only present in CO at 623 K and is assigned to bidentate carbonate. The band at 868 cm^{-1} is consistent with monodentate or polydentate carbonate. The most stable band, at 855 cm^{-1} and 861 cm^{-1} on CeO_2 and Pd/CeO_2, respectively, in CO at room temperature, may be assigned to another type of polydentate

carbonate, here designated polydentate carbonate II. From the greater intensity and absorbance of the polydentate II type carbonates, it may be surmised that they are the more strongly bound of the two types of polydentate species.

On $Ce_{0.75}Zr_{0.25}O_2$ and $Pd/Ce_{0.75}Zr_{0.25}O_2$, assignments are similar. The 823 bands are assigned to hydrogen carbonate.[41,45] The bands at 840 cm^{-1} (835 cm^{-1} on $Pd/Ce_{0.75}Zr_{0.25}O_2$) and 878 cm^{-1} exhibit similar stability and are thus both assigned to bidentate carbonate. The 870 cm^{-1} band may be assigned to monodentate or a type of polydentate carbonate. The high intensity bands at 859 cm^{-1} and 861 cm^{-1}, respectively on $Ce_{0.75}Zr_{0.25}O_2$ and $Pd/Ce_{0.75}Zr_{0.25}O_2$ in CO at room temperature, are consistent with another, more stable type of polydentate carbonate, here designated polydentate carbonate II. The stabilities of the two types of polydentate carbonates are similar to those assigned on CeO_2 and Pd/CeO_2. The behavior of the 849 cm^{-1} (847 cm^{-1} on $Pd/Ce_{0.75}Zr_{0.25}O_2$) is ambiguous and assignment would be imprudently speculative. The band assignments are summarized in Table 3.

Table 3. Band positions (cm^{-1}) for carbonate out-of-plane wagging modes

Sample	Hydrogen carbonate $\pi(CO_3)$	Bidentate carbonate $\pi(CO_3)$	Monodentate carbonate $\pi(CO_3)$	Polydentate carbonate I $\pi(CO_3)$	Polydentate carbonate II $\pi(CO_3)$
CeO_2	823	840	868	868	855
Pd/CeO_2	823	841	868	868	861
$Ce_{0.75}Zr_{0.25}O_2$	823	840, 878	870	870	859
$Pd/Ce_{0.75}Zr_{0.25}O_2$	822	835, 878	870	870	861

8.0 SUMMARY AND FUTURE WORK

8.1 SUMMARY OF MAJOR RESULTS AND CONTRIBUTIONS OF THIS WORK

This work investigated the interaction of CO and O_2 with ceria-based catalysts reduced to varying degrees. *In situ* Raman spectroscopy was used to examine the interaction of CO with Pd/CeO_2, $Pd/Ce_{0.75}Zr_{0.25}O_2$, Pd/ZrO_2, and the supports alone. This work reported the first unambiguous evidence for CO disproportionation on CeO_2 and $Ce_{0.75}Zr_{0.25}O_2$, namely, the appearance of carbon bands at 1582 and 1331 cm^{-1} on those catalysts following CO exposure at 623 K. One previous IR spectroscopic study observed carbonate bands following CO exposure to reduced CeO_{2-x}, and inferred that the reaction occurred.[70] On CeO_2, exposure of the carbonaceous deposits to oxygen at room temperature resulted in surface formate formation. By the principle of microscopic reversibility, it was proposed that CO interacts with reduced CeO_2 through the oxygen end of the molecule, not the carbon as commonly suggested,[5,42] as an intermediate to the ceria surface formate product.

Carbon monoxide disproportionation was observed on high surface area CeO_2 and 1% Pd/CeO_2 using Raman and infrared spectroscopy and HRTEM. HRTEM images confirm carbon formation on CeO_2 and Pd/CeO_2; however, the technique did not allow determination of the active sites for CO disproportionation on Pd/CeO_2. In order to clarify the location of carbon formation on the catalyst, the rates of carbon formation on Pd/CeO_2 and the bare support were

calculated based on spectroscopic evidence. Rate data indicated that initially the most active sites for CO disproportionation on Pd/CeO_2 are Pd, but those sites are quickly blocked by coke. At longer CO exposure times, the ceria support becomes active for the CO disproportionation reaction. A mechanism for CO disproportionation on CeO_2 involving aggregated oxygen vacancy sites is proposed; the sites may be thought of as nano-domains of metallic Ce^{3+}. At the aggregated vacancy, the degree of electron density localization controls the rates at which CO acts as an electron donor or acceptor to form an energetically activated complex. This work showed that aggregated electron vacancies provide active sites for the autocatalytic disproportionation of CO on CeO_{2-x}.

Several groups have performed recent theoretical calculations on CeO_2 and the reduced CeO_2 surface.[6,127,155] In this active field, there is a current consensus that the electrons localize on Ce^{3+} cations adjacent to single oxygen vacancies, contrary to the delocalized electrons in the metallic nano-domains proposed in this work. Current theory and computing power limits the application of theoretical calculations to large aggregated oxygen vacancies. However, future calculations should show that electrons become delocalized when the oxygen vacancy clusters reach a critical size.

In addition, the stability of carbonate species formed upon exposure of CO to Pd/CeO_2, $Pd/Ce_{0.75}Zr_{0.25}O_2$, Pd/ZrO_2, and the supports was investigated using FTIR. On $Pd/Ce_{0.75}Zr_{0.25}O_2$ and $Ce_{0.75}Zr_{0.25}O_2$, carbonates were less strongly bound after oxidation compared to reduction. The oxide-carbonate bond was weakened upon oxidation of Ce^{3+} to Ce^{4+}, which indicates that the Ce^{4+} sites in $Ce_{0.75}Zr_{0.25}O_2$ were the active sites for carbonate destabilization. In contrast, the Ce^{4+} and Ce^{3+} sites on CeO_2 stabilize carbonates to a similar degree after both oxidation and reduction, which indicates that site blocking by carbonates may play a role in the increased

oxygen storage capacity of ceria-zirconia catalysts compared to ceria catalysts alone. The results of this study also assign previously indistinct[41,45,151,152] bands in the CO_3 out of plane bending region to monodentate, bidentate, and polydentate carbonate species on CeO_2 and $Ce_{0.75}Zr_{0.25}O_2$.

8.2 RECOMMENDATIONS FOR FUTURE WORK

The conclusions presented in this dissertation indicate that control of the nature of the reactant-catalyst interaction is possible by tailoring the degree of reduction of metal oxides. In order to favor CO as an electron acceptor (CO as an oxidant), the long exposure studies presented on CeO_2 and Pd/CeO_2 could be extended to other, more reducible oxide materials, such as ceria-zirconia or ceria-hafnia mixed oxides. It is reasonable that the formation of aggregated vacancies will be more rapid on more reducible materials, thus requiring less thermal energy for formation of the nanometallic active sites.

Isotopic studies using $C^{18}O$ (with a mass spectrometer to monitor gaseous products) could further elucidate the relative rates at which CO acts as an electron donor or acceptor on the oxide, and test the hypothesis that the disproportionation becomes autocatalytic. Scheme 6, reproduced here for convenience, allows examination of the effect of $C^{18}O$.

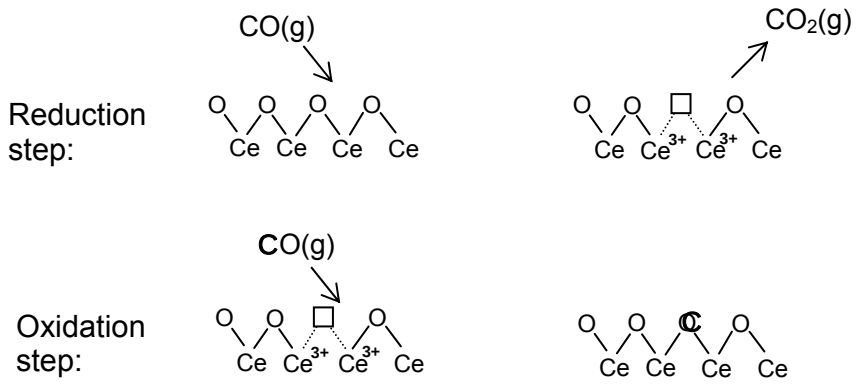

Scheme 6. CO reaction pathway to carbon

It would be expected that at early times on stream the CO_2 produced would consist of mostly $C^{18}O^{16}O$, because one ^{16}O would come from the ceria lattice during the reduction step. In fact the production of $C^{18}O^{16}O$ could be considered a measure of the OSC complete, as termed in the automotive literature. During $C^{18}O$ exposure, the reduction step would continually fill the oxygen vacancies with ^{18}O with concurrent carbon deposition. At later times on stream, production of $C^{18}O_2$ would indicate that the carbon monoxide was oxidized at an oxygen site that was located near a carbon deposit, since the vacancy had been filled by labeled $C^{18}O$. As ^{16}O is depleted from the ceria surface, the concentration of $C^{18}O^{16}O$ produced will decrease. It may be observed that the rate of production of $C^{18}O_2$ rapidly increases after 10 – 14 h on stream, assuming conditions similar to the Raman experiments performed in this work. The rapid increase in production of $C^{18}O_2$ would support the hypothesis that the CO disproportionation becomes autocatalytic on ceria after long times on stream.

The mass spectrometer (MS) experiments may be carried out by sampling the effluent from the current *in situ* Raman system. This would allow direct comparison to the experimental

conditions used in this work. Because MS operates at low pressure, it is necessary to reduce the sample volume entering the instrument. In addition, the delivery volume must be carefully controlled and calibrated in order to quantify the MS signal. This may be accomplished by using an automatic sampling valve with a 100 microliter sampling loop, using a carrier gas with a ppm-level tracer gas, such as Ar. In addition, a 3-way splitter valve may be used to further reduce the sample volume entering the MS. The MS sample injection schematic is shown in Fig. 37.

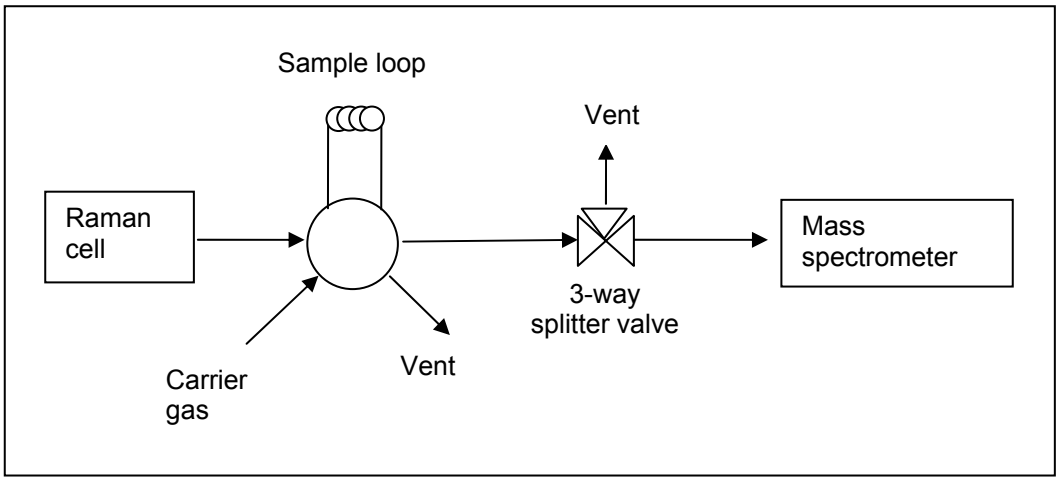

Figure 37. Mass spectrometer sample injection schematic

In addition to studies performed with the spectroscopic equipment used for this work, it would be interesting to use noncontact atomic force microscopy (AFM), and/or scanning tunneling microscopy (STM) to characterize the reduced oxides after different extents of CO exposure. The microscopic methods would be able to directly image the aggregated vacancies. Similarly, X-ray absorption near-edge structure (XANES) could be used to characterize the extent of reduction of the ceria. Assistance from outside laboratories at the University of Pittsburgh or other institutions should be obtained for the surface science studies mentioned; the instruments are not available in the d'Itri lab.

As an alternate to surface studies of the phenomena observed in this work, future studies of CO as an oxidant could be applied directly to macroscopic reaction engineering problems. One of the major challenges in oxidation catalysis is maximizing the selectivity and yield of the desired product. In the case of catalytic partial oxidation, it is a constant challenge to stop short of total oxidation, and yield of the desired product often suffers at the expense of selectivity. By controlling the nature of the active site at the aggregated oxygen vacancy, it should be possible to tailor activated oxygen species to perform desired partial oxidation reactions. This macroscopic application could be used to probe the reactivity of the oxygen species at the aggregated vacancy.

For example, propylene partial oxidation to propylene oxide could be carried out over a reducible oxide catalyst with some partial pressure of CO to activate the oxygen at the aggregate. A conventional temperature controlled reaction kinetics system, with a gas chromatograph detector, could be used to measure the yield and selectivity. The reactor volume and catalyst particle size should be small in order to avoid mass and heat transfer effects; a 10 mm i.d. quartz microreactor is recommended. Gases should be delivered through regulators and the flow should be controlled with electronic mass flow controllers. Micron filters and check valves may also be

used in the gas delivery lines to prevent against back-mixing, and the CO line should be equipped with a carbonyl trap. The lines should be heated in order to avoid condensation of products. A schematic of the kinetics system is shown in Fig. 38.

Future studies may also be carried out using theoretical DFT + U molecular calculation studies. The U parameter approach for modeling metal oxides corrects for the on-site Coulomb interactions in the d and f states.[155] Previous DFT + U studies on reduced ceria have focused on single oxygen vacancies and found that the electron density localized on the two adjacent Ce^{3+} cations. Future studies on ceria containing aggregated oxygen vacancies should be conducted in order to predict the degree of electron localization. Because the d'Itri group does not currently perform computational chemistry, it will be necessary to collaborate with another group at the University of Pittsburgh, or an outside institution such as the National Energy Technology Laboratory, to perform these studies.

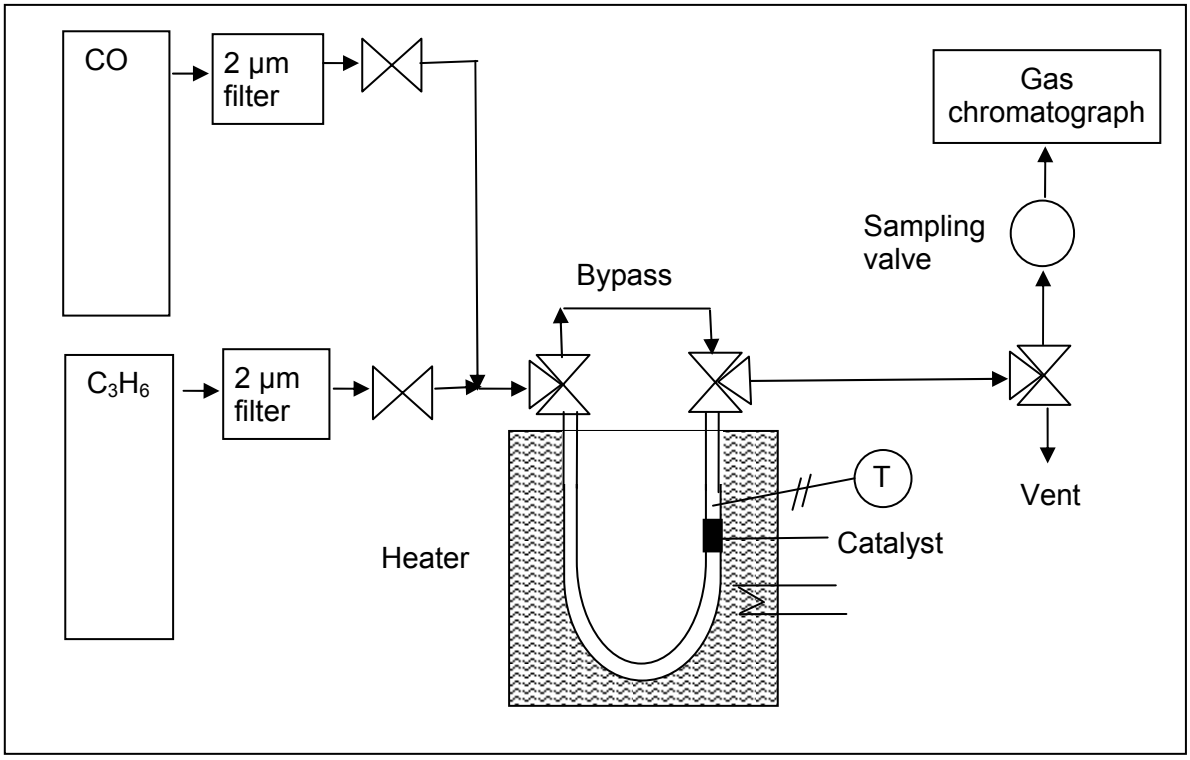

Figure 38. Reaction kinetic system schematic

BIBLIOGRAPHY

(1) Martinez-Arias, A., Conesa, J., Fernandez-Garcia, M. and Anderson, J., Supported Metals in Vehicle Emission Control. In *Supported Metals in Catalysis*, J. Anderson, Eds. Imperial College Press: London, 2005; pp. 283-325.

(2) Trovarelli, A., Structural properties and nonstoichiometric behavior of CeO_2. In *Catalysis by Ceria and Related Materials*, A. Trovarelli, Eds. 2002; pp. 15-50.

(3) Trovarelli, A., Structural and Oxygen Storage/Release Properties of CeO_2-based Solid Solutions. *Comm. Inorg. Chem.* **20** (1999) 263-284.

(4) Bevan, D. J. M. and Kordis, J., Mixed oxides of the type MO_2 (Fluorite)-M_2O_3 I. Oxygen dissociation pressures and phase relationships in the system CeO_2-Ce_2O_3 at high temperatures. *J. Inorg. Nucl. Chem.* **26** (1964) 1509-1523.

(5) Kung, H. H., *Transition Metal Oxides: Surface Chemistry and Catalysis;* Elsevier: New York, 1989.

(6) Esch, F., Fabris, S., Zhou, L., Montini, T., Africh, C., Fornasiero, P., Comelli, G. and Rosei, R., Electron Localization Determines Defect Formation on Ceria Substrates. *Science* **309** (2005) 752-755.

(7) Fukui, K., Namai, Y. and Iwasawa, Y., Imaging of surface oxygen atoms and theis defect structures on CeO2(111) by noncontact AFM. *App. Surf. Sci.* **188** (2002) 252-256.

(8) Pushkarev, V. V., Kovalchuk, V. I. and d'Itri, J. L., Probing Defect Sites on the CeO_2 Surface with Dioxygen. *J. Phys. Chem. B* **108** (2004) 5341-5348.

(9) Li, C., Domen, K., Maruya, K. and Onishi, T., Dioxygen adsorption on well-outgassed and partially reduced cerium oxide studied by FT-IR. *J. Am. Chem. Soc.* **111** (1989) 7683-7687.

(10) Descorme, C., Madier, Y. and Duprez, D., Infrared Study of Oxygen Adsorption and Activation on Cerium-Zirconium Mixed Oxides. *J. Catal.* **196** (2000) 167-173.

(11) Hilaire, S., Wang, X., Luo, T., Gorte, R. and Wagner, J., A comparative study of water-gas-shift reaction over ceria-supported metallic catalysts. *App. Catal. A* **258** (2004) 271-276.

(12) Morgensen, M., Ceria-based electrodes. In *Catalysis by Ceria and Related Materials*, A. Trovarelli, Eds. 2002; pp. 453-481.

(13) Yao, H. and Yu Yao, Y., Ceria in automotive exhaust catalysts 1. Oxygen storage. *J. Catal.* **86** (1984) 254-265.

(14) Fisher, G. B., Theis, J. R., Casarella, M. V. and Mahan, S. T., The Role of Ceria in Automotive Exhaust Catalysis and OBD-II Catalyst Monitoring. *SAE paper # 931034* (1993)

(15) Cuif, J.-P., Blanchard, G., Touret, O., Marczi, M. and Quemere, E., New generation of rare earth compounds for automotive catalysis. *SAE paper # 961906* (1996)

(16) Sugiura, M., Ozawa, M., Suda, A., Suzuki, T. and Kanazawa, T., Development of Innovative TWC containing ceria-zirconia solid solutions with high OSC. *Bull. Chem. Soc. Jpn.* **78** (2005) 752-767.

(17) Cuif, J.-P., Deutsch, S., Marczi, M., Jen, H.-W., Graham, G. W., Chun, W. and McCabe, R. W., High temperature stability of ceria-zirconia supported Pd model catalysts. *SAE paper # 980668* (1998)

(18) Tanaka, H. and Yamamoto, M., Improvement in Oxygen Storage Capacity. *SAE paper # 960794* (1996)

(19) Zhang, Y., Andersson, S. and Muhammad, M., Nanophase catalytic oxides: I. Synthesis of doped cerium oxides as oxygen storage promoters. *App. Catal. B* **6** (1995) 325-337.

(20) Pijolat, M., Prin, M., Soustelle, M., Touret, O. and Nortier, P., Thermal Stability of Doped Ceria: Experiment and Modeling. *J. Chem. Soc., Faraday Trans.* **91** (1995) 3941-3948.

(21) Pijolat, M., Prin, M., Soustelle, M., Touret, O. and Nortier, P., Improvement of the thermal stability of ceria support. *Stud. Surf. Sci. Catal.* **96** (1995) 325-333.

(22) Kaspar, J., Fornasiero, P. and Graziani, M., Use of CeO_2-based oxides in the three-way catalysis. *Catal. Today* **50** (1999) 285-298.

(23) Fornasiero, P., Balducci, G., Di Monte, R., Kaspar, J., Sergo, V., Gubitosa, G., Ferrero, A. and Graziani, M., Modification of the redox behavior of CeO_2 induced by structural doping with ZrO_2. *J. Catal.* **164** (1996) 173-183.

(24) Ozawa, M., Kimura, M. and Isogai, A., The application of Ce-Zr oxide solid solution to oxygen storage promoters in automotive catalysts. *J. Alloys Compd.* **193** (1993) 73-75.

(25) Kaspar, J. and Fornasiero, P., Structural properties and thermal stability of ceria-zirconia and related materials. In *Catalysis by Ceria and Related Materials*, A. Trovarelli, Eds. 2002; pp. 217-241.

(26) Di Monte, R. and Kaspar, J., Nanostructured CeO_2-ZrO_2 mixed oxides. *J. Mater. Chem.* **15** (2005) 633-648.

(27) Cuif, J., Blanchard, G., Touret, O., Seigneurin, A., Marczi, M. and Quemere, E., $(Ce,Zr)O_2$ Solid Solutions for Three-Way Catalysts. *SAE paper # 970463* (1997) 35-47.

(28) Permana, H., Belton, D. N., Rahmoeller, K. M., Schmieg, S. J., Hori, C. E., Ng, K. Y. S. and Brenner, A., Reactor Evaluation of Ceria-Zirconia as An Oxygen Storage Material for Automotive Catalysts. *SAE paper # 970462* (1997) 23-33.

(29) Tauster, S. J., Dettling, J. C. and Rabinowitz, H. N., Patent EP 427493 (1991) Three-way catalyst for exhaust gas treatment including a ceria-containing zirconia support.

(30) Duprez, D. and Descorme, C., Oxygen storage/redox capacity and related phenomena on ceria-based catalysts. In *Catalysis by Ceria and Related Materials*, A. Trovarelli, Eds. 2002; pp. 243-280.

(31) Madier, Y., Descorme, C., Le Govic, A. M. and Duprez, D., Oxygen Mobility in CeO_2 and $Ce_xZr_{(1-x)}O_2$ Compounds: Study by CO Transient Oxidation and $^{18}O/^{16}O$ Isotopic Exchange. *J. Phys. Chem. B* **103** (1999) 10999-11006.

(32) Kim, T., Vohs, J. M. and Gorte, R. J., Thermodynamic Investigation of the Redox Properties of Ceria-Zirconia Solid Solutions. *Ind. Eng. Chem. Res.* **45** (2006) 5561-5565.

(33) Fornasiero, P., DiMonte, R., Ranga Rao, G., Kaspar, J., Meriani, S., Trovarelli, A. and Graziani, M., Rh-loaded CeO_2-ZrO_2 Solid solutions as highly effective oxygen exchangers: dependence on the reduction behavior and the OSC on the structural properties. *J. Catal.* **151** (1995) 168-177.

(34) Mamontov, E., Egami, T., Brezny, R., Koranne, M. and Tyagi, S., Lattice Defects and Oxygen Storage Capacity of Nanocrystalline Ceria and Ceria-Zirconia. *J. Phys. Chem. B* **104** (2000) 11110-11116.

(35) Vlaic, G., Di Monte, R., Fornasiero, P., Fonda, E., Kaspar, J. and Graziani, M., Redox Property-Local Structure Relationships in the Rh-Loaded CeO_2-ZrO_2 Mixed Oxides. *J. Catal.* **182** (1999) 378-389.

(36) Vlaic, G., Fornasiero, P., Geremia, S., Kaspar, J. and Graziani, M., Relationship between the Zirconia-Promoted Reduction in the Rh-Loaded $Ce_{0.5}Zr_{0.5}O_2$ Mixed Oxide and the Zr-O Local Structure. *J. Catal.* **168** (1997) 386-392.

(37) Dmowski, W., Louca, D., Egami, T. and Brezny, R., Local Atomic Structure of CeO_2/ZrO_2 Catalyst Support Determined by Pulsed Neutron Scattering. *Ceram. Trans.* **73** (1997) 119-125.

(38) Conesa, J. C., Computer Modeling of Local Level Structures in (Ce,Zr) Mixed Oxide. *J. Phys. Chem. B* **107** (2003) 8840-8853.

(39) Kiskinova, M., Interaction of CO with single crystal metal surfaces. *Stud. Surf. Sci. Catal.* **64** (1991) 37-86.

(40) Chang, R., *Physical Chemistry for the Chemical and Biological Sciences;* University Science Books: Sausalito, CA, 2000.

(41) Binet, C., Jadi, A. and Lavalley, J. C., IR study of carbon dioxide and carbon monoxide adsorption onto ceria- effect of the reduction state of ceria. *J. Chim. Phys. Phys.-Chim. Biol.* **89** (1992) 1779-1797.

(42) Li, C., Sakata, Y., Arai, T., Domen, K., Maruya, K. and Onishi, T., Adsorption of carbon monoxide and carbon dioxide on cerium oxide studied by Fourier-transform infrared spectroscopy. 2. Formation of formate species on partially reduced cerium dioxide at room temperature. *J. Chem. Soc., Faraday Trans. 1* **85** (1989) 1451-1461.

(43) Holmgren, A., Andersson, B. and Duprez, D., Interactions of CO with Pt/ceria catalysts. *Appl. Catal. B* **22** (1999) 215-230.

(44) Busca, G. and Lorenzelli, V., Infrared Spectroscopic identification of species arising from reactive adsorption of carbon oxides on metal oxide surfaces. *Mater. Chem.* **7** (1982) 89-126.

(45) Binet, C., Daturi, M. and Lavalley, J. C., IR Study of polycrystalline ceria properties in oxidised and reduced states. *Catal. Today* **50** (1999) 207-225.

(46) Li, C., Sakata, Y., Arai, T., Domen, K., Maruya, K. and Onishi, T., Carbon monoxide and carbon dioxide adsorption on cerium oxide studied by Fourier-transform infrared spectroscopy. 1. Formation of carbonate species on dehydroxylated cerium dioxide at room temperature. *J. Chem. Soc., Faraday Trans. 1* **85** (1989) 929-943.

(47) Binet, C., Badri, A. and Lavalley, J.-C., A Spectroscopic Characterization of the Reduction of Ceria from Electronic Transitions of Intrinsic Point Defects. *J. Phys. Chem.* **98** (1994) 6392-6398.

(48) Nakamoto, K., *Infrared and Raman Spectra of Inorganic and Coordination Compounds;* 5^{th}; John Wiley & Sons: New York, 1997.

(49) Weber, W., Hass, K. and McBride, J., Raman study of CeO_2: second-order scattering, lattice dynamics, and particle-size effects. *Phys. Rev. B* **48** (1993) 178-185.

(50) Tuinstra, F. and Koenig, J. L., Raman spectrum of graphite. *J. Chem. Phys.* **53** (1970) 1126-1130.

(51) Ferrari, A. C. and Robertson, J., Interpretation of Raman spectra of disordered and amorphous carbon. *Phys. Rev. B* **61** (2000) 14095-14107.

(52) Castiglioni, C., Mapelli, C., Negri, F. and Zerbi, G., Origin of the D line in the Raman spectrum of graphite: A study based on Raman frequencies and intensities of polycyclic aromatic hydrocarbon molecules. *J. Chem. Phys.* **114** (2001) 963-974.

(53) Cheng, H., Reiser, D. B. and Dean, S., Jr., On the mechanism and energetics of Boudouard reaction at FeO(1 0 0) surface 2CO->C+CO_2. *Catal. Today* **50** (1999) 579-587.

(54) Nakano, H., Kawakami, S., Fujitani, T. and Nakamura, J., Carbon deposition by disproportionation of CO on a Ni(977) surface. *Surf. Sci.* **454-456** (2000) 295-299.

(55) Martra, G., Marchese, L., Arena, F., Parmaliana, A. and Coluccia, S., Surface structure of Ni/MgO catalysts: effects of carbon and hydrogen on the reactivity towards CO. HRTEM and FTIR studies. *Topics Catal.* **1** (1994) 63-73.

(56) Highfield, J. G., Bossi, A. and Stone, F. S., Dispersed-metal/oxide catalysts prepared by reduction of high surface area oxide solid solutions. *Stud. Surf. Sci. Catal.* **16** (1983) 181-192.

(57) Govindaraj, A., Sen, R., Santra, A. K. and Nagaraju, B. V., Carbon structures obtained by the disproportionation of carbon monoxide over nickel catalysts. *Mater. Res. Bull.* **33** (1998) 663-667.

(58) Guinot, J., Audier, M., Coulon, M. and Bonnetain, L., Formation and characterization of catalytic carbons obtained from carbon monoxide disproportionation over an iron-nickel catalyst. I. Fragmentation and rates of carbon deposition. *Carbon* **19** (1981) 95-98.

(59) Geurts, F. W. A. H. and Sacco, A., Jr., The relative rates of the Boudouard reaction and hydrogenation of carbon monoxide over iron and cobalt foils. *Carbon* **30** (1992) 415-418.

(60) Moeller, P. and Papp, H., Heats of adsorption and reaction of carbon monoxide on iron/manganese oxide catalysts. *Adsorpt. Sci. Technol.* **4** (1987) 176-184.

(61) Nakamura, J., Tanaka, K. and Toyoshima, I., Reactivity of deposited carbon on cobalt-alumina catalyst. *J. Catal.* **108** (1987) 55-62.

(62) Gavril, D., Koliadima, A. and Karaiskakis, G., Adsorption Studies of Gases on Pt-Rh Bimetallic Catalysts by Reversed-Flow Gas Chromatography. *Langmuir* **15** (1999) 3798-3806.

(63) Ichikava, S., Poppa, H. and Boudart, M., The effect of particle size on the reactivity of supported palladium. *Catal. Mater.* **248** (1984) 439-451.

(64) Matolin, V. and Gillet, E., Carbon monoxide disproportionation over supported palladium particles: a TPD and static SIMS study. *Surf. Sci.* **238** (1990) 75-82.

(65) Gredig, S., Tagliaferri, M., Maciejewski, M. and Baiker, A., Oxidation and disproportionation of carbon monoxide over Pd/ZrO2 catalysts prepared from glassy Pd-Zr alloy and by co-precipitation. *Stud. Surf. Sci. Catal.* **96** (1995) 285-294.

(66) Yokomizo, G. H., Louis, C. and Bell, A. T., Thermal desorption and disproportionation of carbon monoxide adsorbed on ruthenium/silica. *J. Catal.* **120** (1989) 15-21.

(67) Orita, H., Naito, S. and Tamaru, K., Reactivity of surface carbon deposited on supported rhodium catalysts by the disproportionation of carbon monoxide. *J. Catal.* **111** (1988) 464-467.

(68) Zecchina, A., Coluccia, S., Spoto, G., Scarano, D. and Marchese, L., Revisiting magnesium oxide-carbon monoxide surface chemistry: an IR investigation. *J. Chem. Soc., Faraday Trans.* **86** (1990) 703-709.

(69) Watanabe, M. and Kadowaki, T., Dissociation reactions of CO gas on Fe and Fe_3O_4 surfaces observed by Raman-ellipsometry spectroscopy. *Appl. Surf. Sci.* **28** (1987) 147-166.

(70) Li, C., Sakata, Y., Arai, T., Domen, K., Maruya, K. and Onishi, T., Carbon monoxide disproportionation at mild temperatures over partially reduced cerium oxide. *J. Chem. Soc., Chem. Commun.* (1991) 410-411.

(71) Wang, Y., Alsmeyer, D. C. and McCreery, R. L., Raman spectroscopy of carbon materials: structural basis of observed spectra. *Chem. Mater.* **2** (1990) 557-563.

(72) Jawhari, T., Roid, A. and Casado, J., Raman spectroscopic characterization of some commercially available carbon black materials. *Carbon* **33** (1995) 1561-1565.

(73) Dillon, R. O. and Woollam, J. A., Use of Raman scattering to investigate disorder and crystallite formation in as-deposited and annealed carbon films. *Phys. Rev. B* **29** (1984) 3482.

(74) Nemanich, R. J. and Solin, S. A., First- and second-order Raman scattering from finite-size crystals of graphite. *Phys. Rev. B* **20** (1979) 392-401.

(75) Nathan, M. I., Smith, J. E. and Tu, K. N., Raman spectrum of glassy carbon. *J. Appl. Phys.* **45** (1974) 2370-2371.

(76) Knight, D. S. and White, W. B., Characterization of diamond films by Raman spectroscopy. *J. Mater. Res.* **4** (1989) 385-393.

(77) Al-Jishi, R. and Dresselhaus, G., Lattice-dynamical model for graphite. *Phys. Rev. B* **26** (1982) 4514.

(78) Matthews, M. J., Pimenta, M. A., Dresselhaus, G., Dresselhaus, M. S. and Endo, M., Origin of the dispersive effects of the Raman D band in carbon materials. *Phys. Rev. B* **59** (1999) R6585-R6588.

(79) Yaws, C., *The Yaws Handbook of Thermodynamic Properties for Hydrocarbons and Chemicals;* Gulf Publishing Co.: Houston, TX, 2006.

(80) Swanson, M., Pushkarev, V. V., Kovalchuk, V. I. and d'Itri, J. L., The dynamic surface chemistry during the interaction of CO with ceria captured by Raman spectroscopy. *Catal. Lett.* **116** (2007) 41-45.

(81) Swanson, M., Pushkarev, V. V., Kovalchuk, V. I. and D'Itri, J. L., A mechanistic investigation of formate formation on ceria based oxides. *J. Catal.* In preparation.

(82) De Leitenburg, C., Trovarelli, A. and Kaspar, J., A temperature-programmed and transient kinetic study of CO_2 activaton and methanation over CeO_2 supported noble metals. *J. Catal.* **166** (1997) 98-107.

(83) Martin and Duprez, D., Mobility of surface species on oxides 1. *J. Phys. Chem.* **100** (1996) 9429-9438.

(84) Bedrane, S., Descorme, C. and Duprez, D., Investigation of the oxygen storage process on ceria- and ceria-zirconia-supported catalysts. *Catal. Today* **75** (2002) 401-405.

(85) Swanson, M., Pushkarev, V. V., Kovalchuk, V. I. and d'Itri, J. L., When CO oxidizes a metal oxide. *Science* In work.

(86) Swanson, M., Pushkarev, V. V., Kovalchuk, V. I. and d'Itri, J. L., Relative rates for CO disproportionation on Pd and CeO_2: Is CeO_2 the better catalyst? *J. Phys. Chem. C* In preparation.

(87) Swanson, M., Pushkarev, V. V., Kovalchuk, V. I. and d'Itri, J. L., Carbonate formation and stability on ceria-zirconia supported Pd catalysts. *J. Mol. Catal. A: Chem.* In preparation.

(88) Sharma, S., Hilaire, S., Vohs, J. M., Gorte, R. J. and Jen, H. W., Evidence for Oxidation of Ceria by CO_2. *J. Catal.* **190** (2000) 199-204.

(89) Hepburn, J. S. and Gandha, H. S., The Relationship Between Catalyst Hydrocarbon Conversion Efficiency and Oxygen Storage Capacity. *SAE paper #920831* (1992)

(90) Holmgren, A. and Andersson, B., Oxygen storage dynamics in $Pt/CeO_2/Al_2O_3$ catalysts. *J. Catal.* **178** (1998) 14-25.

(91) Campbell, C. T. and Peden, C. H. F., Chemistry: Oxygen vacancies and catalysis on ceria surfaces. *Science* **309** (2005) 713-714.

(92) Bozon-Verduraz, F. and Bensalem, A., IR studies of cerium dioxide: influence of impurities and defects. *J. Chem. Soc., Faraday Trans.* **90** (1994) 653-657.

(93) Vicario, G., Balducci, G., Fabris, S., de Gironcoli, S. and Baroni, S., Interaction of hydrogen with cerium oxide surfaces: a quantum mechanical computational study. *J. Phys. Chem. B* **110** (2006) 19380-19385.

(94) Laachir, A., Perrichon, V., Badri, A., Lamotte, J., Catherine, E., Lavalley, J. C., El Fallah, J., Hilaire, L., Le Normand, F., Quemere, E., Sauvion, N. and Touret, O., Reduction of cerium dioxide by hydrogen. Magnetic susceptibility and Fourier-transform infrared, ultraviolet and x-ray photoelectron spectroscopy measurements. *J. Chem. Soc., Faraday Trans.* **87** (1991) 1601-1609.

(95) Meunier, F. C., Tibiletti, D., Goguet, A., Reid, D. and Burch, R., On the reactivity of carbonate species on a Pt/CeO2 catalyst under various reaction atmospheres: Application of the isotopic exchange technique. *App. Catal. A* **289** (2005) 104-112.

(96) Binet, C., Badri, A., Boutonnet-Kizling, M. and Lavalley, J. C., FTIR study of carbon monoxide adsorption on ceria: CO_2^{2-} carbonite dianion adsorbed species. *J. Chem. Soc., Faraday Trans.* **90** (1994) 1023-1028.

(97) Ichikawa, S., Suda, J., Sato, T. and Suzuki, Y., Lattice dynamics and temperature dependence of the first-order Raman spectra for α-SiO_2 crystals. *J. Raman Spectrosc.* **34** (2003) 135-141.

(98) Bertheville, B. and Bill, H., The temperature dependence of the Raman T_{2g} lattice mode in K_2S crystals. *Solid State Ionics* **139** (2001) 159-162.

(99) Li, C., Domen, K., Maruya, K. and Onishi, T., Oxygen exchange reactions over cerium oxide: an FT-IR study. *J. Catal.* **123** (1990) 436-442.

(100) Long, R. Q., Huang, Y. P. and Wan, H. L., Surface oxygen species over cerium oxide and heir reactivities with methand and ethane by means of in situ confocal microprobe raman spectroscopy. *J. Raman Spectrosc.* **29** (1997) 29-32.

(101) Li, C., Domen, K., Maruya, K. and Onishi, T., Spectroscopic identification of adsorbed species derived from adsorption and decomposition of formic acid, methanol, and formaldehyde on cerium oxide. *J. Catal.* **125** (1990) 445-455.

(102) Lavalley, J. C., Saussey, J. and Rais, T., Infrared study of the interaction between CO and H_2 on ZnO: Mechanism and sites of formation of formyl species. *J. Mol. Catal.* **17** (1982) 289-298.

(103) Saussey, J., Lavalley, J. C., Lamotte, J. and Rais, T., I.R. Spectroscopic evidence of formyl species formed by CO and H_2: Co-adsorption on ZnO and Cu-ZnO. *J. Chem. Soc., Chem. Commun.* (1982) 278-279.

(104) Jin, T., Zhou, Y., Mains, G. J. and White, J. M., Infrared and X-ray Photoelectron Spectroscopy Study of CO and CO_2 on Pt/CeO_2. *Journal of Physical Chemistry* **91** (1987) 5931-5937.

(105) Kung, M. C. and Kung, H. H., IR Studies of NH_3, pyridine, CO, and NO adsorbed on transition metal oxides. *Catal. Rev.: Sci. & Eng.* **27** (1985) 425-460.

(106) Zhao, S., Luo, T. and Gorte, R. J., Deactivation of the water-gas-shift activity of Pd/ceria by Mo. *J. Catal.* **221** (2004) 413-420.

(107) Nemanich, R. J., Lucovsky, G. and Solin, S. A., *Solid State Commun.* **23** (1977) 177.

(108) Escribano, R., Sloan, J. J., Siddique, N., Sze, N. and Dudev, T., Raman spectroscopy of carbon-containing particles. *Vib. Spec.* **26** (2001) 179-186.

(109) Poscik, I., Hundhausen, M., Koos, M. and Ley, L., Origin of the D peak in the Raman spectrum of microcrystalline graphite. *J. Non-Cryst. Solids* **230** (1998) 1083-1086.

(110) Kastner, J., Pichler, T., Kuzmany, H., Curran, S., Blau, W., Weldon, D. N., Delamesiere, M., Draper, S. and Zandbergen, H., Resonance Raman and infrared spectroscopy of carbon nanotubes. *Chem. Phys. Lett.* **221** (1994) 53-58.

(111) Bensalem, A., Muller, J.-C., Tessier, D. and Bozon-Verduraz, F., Spectroscopic study of CO adsorption on palladium-ceria catalysts. *Journal of the Chemical Society, Faraday Transactions* **92** (1996) 3233-3237.

(112) Bensalem, A., Muller, J.-C., Tessier, D. and Bozon-Verduraz, F., Spectroscopic study of CO adsorption on palladium-ceria catalysts. *J. Chem. Soc., Faraday Trans.* **92** (1996) 3233-3237.

(113) Nistor, L. C., Van Landuyt, J., Ralchenko, V. G., Kononenko, E. D., Obraztsova, V. E. and Strelnisky, V. E., Direct observaton of Laser-induced crystallizaton of a-C:H films. *Appl. Phys. A* **58** (1994) 137.

(114) Shelef, M. and McCabe, R. W., Twenty-five years after introduction of automotive catalysis: what next? *Catal. Today* **62** (2000) 35-50.

(115) Trovarelli, A., Catalytic properties of ceria and ceria-containing materials. *Catal. Rev.* **38** (1996) 439-520.

(116) Mugniery, X., Chafik, T., Primet, M. and Bianchi, D., Characterization of the sites involved in the adsorption of CO on ZrO_2 and ZnO/ZrO_2 methanol synthesis aerogel catalysts. *Catal. Today* **52** (1999) 15-22.

(117) Bianchi, D., Chafik, T., Khalfallah, M. and Teichner, S. J., Intermediate species on zirconia supported methanol aerogel catalysts. II. Adsorption of CO on pure zirconia and on zirconia containing zinc oxide. *App. Catal. A* **105** (1993) 223-249.

(118) Kalies, H., Pinto, N., Pajonk, G. M. and Bianchi, D., Hydrogenation of formate species formed by CO chemisorption on a zirconia aerogel in the presence of platinum. *App. Catal. A* **202** (2000) 197-205.

(119) Yashima, M., Arashi, H., Kakihana, M. and Yoshimura, M., Raman Scattering Study of Cubic-Tetragonal Phase Transition in $Zr_{1-x}Ce_xO_2$ Solid Solution. *J. Am. Ceram. Soc.* **77** (1994) 1067-1071.

(120) Reddy, B. M., Khan, A., Lakshmanan, P., Aouine, M., Loridant, S. and Volta, J.-C., Structural Characterization of Nanosized CeO_2-SiO_2, CeO_2-TiO_2, and CeO_2-ZrO_2 Catalysts by XRD, Raman, and HREM Techniques. *J. Phys. Chem. B* **109** (2005) 3355-3363.

(121) Fornasiero, P., Spenghini, A., Di Monte, R., Bettinelli, M., Kaspar, J., Bigotto, A., Sergo, V. and Graziani, M., Laser Excited Luminescence of Trivalent lanthanide Impurities and Local Structure in CeO2-ZrO2 Mixed Oxides. *Chem. Mater.* **16** (2004) 1938-1944.

(122) Deshmukh, S. S., Zhang, M., Kovalchuk, V. I. and d'Itri, J. L., Effect of SO_2 on CO and C_3H_6 oxidation over CeO_2 and $Ce_{0.75}Zr_{0.25}O_2$. *App. Catal. B* **45** (2003) 135-145.

(123) Fisher, I. A. and Bell, A. T., In situ infrared study of methanol synthesis from H_2/CO over Cu/SiO_2 and $Cu/ZrO_2/SiO_2$. *J. Catal.* **178** (1998) 153-173.

(124) Pokrovski, K., Jung, K. T. and Bell, A. T., Investigation of CO and CO2 adsorption on tetragonal and monoclinic zirconia. *Langmuir* **17** (2001) 4297-4303.

(125) Blyholder, G., Molecular Orbital view of Chemisorbed Carbon Monoxide. *J. Phys. Chem.* **68** (1964) 2772-2777.

(126) Steinfeld, J. I., Francisco, J. S. and Hase, W. L., *Chemical Kinetics and Dynamics;* Prentice Hall: Englewood Cliffs, NJ, 1989.

(127) Ganduglia-Pirovano, M. V., Hofmann, A. and Sauer, J., Oxygen vacancies in transition metals and rare earth oxides: current state of understanding and remaining challenges. *Surf. Sci. Rep.* **62** (2007) 219-270.

(128) Mars, P. and van Krevelen, P. W., *Spec. Suppl. Chem. Eng. Sci.* **3** (1954) 41-59.

(129) Badri, A., Binet, C. and Lavalley, J.-C., Metal-support interaction in Pd/CeO2 catalysts. Part 2. Ceria textural effects. *J. Chem. Soc., Faraday Trans.* **92** (1996) 1603-1608.

(130) Bensalem, A., Muller, J.-C., Tessier, D. and Bozon-Verduraz, F., Spectroscopic study of CO adsorption on palladium-ceria catalysts. *J. Chem. Soc., Faraday Trans.* **93** (1997) 1861.

(131) Bozo, C., Guilhaume, N. and Herrmann, J.-M., Role of the Ceria-Zirconia Support in the Reactivity of Platinum and Palladium Catalysts for Methane Total Oxidation under Lean Conditions. *J. Catal.* **203** (2001) 393-406.

(132) Ciuparu, D., Bensalem, A. and Pfefferle, L., Pd–Ce interactions and adsorption properties of palladium: CO and NO TPD studies over Pd–Ce/Al2O3 catalysts. *App. Catal. B* **26** (2000) 241-255.

(133) Fernandez-Garcia, M., Martinez-Arias, A., Salamanca, L. N., Coronado, J. M., Anderson, J. A., Conesa, J. C. and Soria, J., Influence of Ceria on Pd Activity for the CO+O2 Reaction. *J. Catal.* **187** (1999) 474-485.

(134) Tiznado, H., Fuentes, S. and Zaera, F., Infrared Study of CO Adsorbed on Pd/Al_2O_3-ZrO_2. Effect of Zirconia Added by Impregnation. *Langmuir* **20** (2004) 10490-10497.

(135) Wang, J. A., Dominguez, J. M., Montoya, A., Castillo, S., Navarrete, J., Moran-Pineda, M., Reyes-Gasga, J. and Bokhimi, X., New Insights into the Defective Structure and Catalytic Activity of Pd/Ceria. *Chem. Mater.* **14** (2002) 4676-4683.

(136) Bedrane, S., Descorme, C. and Duprez, D., Oxygen storage and oxygen mobility on ceria and ceria-zirconia supported noble metals. *Stud. Surf. Sci. Catal.* **138** (2001) 125-134.

(137) Duprez, D., Descorme, C., Birchem, T. and Rohart, E., Oxygen storage and mobility on model three-way catalysts. *Topics Catal.* **16/17** (2001) 49-56.

(138) Deshmukh, S. S., Borovkov, V. Y., Kovalchuk, V. I. and d'Itri, J. L., FTIR Spectroscopic and Reaction Kinetics Study of the Interaction of CF_3CFCl_2 with gamma-Al_2O_3. *J. Phys. Chem. B* **104** (2000) 1277-1284.

(139) Wang, J., Dominguez, J., Montoya, A., Castillo, S., Navarrete, J., Moran-Pineda, M., Reyes-Gasga, J. and Bokhimi, X., New Insights into the Defective Structure and Catalytic Activity of Pd/Ceria. *Chem. Mater.* **14** (2002) 4676-4683.

(140) Vander Wal, R. L., A TEM Methodology for the Study of Soot Particle Structure. *Combust. Sci. Technol.* **126** (1997) 333-351.

(141) Huang, M. and Fabris, S., Role of surface peroxo and superoxo species in the low-temperature oxygen buffering of ceria: DFT calculations. *Phys. Rev. B* **75** (2007) 081404(R).

(142) Perkins, C. L., Henderson, M. A., Peden, C. H. F. and Herman, G. S., Self-diffusion in ceria. *J. Vac. Sci. Technol., A* **19** (2001) 1492-1496.

(143) In fact, the presence of gas phase O_2 increases the stability of all three surface peroxide species; the temperature at which each peroxide species transformed into lattice oxygen was roughly 15 K higher than in the presence of He.[47] Healing of the vacancies by lattice oxygen diffusion may also be considered as a possibility for the difference in intensity distribution, but solid diffusion is a slow process at room temperature; surface oxygen exchange with the ceria bulk is not observed at temperatures less than 500 K.[76,77]

(144) Cuif, J.-P., Blanchard, G., Touret, O., Seigneurin, A., Marczi, M. and Quemere, E., (Ce, Zr)O2 solid solutions for three-way catalysts. *SAE Paper # 970463* (1997) 35-47.

(145) Sheppard, N. and Nguyen, T. T., The Vibrational Spectra of Carbon Monoxide chemisorbed on the surfaces fo metal catalysis- a suggested scheme of interpretation. In *Advances in Infrared and Raman Spectroscopy*, R. J. H. Clark and R. E. Hester, Eds. Heyden: Philadelphia, 1978; pp.

(146) Dulaurent, O., Chandes, K., Bouly, C. and Bianchi, D., Heat of Adsorption of Carbon Monoxide on a Pd/Al_2O_3 Solid Using in Situ Infrared Spectroscopy at High Temperatures. *J. Catal.* **188** (1999) 237-251.

(147) Kondo, J., Abe, H., Sakata, Y., Maruya, K., Domen, K. and Onishi, T., Infrared studies of adsorbed species of H_2, CO and CO_2 over ZrO_2. *J. Chem. Soc., Faraday Trans. 1* **84** (1988) 511-519.

(148) Hertl, W., Surface Chemistry of Zirconia Polymorphs. *Langmuir* **5** (1989) 96-100.

(149) Guglielminotti, E., Infrared study of syngas adsorption on zirconia. *Langmuir* **6** (1990) 1455-1460.

(150) Guerrero-Ruiz, A., Yang, S., Xin, Q., Maroto-Valiente, A., Benito-Gonzalez, M. and Rodriguez-Ramos, I., Comparative Study by Infrared Spectroscopy and Microcalorimetry of the CO Adsorption over Supported Palladium Catalysts. *Langmuir* **16** (2000) 8100-8106.

(151) Daturi, M., Binet, C., Lavalley, J. C. and Blanchard, G., Surface FTIR investigations on $Ce_xZr_{1-x}O_2$ system. *Surf. Interface Anal.* **30** (2000) 273-277.

(152) Daturi, M., Binet, C., Lavalley, J. C., Galtayries, A. and Sporken, R., Surface Investigation on $Ce_xZr_{1-x}O_2$ compounds. *Phys. Chem. Chem. Phys.* **1** (1999) 5717-5724.

(153) Song, Z., Nishiguchi, H., Liu, W., Yamada, H., Takami, A., Kudo, K., Nagaoka, K. and Takita, Y., Redox properties of CeO_2 and $Pt\text{-}Rh/CeO_2$ studied by TAP method. *Catal. Lett.* **111** (2006) 169-171.

(154) Song, Z., Liu, W. and Nishiguchi, H., Quantitative analyses of oxygen release.storage and CO_2 adsorption on ceria and Pt-Rh/ceria. *Catal. Comm.* **8** (2007) 725-730.

(155) Nolan, M., Parker, S. C. and Watson, G. W., The electronic structure of oxygen vacancy defects at the low index surfaces of ceria. *Surface Science* **595** (2005) 223-232.